EFFECTS OF DIMETHYLARGININE DIMETHYLAMINOHYDROLASE 1 AND ADENOSINE MONOPHOSPHATE-ACTIVATED PROTEIN KINASE ALPHA 2 GENE DELETION ON PULMONARY HYPERTENSION IN MICE

A Dissertation
SUBMITTED TO THE FACULTY OF
UNIVERSITY OF MINNESOTA
BY

Dongmin Kwak

IN PARTIAL FULFILLMENT OF THE REQUIREMENTS
FOR THE DEGREE OF
DOCTOR OF PHILOSOPHY

Arthur S. Leon, Yingjie Chen

June 2015

Dedication

To Sun Hae, Erin, Taejoon

Preface

Pulmonary arterial hypertension (PAH) is generally defined as a sustained elevation of pulmonary arterial pressure without left ventricular failure. Nitric Oxide (NO) is an endogenously produced, locally acting gas that exerts multiple actions that help to maintain lung vascular function, while development of PAH is associated with reduced lung vascular NO bioavailability. Dimethylarginine dimethylaminohydrolase-1 (DDAH1) is the critical enzyme for the degradation of endogenous NO synthase inhibitor ADMA to enhance NO production. Adenosine monophosphate-activated protein kinase (AMPK) is an enzyme that also exerts multiple actions to regulating cardiovascular function partially though modulating NO production. This dissertation tries to identify the effects of DDAH1 and AMPKα2 on hypoxia-induced PAH and the underlying molecular mechanisms. The findings from these studies provide new insight into the molecular mechanism of the development of PAH and right heart hypertrophy/failure.

The dissertation has been divided into 2 chapters. The first chapter is determining effect of DDAH1 gene deletion on hypoxia+SU5416-induced pulmonary arterial hypertension and the second chapter is determining effect of AMPKα2 gene deletion on hypoxia+SU5416-induced pulmonary arterial hypertension. The data presented in these chapters are resulted from a research team in Dr. Yingjie Chen's laboratory. I was one of the major contributors for these chapters where I was responsible for most areas of concept formation, data collection and analysis, as well as the majority of manuscript

composition. I will be the first author for two manuscripts to be published and these manuscripts are based on the data presented in these two chapters.

Table of Contents

List of Tables

List of Figures

Figure (By Chapter 2)

CHAPTER 1

Effect of dimethylarginine dimethylaminohydrolase 1 (DDAH1) gene deletion on pulmonary arterial hypertension in mice

1. Introduction

Pulmonary arterial hypertension (PAH) is a progressive disease with a very poor prognosis. PAH is characterized by a progressive elevation of pulmonary arterial pressure, ultimately inducing right ventricular failure (1, 2). Previous studies have demonstrated that PAH and subsequent right ventricular hypertrophy is associated with diminished lung nitric oxide (NO) and cGMP bioavailability. While treatments that augment the NO-soluble guanylate cyclase-cGMP system have shown promise in attenuating PAH in animal model (3), and in human (4). However, the mortality rate for PAH remains extremely high (5), suggesting better understanding of biological factors involved in PAH development is necessary.

Asymmetric dimethylarginine (ADMA) and L-N^G-Monomethylarginine (L-NMMA) are endogenous NO synthase inhibitors that compete with L-arginine to attenuate NO production (6). Plasma ADMA levels are increased in experimental PAH models in animals (7, 8) and in patients with PAH (9), and may contribute to reduced NO generation observed in this disease. ADMA is eliminated by the action of Dimethylarginine dimethylaminohydrolase (DDAH), which converts ADMA to L-citrulline and dimethylamine. ADMA is also eliminated from circulation through renal excretion (10). DDAH activity was reduced and negatively correlated with ADMA levels in rats with

chronic hypoxia-induced pulmonary hypertension, suggesting DDAH deficiency may contribute to the increased ADMA levels and impaired NO production in PAH (7, 8).

It is reported that there are two isoforms of DDAH (DDAH1 and DDAH2) that are encoded by two different genes (11). DDAH1 was initially identified as the enzyme responsible for degrading ADMA and L-NMMA (6). Recent studies have demonstrated that loss of function mutations in DDAH1 are associated with increased occurrence of coronary heart disease, thrombosis, and stroke (12, 13). DDAH2 was also reported to degrade ADMA and L-NMMA *in vitro*, similar to DDAH1 (14). It consequently was assumed that *in vivo* metabolism of NOS inhibitors would reflect the combined activity of both isoforms. However, we have demonstrated that DDAH1 is the essential enzyme or the only enzyme for ADMA degradation (6), and that DDAH1 localized specifically in vascular endothelium plays an important role in regulating systemic and lung ADMA (15, 16).

Previous studies have demonstrated that PAH is associated with decreased lung DDAH activity and increased ADMA levels (7, 11), but the actual impact of DDAH1 dysfunction in PAH development has not been examined. In addition, DDAH1 is expressed in both vascular endothelial cells and cardiomyocytes (17, 18), but the impact of cardiomyocyte DDAH1 expression in right ventricular (RV) hypertrophy that accompanies PAH is unknown.

1.1. Purpose and specific aims of the study

The purpose of this study is to investigate whether DDAH1 plays an important role in attenuating PAH.

The specific aims of this study are:

(1) To determine the overall impact of DDAH1 in PAH development and progression.

(2) To determine the impact of cardiomyocyte DDAH1 on PAH induced RV hypertrophy and dysfunction.

1.2. Hypotheses

This project will test the following two hypotheses:

- Increased systemic and lung ADMA by global DDAH1 KO will exacerbate PAH development.
- Cardiomyocyte DDAH1 expression plays a protective role in RV adaptation to pulmonary hypertension, so that cardiomyocyte specific DDAH1 KO will exacerbate RV hypertrophy and dysfunction as compared to WT mice under equivalent levels of PAH.

Overall, by using novel DDAH1 mouse strains, these studies will define the causal role of DDAH1 dysfunction in development of PAH and RV hypertrophy. The findings will help to determine whether intervention(s) to augment DDAH1 could represent a new therapeutic strategy for treatment of PAH and RV hypertrophy.

1.3. Significance of the study

The study will explore unique new knowledge defining the causal role of DDAH1 dysfunction in PAH development and right ventricular hypertrophy. The findings will help determine the therapeutic potential of increasing DDAH1 activity in protecting the lung against PAH development. This is important, since agents that increase DDAH1 protein expression have been identified, including a farnesoid X receptor agonist (INT-747) (19) that is currently in a Phase II clinical trial to treat primary biliary cirrhosis. Using global DDAH KO mice will make it possible for the first time to determine the effect of chronic DDAH1 dysfunction on PAH development and RV hypertrophy. Using the novel cardio-DDAH KO mouse will help determine the impact of cardiac-specific DDAH1/ADMA/NOS signaling on PAH induced RV hypertrophy.

2. Literature Review

2.1. Pulmonary arterial hypertension

PAH is a syndrome resulting from restricted blood flow through the pulmonary arterial circulation, resulting in increased pulmonary vascular resistance and ultimately, right heart failure (20). An imbalance in the vasoconstrictor/vasodilator milieu has served as the basis for current medical therapies, although increasingly it is recognized that PAH also involves an imbalance of proliferation and apoptosis. It is now believed that the predominant cause of increased pulmonary vascular resistance is loss of vascular luminal cross sectional area due to vascular remodeling produced by excessive cell proliferation and reduced rates of apoptosis, while excessive vasoconstriction plays a significant role in approximately 20% of patients (21, 22).

While a single primary cause of PAH has not been clearly identified, improved understanding of the disease pathways in PAH has led to therapeutic strategies, including the administration of prostanoids, antagonism of endothelin receptors, and inhibition of PDE-5. Future therapeutic options identified by basic studies include inhibiting pyruvate dehydrogenase kinase (PDK), the serotonin transporter (5-HTT), the anti-apoptotic protein survivin, several transcription factors (hypoxia inducible factor-1 alpha, nuclear factor activating T lymphocytes), and augmenting voltage-gated potassium channel activity.

PAH is a panvasculopathy that predominantly affects small pulmonary arteries (23). PAH is characterized by a variety of arterial abnormalities including intimal hyperplasia, medial hypertrophy, adventitial proliferation, thrombosis in situ, varying degrees of

inflammation, and plexiform arteriopathy. An individual patient may manifest all of these lesions, and the distribution of lesions may be diffuse or focal. The understanding of the natural history of the evolution of vascular lesions in PAH, except for patients with coronary heart disease, is limited because biopsies are rarely obtained in adult patients. However, it is believed that medial hypertrophy is an earlier and more reversible lesion than intimal fibrosis or plexogenic arteriopathy.

RV function is a major determinant of functional capacity and prognosis in PAH (20). While RV hypertrophy and dilatation are initiated by increased afterload, the adequacy of the RV's compensatory response is quite variable among individuals. It remains unclear why some RVs exhibit compensatory hypertrophy and maintain function, while others decompensate, exhibiting ventricular wall thinning, dilatation, and reduced RV ejection fraction. The neonatal RV is much more tolerant of increased PVR, partially explaining the better survival in children with PAH associated with coronary heart disease. RV function could potentially be improved by effective therapies to reduce pulmonary vascular obstruction or by directly improving RV contractile function.

2.2. Endothelial Dysfunction contributes to PAH

In the human vascular system, the endothelium has an important role in the regulation of blood flow, vascular remodeling and repair. The outcome of PAH is the elevation of pulmonary vascular resistance mediated by vasoconstriction and obstructive cellular proliferation of the pulmonary vasculature. Through the synthesis and release of vasoactive factors, the endothelium plays a critical role in maintaining the delicate and precise balance between vasoconstrictor (such as endothelin-1 and thromboxane A2) and vasodilator (such as prostaglandin 1 and NO) in PAH. Endothelial damage and dysfunction disrupt this homeostasis, changing the balance to vasoconstriction. Several studies have suggested that dysfunction in NO signaling pathways contribute to the pathological remodeling of the pulmonary vasculature during the development of PAH (24, 25).

2.3. Decreased NO bioavailability contributes to PAH

NO in the cardiovascular and pulmonary system

NO is a critical regulator of many biological processes. In mammalian cells, NO is synthesized by a family of enzymes called NO synthases, which catalyze the production of NO from the amino acid L-arginine (26). There are 3 known nitric oxide synthases; eNOS, which is an endothelial nitric oxide synthase, iNOS which is an inducible NOS, and nNOS which a neuronal NOS. NO has particularly important influence on the cardiovascular system, where it regulates vascular tone and blood pressure, platelet aggregation and cardiac contractility. While defects in NO synthesis exacerbate some diseases such as cardiovascular disease and pulmonary hypertension, excess NO production can also promote certain pathological conditions such as septic shock. In addition to important roles in the cardiovascular system, NO participates in host defense against foreign cells and regulates inflammation. This section will discuss the role of nitric oxide in regulating cardiovascular and pulmonary vascular functions, homeostasis, and the immune system.

Physiological roles of eNOS

NO is produced and released by the endothelium to promote smooth muscle relaxation (27). The main source of NO in the endothelium is eNOS, which generates NO from the amino acid L-arginine (28). eNOS expression and activity are stimulated by increased shear stress. eNOS is calcium-and calmodulin-dependent, and releases picomoles of nitric oxide in response to stimulation (29). Endothelial NO then diffuses into smooth muscle cells where it activates guanylate cyclase, which produces cyclic GMP, resulting in smooth muscle cell relaxation and vasodilation. In this manner, NO produced by

endothelial cells regulates vascular tone and blood pressure. The methylated L-arginine analogues ADMA and L-NMMA are inhibitors of NOS that has provided important information on the role of nitric oxide in biological processes.

Evidence that endothelial NO plays an important homeostatic role came from studies using the NOS inhibitor L-NMMA or eNOS KO mice, both which showed that inhibition of eNOS activity causes hypertension (30). L-NMMA is a potent vasoconstrictor in vitro and produces a hypertensive response in animals and humans (29). In absence of vascular endothelium, L-NMMA has no intrinsic constrictor activity on vascular smooth muscle suggesting its vasoconstrictor effects are mediated by the endothelium (29). These findings indicate that the endothelium mediates NO dependent smooth muscle contractility through NOS, which is essential for the regulation of blood flow and pressure. In addition to regulating smooth muscle contractility, NO can regulate cardiomyocyte contractility through the NO/soluble guanylate cyclase/cyclic GMP dependent activation of PKG, which reduces cardiomyocyte contractility. This is believed to be due in part to PKG phosphorylation of troponin I and reduction of calcium sensitivity. NO also prolongs diastole, resulting in increased filling.

Maladaptive effects of NO in vascular system

While NO production is important for maintaining normal vascular tone, and blood pressure, excessive or inappropriate release of NO can also be detrimental. A calcium-independent isoform of nitric oxide synthase known as inducible nitric oxide synthase (iNOS) can be induced in vessel walls by certain cytokines and by endotoxin lipopolysaccharides. This induction occurs in both endothelial and smooth muscle cells, promoting severe vascular relaxation, hypotension and endotoxic shock. This pathological form of vascular relaxation is directly related to the production of NO and while resistant to most vasoconstrictors, it can be reversed by anti inflammatory treatments or inhibitors of nitric oxide synthase.

Endotoxin also induces iNOS expression in venous smooth muscle (31) and in the myocardium and endocardium (32). Enhanced synthesis of nitric oxide by iNOS may therefore contribute to the venous pooling and cardiac dysfunction associated with endotoxemia. Furthermore, induction of iNOS under certain stress conditions is also associated with cardiac dysfunction (33). Therefore, in the heart as in the vasculature, NO may have a physiological role when generated by the constitutive enzyme that is normally present in the myocardium but may also exert pathological effects, such as dilatation and tissue damage, when generated in large quantities and for long periods by the inducible enzyme.

Inhibitors of iNOS can reverse or prevent hypotension induced in animals by lipopolysaccharide, tumor necrosis factor, hemorrhagic shock or anaphylactic shock (29). In patients with septic shock, low dose of L-NMMA added to standard therapy

reversed hypotension in this condition (30). Experiments in animals indicate that a sub-maximal level of NOS inhibition is essential for the outcome of treatment because high doses of NOS inhibitor lead to severe vasoconstriction, end-organ damage, and rapid death. This finding is not surprising in a condition such as septic shock, in which hypotension occurs in the presence of increased circulating concentrations of vasoconstrictors. One solution to this problem may be to inhibit the endogenous generation of nitric oxide completely while at the same time giving a nitro-vasodilator to reverse the hypertension and maintain vascular homeostasis (34). This treatment would also counteract the increased aggregation of platelets that might occur during the inhibition of NO synthesis (35).

2.4. ADMA attenuates NO production

NO is a vasodilator. NO also promotes endothelial cell survival and proliferation, inhibits excessive proliferation of vascular smooth muscle cells, and suppresses adhesion of platelets and inflammatory cells to the vessel wall (36). As NOS are the major source of NO, factors that regulate NOS activity play an important role in cardiovascular physiology, where NO is an important signaling molecule. NOS activity is controlled by several factors, including the endogenous NOS inhibitors ADMA and L-NMMA (37). ADMA and L-NMMA compete with L-arginine for NOS attenuating NO production. ADMA is a strong independent marker for cardiovascular morbidity and mortality (38).

Generation of ADMA

Methylation of arginine residues in proteins by arginine methylltransferases (PRMTs) is the main source of ADMA (39). When the proteins are hydrolyzed, free methylarginines appear in the cytosol. PRMTs are distinguished as type-I and type-II. Type-I catalyze the formation of ADMA, whereas type-II catalyze symmetrical dimethylation of arginine to form Symmetric dimethylarginine (SDMA). Both types lead to formation of L-NMMA (40). ADMA and L-NMMA are inhibitors of NOS, but SDMA is not a NOS inhibitor (6).

Type-1 PRMTs (41), are widely distributed throughout the body (42), and protein arginine methylation has been implicated in many processes, including RNA/protein interactions, transcriptional regulation, DNA repair, protein localization, protein-protein interaction, signal transduction and recycling or desensitization of receptors. There is limited evidence that elevated plasma levels of ADMA are due to increased methylation of arginine residues, however. Rather, plasma ADMA levels are mostly determined by the rate of elimination.

Elimination of ADMA

ADMA is eliminated by both renal excretion and metabolic degradation. ADMA metabolism is mediated by DDAH. Since DDAH metabolizes ADMA and regulates plasma levels of ADMA, it can directly influence NO production by preventing ADMA inhibition of NOS activity (39).

Humans generate approximately 300mmol of ADMA per day (approximately 60 mg) (44). Of this amount, approximately 50*m*mol/d is excreted in the urine (45). Therefore, ADMA

accumulates in patients with renal failure (45). Kidney transplantation normalization of SDMA is mediated largely by DDAH (46). Earlier studies of DDAH suggested that DDAH1 predominates in tissues containing neuronal NOS, whereas DDAH2 is more prevalent in tissues expressing endothelial NOS (47). However, more recent studies, using more specific antibodies and DDAH1 knockout models, have indicated that DDAH1 is highly expressed in tissues that express eNOS, such as the lung and vasculature (6). The elevation in plasma ADMA that occurs with vascular disease is believed to be due to impaired activity of DDAH (48). Current data indicates that ADMA is eliminated by both renal excretion and metabolic degradation by DDAH1, and that DDAH1 activity in particular, plays the predominant role in eliminating ADMA and L-NMMA (6).

2.5. Protein arginine methyltransferases (PRMTs) in regulating ADMA production

Protein arginine residues are methylated by a family of proteins known as PRMTs. Upon proteolysis of these methylated proteins ADMA and L-NMMA are released into the cytoplasm where they inhibit NO generation by NOS (49). To date, ten mammalian isoforms of the PRMT family have been identified. In mammalian cells, PRMTs have been classified into type I (PRMT-1. -3, -4, -6 and -8) and type II (PRMT -5, -7, and FBXO-11), based on their specific catalytic activity. The enzymatic activity of PRMT -2 and PRMT -9 is unclear (50). Type-I and type-II PRMTs both catalyze the formation of L-NMMA from L-Arginine. In a second step, type-I PRMTs produce ADMA while type-II PRMTs catalyze the formation of SDMA (51, 52). As with other post-translation modifications such as phosphorylation, arginine methylation regulates protein activity. Over the last 40 years, arginine methylation has been extensively studied in prokaryotes and eukaryotes. These efforts have established a pivotal role for arginine methylation in the regulation of transcription, RNA metabolism and protein-protein interactions which thereby influence cellular differentiation, proliferation, survival, and apoptosis (51).

The catalytic activity of PRMTs is characterized by the transfer of a methyl group from S-adenosylmethionine (SAM) to the guanidine nitrogen of arginine (52). Glycine-arginine-rich motifs on proteins are preferential targets for methylation by the majority of PRMTs (53). PRTM-4 and PRMT-5 methylate arginine residues with proline-, glycine, or methionine-rich domain (54). Transfer of one methyl group results in the formation of MMA and transfer of two methyl groups can result in production of ADMA or SDMA. Although protein-arginine methylation has not been shown to be reversible, the Jumonji

domain-containing 6 protein (JMJD-6) has been shown to demethylate histone-arginine residues (55). In addition, prior to proteolysis, protein-incorporated MMA can be converted to citrulline by peptidylarginine deiminase 4 (PAD) (56). LSD-1 is potentially an enzyme that is capable of demethylating protein-arginine residues. LSD-1 has been shown to demethylate histone-lysine residues although it is unclear if it has arginine demethylation activity (57). PRMTs are ubiquitously expressed, however, gene-splicing may allow for tissue specific expression (58). Two isoforms of PRMT have been identified as essential for embryonic development. PRMT-1 is necessary for early post implantation development and PRMT-1 knock-out mice die at approximately embryonic day 6.5 (59). Pawlak et al. also showed that PRMT-1 is responsible for over 85% or total PRMT activity in embryonic stem cells. PRMT-4/CARM-1 knock-put mice die at birth and have disrupted estrogen-responsive gene expression (60).

The activity of PRMT has been found to be regulated by binding of non-substrate proteins. Binding of BTG-1 and BTG-2/TIS-21 has been found to increase activity of PRMT-1 (61). PRMT-3 activity is inhibited by binding of the tumor suppressor DAL-1 (62). PRMT-1 has the ability to form homodimers and deletion of the protein domain facilitating dimerization results in loss of PRMT-1 enzymatic activity (63).

PRMT expression levels can be altered in various disease states. Chen et al. noted increase levels of PRMT-1 protein in diabetic rat retina which was reversed by administration of telmisartan (64). This study also found that exposure of bovine retinal capillary endothelial cells to high glucose causes increased level of ROS production suggesting a possible role of ROS mediated PRMT-1 expression. Exposure of human umbilical vein endothelial cells (HUVECs) to fluid shear stress of > or =15 dyne/cm^2

resulted in a two fold increase in expression of PRMT-1 mRNA via activation of the nuclear factor kappaB pathway (65).

2.6. The critical role of DDAH1 in ADMA degradation

DDAH plays a major role in ADMA degradation. A detailed study of the metabolic fate of ADMA and SDMA in rats confirmed this early idea (12). The excretion of analogous metabolites of ADMA and SDMA indicated a common catabolic pathway for both dimethylarginines. However, there appeared to be an additional pathway that specifically metabolized ADMA. This was demonstrated by the identification of metabolites, mainly citrulline, in the tissue samples and plasma of C-ADMA but not C-SDMA injected rats. The enzyme responsible for this specific pathway was subsequently purified from rat kidney and called DDAH (66), it is now known as DDAH1.

The first evidence that DDAH1 regulates of the NOS pathway came from observations using the DDAH inhibitor, 4124W. Addition of 4124W to an isolated vascular segment induces a gradual vasoconstriction which is reversed by addition of L-arginine to the medium (67). This finding is consistent with the view that ADMA competes with arginine for NOS, is constantly being produced in the course of normal protein turnover and is degraded by DDAH1.

Impairment of DDAH activity is a central mechanism by which cardiovascular risk factors disrupt the NOS pathway. The activity of DDAH is impaired by oxidative stress, which is induced by a wide range of pathological stimuli including oxidized LDL, cholesterol, inflammatory cytokines, hyperhomocystinemia, hyperglycemia, and infectious agents.

These insults inhibit DDAH activity in vitro and in vivo (68). The sensitivity of DDAH to oxidative stress is conferred by a critical sulfhydryl in the active site of the enzyme that is required for the metabolism of ADMA. The sulfhydryl can also be reversibly inhibited by NO in an elegant form of negative feedback (69). Homocysteine mounts an oxidative attack on DDAH to form a mixed disulfide, inactivating the enzyme (68). By oxidizing a sulfhydryl moiety essential for DDAH activity, homocysteine and other risk factors cause ADMA to accumulate and to suppress NOS activity.

In apolipoprotein E-deficient mice, hypercholesterolemia is associated with increased levels of plasma ADMA and impaired angiogenesis (70). The effect of ADMA on angiogenesis can be reversed by administration of L-arginine. This data supports previous observations indicating a critical role of endothelium-derived NO in angiogenesis (70). The role of ADMA in modulating angiogenesis was strengthened by the finding that C6 glioma cells genetically engineered to overexpress DDAH resulted in tumors that were more vascular and grew faster than tumors from wild type cells (71). Expression of DDAH can also be increased by exposing endothelial cells to retinoic acid. The effect is associated with reduced accumulation of ADMA and increased endothelial cGMP levels (72).

In experimental models of pulmonary hypertension, a reduction in pulmonary DDAH activity or expression is associated with an increase in plasma ADMA levels and reduced pulmonary NO synthesis. A reduction in DDAH activity could explain elevated plasma ADMA levels and L-arginine responsiveness in patients with pulmonary hypertension (73). These above studies indicate that DDAH and plasma ADMA levels are important for the regulation of NO synthesis.

Global DDAH1 deletion accumulated ADMA and loss of homeostasis

Hu et al (6) provided strong evidence that DDAH1, rather than DDAH2 is largely responsible for the degradation of ADMA. Our group generated a murine model of global DDAH1 knockout (DDAH1$^{-/-}$) by targeting exon 4 of the DDAH1 gene. The DDAH1$^{-/-}$ mice displayed normal developmental features while showing negligible DDAH activity in kidney, brain, and lung tissues. The abrogation of DDAH enzymatic activity was surprising because expression of the DDAH2 was unaffected. The expression of endothelial NOS, protein arginine methyltransferases 1 and 3, and cationic transporter were also unaffected. With the loss of DDAH activity there were significant elevations in tissue and plasma ADMA and L-NMMA.

In support of a role for DDAH1 in regulating endothelial function, isolated aortic rings from the DDAH1$^{-/-}$ mice manifested impaired endothelium dependent vasodilation in response to acetylcholine, consistent with ADMA induced suppression of NOS. These animals also exhibited a significant increase in blood pressure that was reversed by infusion of L-arginine, consistent with the competitive inhibition of NOS by ADMA (6). Most importantly, tissues obtained from DDAH1 KO mice are unable to degrade ADMA and L-NMMA even the DDAH2 protein expression in these tissues are unaffected (6), indicating that DDAH1 is essential for ADMA and L-NMMA degradation. Consistent with the critical role of DDAH1 in ADMA degradation, ADMA content was not affected by selective DDAH2 gene silencing in cultured cells or in vivo (6).

ADMA plays an important role in the regulation of vascular tone by acting as an endogenous inhibitor of NO synthesis. By inhibiting NO synthesis, plasma ADMA may reduce vascular compliance, increase vascular resistance, and limit blood flow. Furthermore, plasma ADMA may promote atherogenesis as it opposes the vasoprotective effects of NO. Thus, elevations in plasma ADMA may accelerate the progression of atherosclerosis and increase the risk of cardiovascular events.

In summary, DDAH1 is essential for degradation of endogenous NOS inhibitor ADMA, and is thus a critical regulator of endothelial NO production. DDAH1 reduces blood pressure, and would be anticipated to reduce adverse cardiovascular outcomes, particularly in diseases such as pulmonary hypertension where vascular resistance is a primary cause and increased ADMA levels are a defined risk factor. The research is therefore designed to determine the role of DDAH1 in development and progression of PAH and subsequent right ventricular heart failure.

2.7. SU5416 in PAH model generation

Vascular endothelial growth factor (VEGF) is abundantly expressed in the normal lung (74) and has a prosurvival and antiapoptotic role in endothelial cells (EC). SU5416, 3-(3,5-dimethyl-aH-pyrrol-2ylmethylene)-1, 3-dihydroindol-2-one is a selective and potent small molecule inhibitor of the VEGF Receptor 2 (VEGFR2) tyrosine kinase. It has been shown to inhibit VEGF dependent EC proliferation in vitro and in animal models (75, 76), has shown broad in vivo antitumor activity (77) and was the first VEGFR 2 inhibitor to enter clinical development for cancer therapy. Utilized to inhibit tumor growth by limiting angiogenesis, SU5416 was well tolerated, and showed initially promising results in phase I trials in patients with terminal cancers (78). However, expanded phase III trials did not find a statistically significant clinical benefit, and further development of this drug for clinical purposes was discontinued. Nevertheless, SU5416 has continued to be used in research as a way to perturb endothelial cell growth.

Kasahara et al. (79) developed a rodent model of inflammation independent emphysema based on VEGF receptor blockade. This model provides an alternative explanation for emphysema based on the hypothesis that a failure of the lung VEGF receptor signaling may significantly contribute to the unique characteristics of pulmonary emphysema (79). Evidence that lung airspace enlargement in newborn mice treated with a soluble VEGF receptor (80) or lung specific deletion of VEGF using Cre-Lox approach (84) support the data obtained with this model (79). The role of apoptosis in the lung damage observed in emphysema is increasingly being recognized. Emphysema triggered by the VEGF receptor blocker SU5416, which is characterized by the presence of apoptotic alveolar septal cells, is prevented by a broad spectrum caspase inhibitor (79). Moreover, Tuder et

al. (82) demonstrated that a superoxide dismutase mimetic protects against the development of apoptosis and emphysema induced by SU5416 thus suggesting that VEGF receptor blockade triggers lung oxidative stress, which is causally involved in alveolar septal cell death in this emphysema model.

A decade ago, Taraseviciene-Stewart et al. (83) showed that VEGF receptor blockade with the VEGFR-1/VEGFR-2 antagonist SU5416 combined with chronic hypoxia resulted in severe angioproliferative pulmonary arterial hypertension (PAH) with neointimal changes in adult rats. Although classic animal models of pulmonary hypertension (that is, the monocrotaline and hypoxic models) do not form obstructive intimal lesions in the peripheral pulmonary arteries, the SU5416 models has shown pulmonary arterial changes resembling plexiform lesions. Moreover, a recent report clearly demonstrates that severe pulmonary hypertension in a very late stage of the SU5416/hypoxia/normoxia exposed rat is accompanied by the formation of plexiform like lesions that are indistinguishable from the pulmonary arteriopathy of human pulmonary arterial hypertension (84). The finding that SU5416 promotes plexiform lesions, which is a endothelial hyperproliferative disorder is rather surprising, given that this drug inhibits endothelial cell growth and angiogenesis. However, as described below, the suspected mechanism SU5416 induced plexiform lesions makes this drug highly useful for understanding pathology and treatment of PAH. (85-89).

The SU5416 model and rodent models of PAH

Tuder et al. (90) demonstrated immunohistochemically and via in situ hybridization that the EC in the plexiform lesions, not in the normal vasculature, express mRNA and protein for VEGF (the survival factor for EC) and VEGFR-2, thus suggesting that the formation of these lesions in PAH involves a process of disordered angiogenesis. Moreover, in PAH, the population of lung EC expands in a monoclonal pattern (91), and these EC contain an inactivating mutation of the transforming growth factor receptor II (92). Therefore, Taraseviciene-Stewart et al. (83) postulated that the occlusive neointimal lesions increase from a process of dysregulated angiogenesis that has several features in common with that seen in neoplastic processes. They used SU5416 to treat the rodent model of mild to moderate pulmonary hypertension under the chronic hypoxia. The results unexpectedly showed that in chronically hypoxic rats, SU5416 causes pulmonary arterial EC death, followed by obliteration of the precapillary arterial lumen by the proliferating EC, which is associated with a severe, irreversible PAH (83). Moreover, the effect of the VEGF receptor blockade could be reversed by inhibitors of apoptosis, suggesting that increased apoptosis of EC in response to the loss of survival signaling creates conditions favoring the emergence of apoptosis resistant cells with increased growth potential. Importantly, in this model, it was shown that chronic hypoxia plus VEGF receptor blockade caused severe pulmonary hypertension, which persisted, and even progressed, after the animals were no longer being subjected to the hypoxic stimulus. Moreover, the defining pulmonary vascular alteration, arterial occlusion by proliferating ECs, was not reversible upon re-exposure to normoxia and removal of SU5416 (83).

This model of severe PAH was therefore considered to be useful for better addressing the etiological mechanisms involved in the hyperproliferation of EC that characterizes the plexiform lesions of human PAH (83, 84).

In contrast to the SU5416 model, other classical rodent models of mild to moderate pulmonary hypertension, (i.e. the chronic hypoxia and monocrotaline models) lack clustered proliferating EC in the lumen of the pulmonary arteries (93, 94). In these models, the defining pulmonary vascular alteration, medial muscular thickening of the proliferating SMC, is potentially reversible upon re-exposure to normoxia or with the passage of time after monocrotaline injection (93, 95, 96). Together, these rat models offer the perspective that medial muscular thickening due to proliferating SMC may be reversible, while arterial occlusion by proliferating EC appears to be irreversible (97).

Together, the literature suggests that the pathological features of the SU5416 PAH model is currently the most appropriate small animal model available for investigating development and treatment of PAH.

3. Meterials and Methods

The central aim of the study is to test the hypothesis that DDAH1 plays an important role in attenuating PAH through degrading ADMA. We have engineered novel global DDAH1 knockout (global DDAH1 KO) mice (6, 98), and cardiomyocyte specific DDAH1 knockout mice (cardio DDAH1 KO) mice to study the effects of DDAH1 on PAH and RV hypertrophy.

3.1. Experimental Animals

We used C57BL mice, global DDAH1 KO mice, and cardio DDAH KO mice as control and hypoxia+SU5416 groups. C57BL mice are one of the most widely used inbred strains. Mice were housed in a temperature-controlled ($20^{\circ}C \pm 2^{\circ}C$) environment with a 12-h light-dark cycle, and free access to water and mouse chow provided after weaning at 18 days of age. The Animal Care and Use Program at the University of Minnesota, maintains full accreditation from the Association for Assessment and Accreditation of Laboratory Animal Care, International (AAALAC) and complied with the US Animal Welfare Regulations, the National Research Council (NRC) Guide for the Care and Use of Laboratory Animals, and Public Health Service Policy on the Humane Care and Use of Laboratory Animals. The University of Minnesota has an Animal welfare Assurance on file with the National Institutes of Health's Office of Laboratory Animals Welfare (NIH-OLAW). Training for all personnel involved in animal care is required.

Genotyping Global DDAH1 KO mice

Global DDAH1 KO mice were engineered in our lab by crossing DDAH1$^{flox/flox}$ mice (15) with protamine (Prm)-cre mice (129-Tg(prm-cre)58Og/J, Jackson Laboratory) as we previously reported (6). The DDAH1 gene was deleted in the sperm of the male double heterozygote Prm-cre/DDAH1 flox/+ mice. When these male mice were crossed with wild type female breeders, DDAH$^{+/-}$ mice were generated. The homozygote global DDAH1$^{-/-}$ was generated by inbreeding of the heterozygotes. Polymerase chain reaction was performed for genotyping of the offspring using primer pairs 5'-AAT CTG CAC AGA AGG CCC TCA A-3' and 5'-GGA GGA TCC ATT GTT ACA AGC CCT TAA CGC-3' for the wild type allele and 5'-TGC AGG TCG AGG GAC CTA ATA ACT-3' and 5'-AAC CAC ACT GCT CGA TGA AGT TCC-3' for the knockout (KO) allele.

Generation of Cardio-DDAH1 KO mice

Our lab also generated an inducible cardiomyocyte specific DDAH1 KO strain by using the strategy described in Figure 1. Briefly, adult α-MHC^{MerCreMer} mice, which express a tamoxifen inducible Cre specifically in cardiomyocytes, were crossed with DDAH1$^{flox/flox}$ mice to generate DDAH1$^{flox/flox}$/α-MHC^{MerCreMer}. DDAH1$^{flox/flox}$ mice were used as controls, and are designated as WT for convenience. DDAH1$^{flox/flox}$/α-MHC^{MerCreMer} mice have normal cardiac structure and function during unstressed conditions as compared with either DDAH1$^{flox/flox}$ or α-MHC^{MerCreMer} mice. DDAH1$^{flox/flox}$/α-MHC^{MerCreMer} and DDAH1$^{flox/flox}$ were given 4-hydroxytamoxifen (4-HOT, Sigma) in peanut oil at 20mg/kg per day for 12 injections (i.p.).

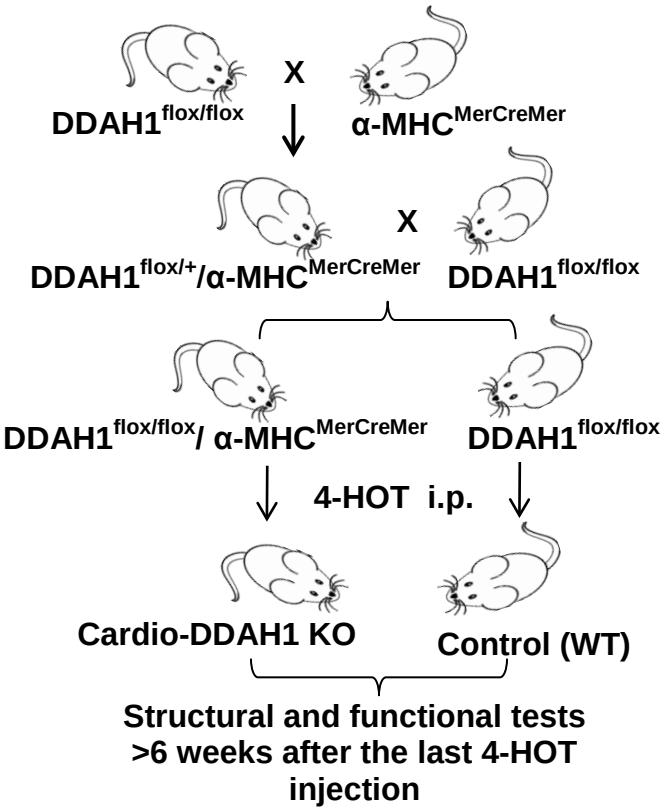

Figure 1. Generation of Cardio-DDAH1 KO mice.

3.2. Experimental protocols and procedure

Global DDAH1 KO, Cardio DDAH1 KO, and C57BL mice were exposed to 2 different conditions as described in Table 1 below. For Sugen 5416 (SU5416) treated mice, the mice in the hypoxia group received subcutaneous weekly injection of SU5416 (25mg/kg, R&D System). Sham group was given vehicle injections. For hypoxia treatment, mice were gradually acclimatized in a hypobaric chamber to hypoxia for 1 week and then maintained at a simulated altitude of 18,500 feet (10% oxygen) for 2 more weeks (figure 2). The chamber was opened once every week for cleaning, feeding, and injection. Animals were monitored daily by our investigators including weekends. After hypoxic exposure for a total of 3 weeks, determination of RV pressure and hypertrophy was performed as described. The mice in the sham group were kept in normobaric conditions for 3 weeks, followed by determination of RV pressure. Heart and lung from all experimental groups were then quickly extracted, weighed, snap frozen in liquid nitrogen and stored at -80°C until analyses.

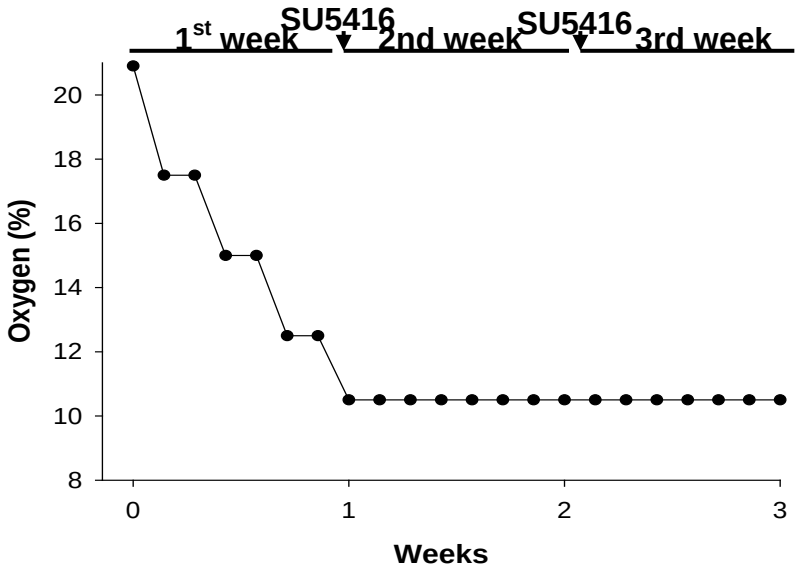

Figure 2. Protocol for hypoxia+SU5416-induced pulmonary arterial hypertension

Table1. Experimental groups.

	A. Sham	**B. Hypoxia + Sugen 5416**
Aim-1	1. Wild type 2. Global DDAH1 KO	3. Wild type 4. Global DDAH1 KO
Aim-2	5. Wild type 6. Cardio-DDAH1 KO	7. Wild type 8. Cardio-DDAH1 KO

Sugen 5416 was given at a dose of 25mg/kg/week in each mouse (for Group-B).

The hypoxia (Group-A) was given vehicle injections. N=12 each group.

3.3. Measurements

Right ventricle catheterization

RV pressure was determined with a 1.2F pressure transducer. RV systolic pressure, RV diastolic pressure, RV dP/dt max and negative dP/dt min were determined during continued anesthesia (15, 99, 100, 101). Mice were first anesthetized with 2% isoflurance and intubated with 20-gauge Teflon tube attached to MiniVent type 845 mouse ventilator (Hugo Sachs Elektronik). A 1.2F pressure catheter (Scisense Inc., Ontario Canada) was introduced through the right common carotid artery into the ascending aorta for measurement of systolic and diastolic blood pressures as described previously (99, 100). For RV hemodynamics, open-chest RV catheterization was performed during anesthesia with 2% isoflurane. Data were collected when steady state was reached (102). The catheter was then advanced into the pulmonary artery for measurement of pressures.

Sample preparation for ADMA and L-NMMA measurement

After the final hemodynamic assessment, the mice were euthanized by exsanguination, and heart, lung, and other major organs were flushed with flushed with PBS and harvested. Lung weight was determined and the left lung was snap-frozen in liquid nitrogen for biochemical analysis. The airways of the top right lobe were perfused with PBS and then fixed in 10% buffered formalin for histological analysis. The blood samples were collected for plasma levels of ADMA, L-arginine, and L-NMMA. The wet weight of RV and of left ventricle (LV) + septum (S) was weighed and the ratio of RV weight to LV+S was calculated as an index of RV hypertrophy (102, 103, 104).

Tissue Homogenization for Western Blots

Lung tissue was minced into fine pieces, weighed and suspended (26:1 v/w) in ice-cold complete lysis buffer A (pH=7.4) comprised of the following: 10 mM HEPES, 350mM NaCl, 20% glycerol, 1% Igepal-CA630, 1mM $MgCl_2$, 0.1 mM DTT, 0.1mM EGTA, and protease inhibitor cocktail (Roche Applied Science). Each lung was homogenized in a PowerGen homogenizer (Fisher Scientific; Waltham, MA) at 4^{o}C. The homogenates were first centrifuged (4^{o}C) for 10 min at 3,000g, and supernatant was separated from the pellet. The supernatant was centrifuged (4^{o}C) for 15 min at 10,000g to obtain the soluble fraction. The nuclear fraction was isolated using this pellet re-suspended by complete lysis buffer B containing the following: 20 mM HEPES, 350 mM NaCl, 10% glycerol, 1 *m*M $MgCl_2$, 0.1 *m*M DTT, and protease inhibitor cocktail (Roche Applied Science) and centrifuged again for 30 min at 12,000g. The supernatant of this fraction contains nuclei. Protein concentration was measured using Spectronic Genesys 5 spectrophotometer (Milton Roy) at 562 nm absorbance.

Procedure for Western Blots

Protein levels were measured by Western blot analysis. Separating gel (375 *m*M Tris-HCl; pH=8.8, 0.4% sodium dodecyl sulfate (SDS); 10% acrylamide) and stacking gel (125 *m*M Tris-HCl; pH=6.8; 0.4% SDS; 10% acrylamide monomer) solutions were made, and polymerization then was initiated by N,N,N',N'– teramethylethylene diamine (TEMED) and ammonium persulfate (APS). Separating and stacking gels were then quickly poured into a gel-box (Hoefer Inc, Holliston, MA). Twenty μg of protein from lung homogenates in sample buffer (100 mM Tris-HCl, pH=6.8, 2% SDS, 30 *m*M dithiothreitol, 25% glycerol) was then loaded into the wells of the 10% SDS-PAGE gels, and electrophoresed at 40V for overnight. The gels were then transferred at 60V for 6 hours onto a nitrocellulose membrane (Bio-Rad, Hercules, CA). Membranes were blocked in 3% nonfat milk in PBS with 0.1% Tween-20 for 1 hour. After blocking, membranes were incubated in 5% bovine serum albumin (BSA) at 4^{o}C overnight with the appropriate primary antibodies: eNOS (1:1000, BD Biosiences), DDAH-1 (1:800,Lifespan Biosciences), DDAH-2 (1:800, Santa Cruz Biotechnology), CAT (1:1000, Santa Cruz Biotechnology), PRMT-1(1:1000, Santa Cruz Biotechnology), and PRMT3 (1:600, Sigma-Aldrich). Following three washes in PBS with 0.4% Tween-20, membranes were incubated with horseradish peroxidase- conjugated secondary antibodies in 3% nonfat milk at room temperature for 120 min. Following three washes in PBS with 0.4% Tween-20, an enhanced chemiluminescence (ECL) detection system (Amersham, Piscataway, NJ) was used for visualization. Densitometry and quantification were performed using a Kodak film cartridge, a scanner interfaced with a microcimpter, and the NIH Image J Analysis software program. To ensure equal loading of protein, Ponceau-S-staining was

performed for each membrane. Membranes were stripped and reprobed for B-actin (1:500, Sigma) and Vinculin (1:1000, Santa Cruz Biotechnology) as loading controls.

Determination of tissue ADMA, L-NMMA, SDMA, and L-arginine

Lung ADMA, L-NMMA, SDMA, and L-arginine levels were determined using a high-through put liquid chromatographic-tandem mass spectrometric method (6, 15, 105).

Briefly, For ADMA, bromcyan-agarose (0.4g) was suspended in 10 ml of 1 *m*M HCl in methanol and incubated for 30 min at room temperature. After incubation, the mixture was filtered and washed five times with 5 ml of 1 *m*M HCl and 5 ml of water. To prepare a copper-ornithine-complex, 0.125 g was dissolved in 1.25 ml of water. Small amounts of CuCo3 were added until a blue color was obtained. After filtration of the solution the filtrate was brought to pH 10 with 10 M KOH. The washed bromcyan agarose was suspended in 1.25 ml of the copper ornithine complex and was shaken overnight at 4 ^{o}C. The next day the suspension was filtered and washed one time with 1 M HCl and ten times with 10 ml water. The ornithine bromcyan agarose was then suspended in a 20 % solution of dimethylamine in water and stirred for 24h at 50^{o}C. The suspension was filtered and washed two times with 10 ml of water. The filtrate together with the washings was concentrated to dryness in a vacuum to remove any remaining dimethylamine. The residue was dissolved in water again and concentrated to dryness in vacuum for a second time. The final residue was dissolved in water to yield a stock solution which was stored at -20 ^{o}C.

Arginine levels were analyzed as described for ADMA with the following modifications: [13C5] ornithine HCl was used instead of [2H6] ornithine HCl to prepare the copper

ornithine complex, and the ornithine bromcyan agarose was suspended in a 20 wt.% solution of dimethylamine. Purity and identify of ADMA was assessed by HPLC and LC-MS. Briefly, fluorescenece (RF2000 fluorescence detector, Dionex, Germering, Germany) was detected as previously described after solid phase extraction (SPE) with carboxylic acid (CBA) cartridges, online o-phthaldehyde (OPA) derivatisation, and separation on a phenyl column from Macherey-Nagel (Duren, Germany), at excitation and emission wavelengths of 340 and 453 nm, respectively, Mass spectra were generated by direct injection without prior chromatography.

Lung DDAH activity was determined as previously described (6, 105).

Briefly, Lung tissue samples (20 mg frozen tissue per determination of DDAH activity from a single organ) were homogenized in PBS buffer with protease inhibitor as described above to minimize possible interference by endogenously released ADMA. The homogenate was centrifuged in a pre-cooled (4^{o}C) centrifuge for 5 min at 12,000 × g. For the DDAH activity assay 50 µl aliquots of the resulting supernatant were added to 50 µl aliquots of PBS buffer containing 20 µM ADMA and incubated for 60 min at 37^{o}C. Reactions were stopped and ADMA was determined as described above. Enzyme activity was calculated as follows using an incubation time of 60 min.

Quantification unlabeled and stable-isotope labeled L-arginine, ADMA and SDMA was performed by LC-tandem MS by a modification. All compounds were analyzed as their butyl ester derivatives. Derivatization was performed in 96 well u shaped 96 well polypropylene plates. After addition of 100 µl of 1 M HCl in 1-butanol, plates were sealed with aluminum foil and u shaped 96 well polyprophlene plates were heated at 65^{o} C on a 96 well aluminum block for 30 min. For evaporation, aluminum seal was removed and open plates were heated at 85 ^{o}C for 30 min. After evaporation of the derivatization

reagent, samples were reconstituted in 100 µl aliquots of methanol water, 50:50 (v/v) containing 0.1 wt.% ammonium formate, pH 4. The pH was adjusted with formic acid. Afterwards, polypropylene plates were transferred to an autosampler (HCS CombiPAL, CTC Analytics, Switzerland), and 10 µl aliquots were injected onto the chromatographic column for each sample.

LC- tandem MS analyses were performed on a Varian (Palo Alto, CA, USA) 1200L Triple Quadrupole MS equipped with two Varian ProStar model 210 HPLC pumps. Separation of analytes from major matrix was achieved with a Chirobiotic T (20mm × 1.0 mm i.d.) microbore guard column packed with teicoplanin covalently bonded to 5 µm particle size spherical silica. Acetonitrile containing 0.1 wt.% ammonium formate water containing 0.1 wt.% ammonium formate, pH 4 (60:40 v/v), served as isocratic eluent at 28^{o}C, with a flow rate of 0.2 ml/min. Nitrogen was used as the nebulzing and drying gas (380^{o}C) at 90 and 180l/h, respectively, For ionization in the positive electrospray ionization (ESI^{+}) mode the needle and shield voltage were set at 5600 and 400 V, respectively.

Histological analysis

Comprehensive histological analysis was performed to determine pulmonary vessel muscularization, fibrosis, and cardiac hypertrophy.

Sample preparation for histological staining

Sample cross-sections were cut (5 μm thick) from the middle portion of lung tissues in a microtome (Leica Biosystems, Buffalo Grove, IL), placed on slides in tissue float bath at 40^{o}C , and incubated overnight at 37^{o}C. The sections were deparaffinized as following steps before stained; 1) Immerse slides in xylene for 5 min. 2) repeat once in fresh xylene for 5 min. 3) immerse slides in 100% ethanol for 5 min in two times. 4) immerse slides in 95% ethanol for 5 min in two times. 5) immerse slides in 70% ethanol for 5 min in two times. 6) immerse slide in 1X PBS for 5 min.

Determination of lung vascular muscularization

For the relative muscularization of pulmonary arterioles, the cross-sections were stained with Hematoxylin, Mayer's (Lillie's modification) and incubated for 5 minutes. Hematoxylin stains a bluish-purple color for smooth muscle cell and mitochondria, while nuclei stain dark blue. Stained sections were rinsed in 2 changes of distilled water to remove excess stain and Eosin Y solution (Modified Alcoholic) were applied for 3 min. Stained sections were rinsed in 3 changes of absolute alcohol before mounting with Vectamount medium (Vector Laboratories). Lung artery muscularization images were visualized and captured using a Zeiss Axio-series microscope and software at a magnitude of 20X. Briefly, in each mouse, 60 intra-acinar arteries (50-200 μm) were

examined and categorized as nonmuscular (NM), partially muscular (PM) or fully muscular (FM). The relative percentage of NM, PM, and FM arteries were calculated (99, 100, 102).

Determination of lung fibrosis

For Lung fibrosis, the tissue sections were stained using Masson's Trichrome Stain Kit from Scy Tek Laboratories. Briefly, the sections were placed in preheated Bouin's Fluid in a water bath at 56^{O} – 64^{O} C in a fume hood and then placed in preheated Bouin's Fluid for 60 min followed by a 10 min cooling period. The slides were rinsed in tap water until sections were completely clear and then equal parts of Weigert's (A) and Weigert's (B) were applied and the slides were stained with working Weigert's Iron Hematoxylin for 5 min. The sections were rinsed in running tap water for 2 min and Biebrich Scarlet/Acid Fuchsin Solution was applied to the slides for 15 min and then rinsed in distilled water. The sections were differentiated in Phosphomolybdic/Phosphotungstic Acid Solution for 15 min until the red collagen stain is visible. Without rinsing, Aniline Blue Solution was applied to sections for 10 min and then rinsed in distilled water. Finally, Acetic Acid Solution (1%) was applied for 5 min and then dehydrated in 2 changes of 95% Alcohol, followed by 2 changes of Absolute Alcohol. Percentage tissue fibrosis was calculated as previously described (99, 102, 106, 107).

Measurement of right ventricular fibrosis and cardiac myocyte hypertrophy

Tissue sections from the central portion of the RV were stained with Sirius Red (Sigma) for detection of fibrosis, and FITC-conjugated wheat germ agglutinin (AF488, Invitrogen) to assist in the evaluation of cardiac myocyte size.

Sirius Red staining

Sirius Red staining was performed as follows; 1) Stain in pico Sirius red for one hour. 2) Rinse in two changes of acidified water. 3) Remove most of the water from the slides by vigorous shaking or blotting with damp filter paper. 4) Dehydrate in three changes of 100% ethanol.

Wheat Germ Agglutinin (WGA) staining

For wheat germ agglutinin (WGA) staining, deparaffinized slides were incubated for 1 hour at room temperature with primary antibody against WGA conjugated to FITC (50 µg/ml) in PBS. Slides were washed 3 times in PBS, mounted in Vectashield with DAPI (Vector Labs) and imaged by fluorescence microscopy. The cross sectional area of at least 120 cells/sample (from 5 areas) and at least 4 samples of each group were averaged. The percent volume fibrosis was determined using the method described previously (108).

3.4. Statistical analysis

Data were first analyzed for normal distribution using a normality test (Kolmogorov-Smirnov) provided by SigmaStat. If data were normally distributed, it was presented as mean ± SE (standard error). If the data were not normally distributed, it was presented as median (±SE). Two-way ANOVA was used to test for differences between gene-deficient mice and wild-type mice under control conditions and after hypoxia+SU5416. Comparisons were made with the Tukey method under the interaction term. Statistical significance was defined as $P<0.05$.

4. Results

4.1. Effect of global DDAH1 KO on hypoxia+SU5416-induced PAH and RV hypertrophy

Effect of global DDAH1 KO on changes of body weight after hypoxia+SU5416

The body weight was monitored weekly as presented in Figure 3. There was no significant difference between wild type and global DDAH1 KO mice body weight at 1 week and 2 weeks after hypoxia+SU5416. After 3 weeks of hypoxia+SU5416 however, global DDAH1 KO mice exhibited a slightly higher loss of body weight as compared to WT mice (82.02 ± 0.86 % of starting weight in wild type hypoxia+SU5416 group versus 78.99 ± 0.86 % in global DDAH1 KO hypoxia+SU5416 group; $p<0.05$). The results indicate that hypoxia+SU5416 caused a similar reduction of body weight in both wild type and Global DDAH1 KO mice, with DDAH1 KO being slightly more susceptible to hypoxia+SU5416 induced body weight loss than WT mice.

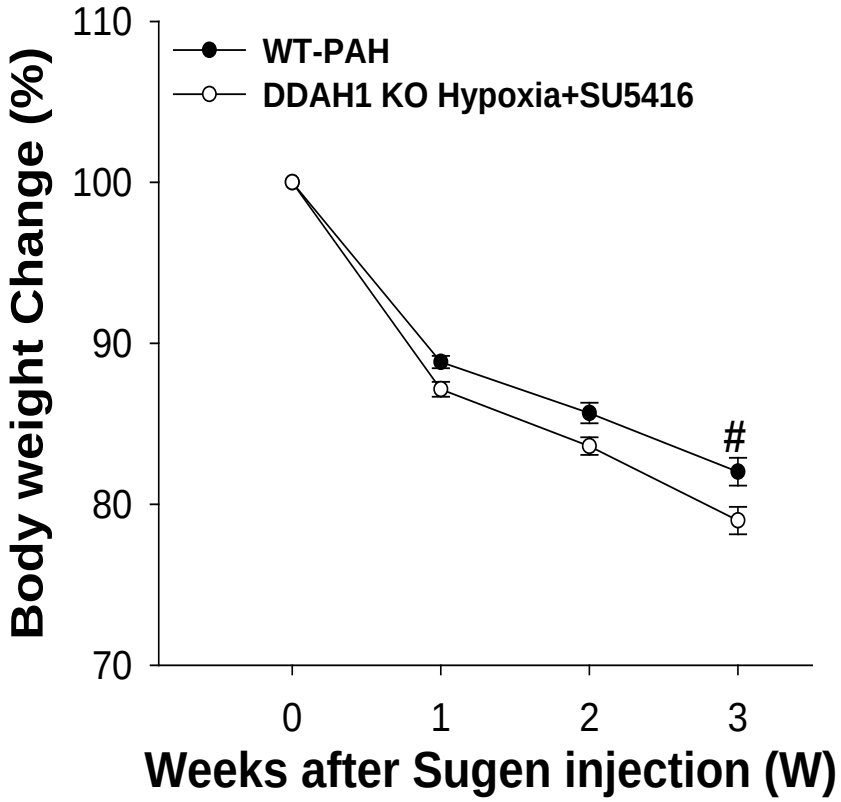

Figure 3. Effect of hypoxia on body weight changes in wild type and global DDAH1 KO mice. Wild type and global DDAH1 KO mice were exposed to hypoxia+SU5416 treatment for 3 weeks and the change (%) of body weight were determined. # indicates $p<0.05$ comparing WT to KO.

Global DDAH1 KO abolished lung DDAH1 expression and DDAH activity.

We determined expression of lung DDAH1 and DDAH2 and total DDAH activity in wild type and global DDAH1 KO mice. DDAH1 expression was undetectable in lungs of global DDAH1 KO mice. DDAH2 expression was unchanged in lungs of global DDAH1 KO mice (Figure 4A). As anticipated, total lung DDAH activity was abolished in global DDAH1 KO mice (Figure 4B).

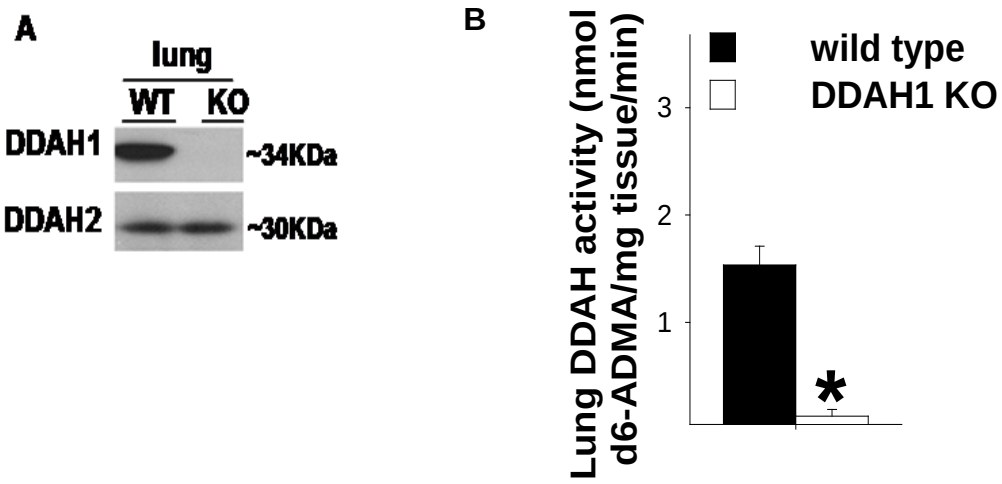

Figure 4. Global DDAH1 KO abolished lung DDAH1 expression and DDAH activity. Representative picture of lung DDAH1 and DDAH2 expression by western blot is presented (A). Lung DDAH activity is presented (B). Data are presented as mean ± SEM. * indicates $p<0.05$ comparing WT to KO.

Global DDAH1 KO impact on hypoxia+SU5416-induced increases of RV pressure

RV pressure was assessed as a surrogate of the pulmonary arterial pressure in wild type and global DDAH1 KO mice under control and hypoxia+SU5416 conditions (Figure 5). RV systolic pressure, RV end-diastolic pressure, RV dp/dtmax, and RV dp/dtmin were not different between wild type and global DDAH1 KO mice under control conditions (Figure 6, Figure 7 and Table 2). However, global DDAH1 KO significantly exacerbated hypoxia+SU5416-induced increases of RV systolic pressure (42.84 ± 1.73 mmHg in wild type hypoxia+SU5416 group versus 48.28 ± 1.18 mmHg in global DDAH1 KO hypoxia+SU5416 group; $p<0.05$) in (Figure 6 and Table 2), RV dp/dtmax (3026.62 ± 166.23 mmHg/s in wild type hypoxia+SU5416 group versus 3475.10 ± 152.54 mmHg/s in global DDAH1 KO hypoxia+SU5416 group; $p<0.05$) , and RV dp/dtmin (-2892.04 ± 232.64 mmHg/s in wild type hypoxia+SU5416 group versus -3179.00 ± 209.62 mmHg/s in global DDAH1 KO hypoxia+SU5416 group; $p<0.05$) (Figure 7 and Table 2). Global DDAH1 KO did not affect RV end diastolic pressure (RV EDP) in mice after hypoxia+SU5416 (Figure 6).

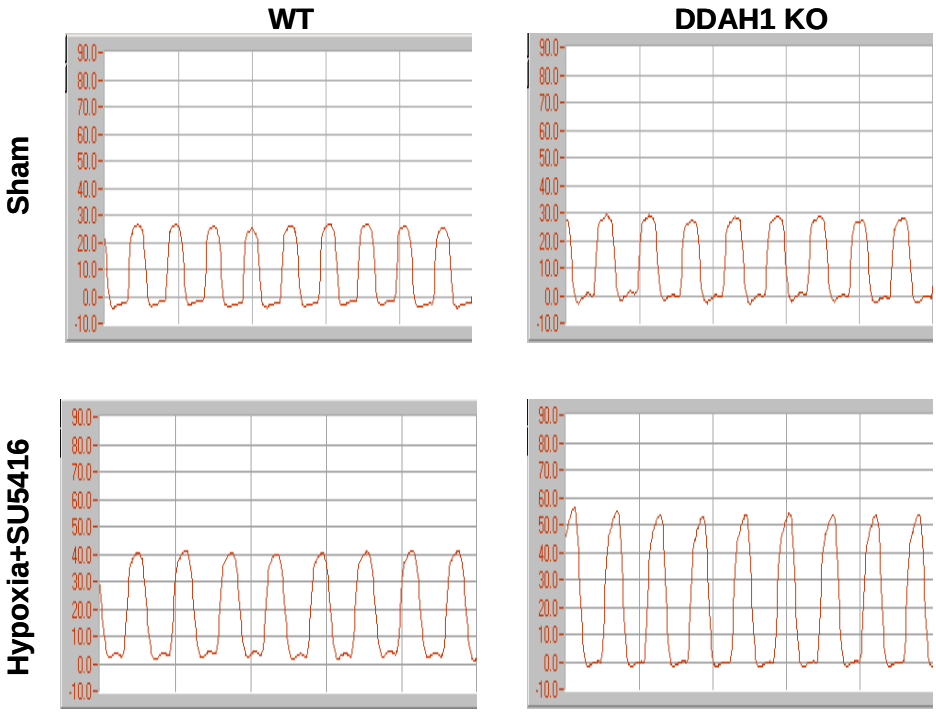

Figure 5. Representative RV pressure tracings from wild type and global DDAH1 KO mice exposed to sham and hypoxia+SU5416 conditions.

Table 2. Hemodynamic data for WT and global DDAH1 KO under sham and hypoxia+SU5416 conditions

Parameters	**WT Sham**	**Global-DDAH1 KO Sham**	**WT Hypoxia+SU5416**	**Global-DDAH1 KO Hypoxia+SU5416**
Number of mice	6	6	9	8
Heart rate (beat/min)	565.83±10.53	551.88±11.13	537.46±17.46	535.82±12.75
RVSP (mmHg)	24.93±1.07	25.19±0.88	42.84±1.73*	48.28±1.18*†
RVEDP(mmHg)	1.35±0.19	1.59±0.29	1.68±0.19	1.89±0.22
RV dp/dt max (mmHg/s)	2508.56±308.79	2537.52±137.81	3026.62±166.23	3475.10±152.54*†
RV dp/dt min (mmHg/s)	-2095.01±334.60	-2351.91±132.89	-2892.04±232.64*	-3179.00±209.62*†

Data are presented as mean ± SEM when normally distributed. *$p<0.05$ as compared with corresponding control conditions; † $p<0.05$ as compared with WT mice under the hypoxia+SU5416 condition.

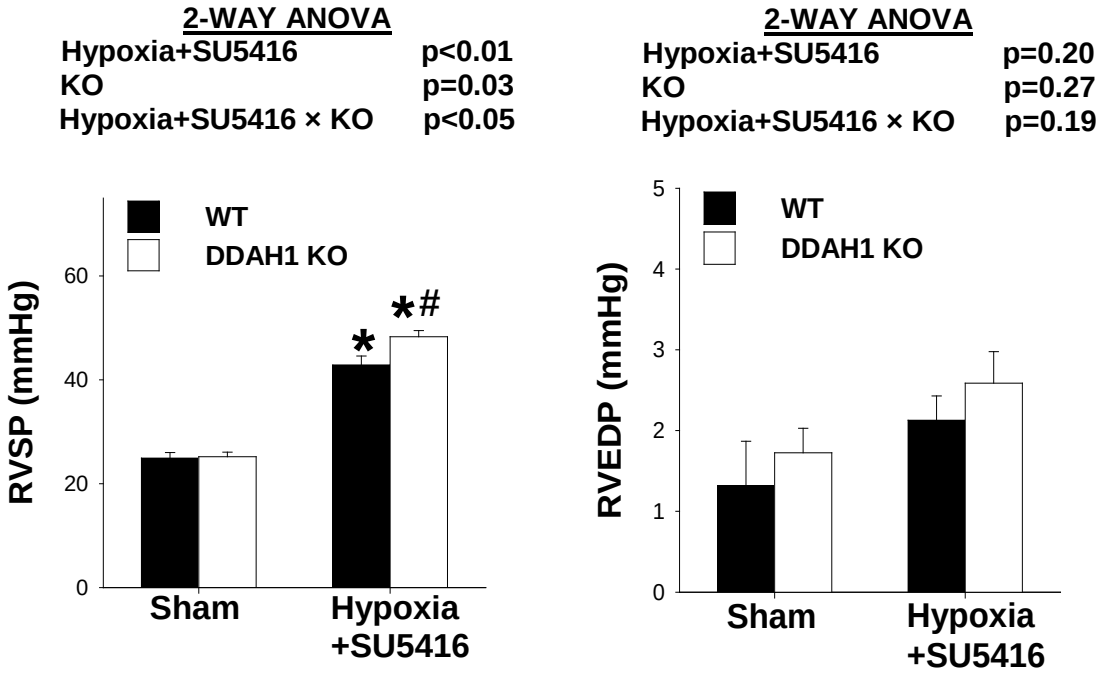

Figure 6. Global DDAH1 KO impact on hypoxia+SU5416 induced increase of RV pressure. RV pressure measurements were obtained by catheterization of right ventricle. RV systolic pressure and RV diastolic pressure were calculated from 7-9 mice in each group. Data were presented as mean ± SEM. * indicates $p<0.05$ comparing hypoxia+SU5416 to sham. # indicates $P<0.05$ comparing WT to KO.

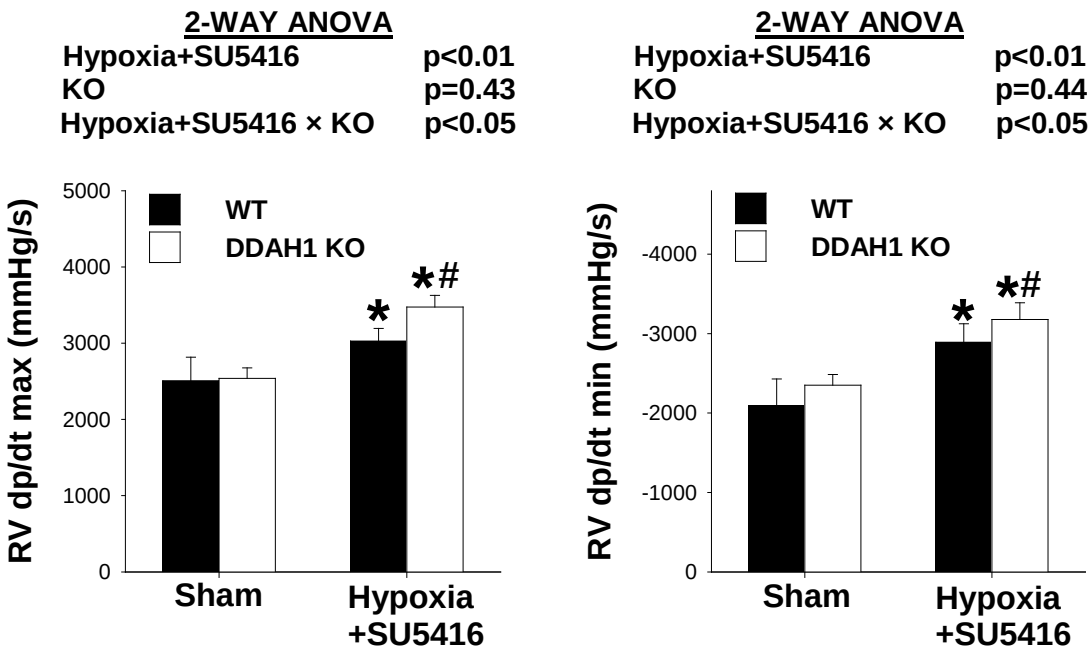

Figure 7. Global DDAH1 KO impact on hypoxia+SU5416-induced increase of RV contractility. RV dp/dtmax and RV dp/dtmin were calculated from 7-9 mice in each group. Data were presented as mean ± SEM. * indicates p<0.05 comparing hypoxia+SU5416 to sham. # indicates P<0.05 comparing WT to KO.

Global DDAH1 KO exacerbated hypoxia+SU5416 induced increases of RV hypertrophy

We measured the RV weight to body weight and ratio of the RV weight to LV (LV + septum) weight to determine RV hypertrophy under control and hypoxia+SU5416 conditions. Global DDAH1 KO had no detectable effect of RV hypertrophy under control conditions as indicated by the similar ratios of RV weight to LV weight between global DDAH1 KO mice and wild type mice, as well as comparable RV weight and RV weight ratios to body weight. Consistent with the greater increase of RV systolic pressure in global DDAH1 KO mice after hypoxia+SU5416, global DDAH1 KO mice exhibited a significantly greater increase of RV to body weight ratio (1.42 ± 0.07 mg/g in wild type hypoxia+SU5416 group versus 1.62 ± 0.04 mg/g in KO hypoxia+SU5416 group; $p<0.05$) and RV to LV (LV + septum) ratio (0.38 ± 0.02 mg/g in wild type hypoxia+SU5416 versus 0.43 ± 0.01 mg/g in KO hypoxia+SU5416; $p<0.05$) compared to wild type mice after hypoxia+SU5416 (Figure 8 and Table 3), indicating that global DDAH1 KO exacerbated hypoxia-induced RV hypertrophy. In addition, Histological analysis indicated that hypoxia+SU5416 increased RV cell size to a greater degree in global DDAH1 KO mice as compared to wild type mice (362.47 ± 10.69 μm^2 in wild type hypoxia+SU5416 group versus 410.81 ± 17.35 μm^2 in KO hypoxia+SU5416 group) (Figure 9 and 10).

Table 3. Anatomic data for WT and DDAH1 KO mice under sham and hypoxia+SU5416 conditions

Parameters	**WT-Sham**	**DDAH1 KO-Sham**	**WT-Hypoxia+SU5416**	**DDAH1 KO-Hypoxia+SU5416**
Number of mice	10	14	22	22
Bodyweight (BW) (g)	33.16 ± 2.56	30.32 ± 0.85	29.11 ± 0.55	29.37 ± 0.49
Tibia length (TL) (mm)	17.56 ± 0.23	17.53 ± 0.09	18.03 ± 0.05	18.33 ± 0.06*
RV weight (mg)	29.07 ± 1.96	27.51 ± 0.57	41.34 ± 2.30*	47.57 ± 1.33*†
LV + septum (mg)	101.75 ± 6.88	95.41 ± 1.78	110.66 ± 3.36	110.96 ± 3.38*
Ratio of RV to LV + septum	0.29± 0.01	0.29 ± 0.01	0.38 ± 0.02*	0.43± 0.01*†
Lung mass (mg)	158.64 ± 7.55	147.27 ± 2.61	213.34 ± 3.36*	222.00 ± 3.63*†
Right atria weight (mg)	3.53 ± 0.17	3.48 ± 0.10	6.39 ± 0.52*	6.48 ± 0.62*
Left atria weight (mg)	4.00 ± 0.20	3.76 ± 0.14	5.34 ± 0.25*	5.36 ± 0.35*
Kidney weight (mg)	378.92 ± 21.38	357.79 ± 16.99	338.48 ± 5.91	356.20 ± 8.61
Ratio of RV to BW (mg/g)	0.89 ± 0.03	0.91 ± 0.03	1.42± 0.07*	1.62 ± 0.04*†
Ratio of LV to BW (mg/g)	3.12 ± 0.15	3.17 ± 0.09	3.80 ± 0.09*	3.78± 0.10*
Ratio of lung to BW (mg/g)	4.93 ± 0.25	4.90 ± 0.15	7.37 ± 0.15*	7.57 ± 0.11*
Ratio of RA to BW (mg/g)	0.11 ± 0.01	0.12 ± 0.01	0.25 ± 0.03*	0.23 ± 0.02*
Ratio of LA to BW (mg/g)	0.13 ± 0.01	0.14 ± 0.01	0.22± 0.02*	0.22 ± 0.02*
Ratio of kidney to BW (mg/g)	11.68 ± 0.52	11.85 ± 0.57	11.67 ± 0.23	12.16 ± 0.28
Ratio of RV to TL (mg/mm)	1.65 ± 0.09	1.57 ± 0.04	2.29 ± 0.13*	2.60 ± 0.07*†
Ratio of LV to TL (mg/mm)	5.77 ± 0.32	5.36 ± 0.09	6.13 ± 0.18	6.06 ± 0.18*
Ratio of lung to TL (mg/mm)	9.01 ± 0.36	8.27 ± 0.14	11.83 ± 0.19*	12.11 ± 0.37*
Ratio of RA to TL (mg/mm)	0.20 ± 0.01	0.20 ± 0.01	0.41 ± 0.04*	0.41 ± 0.29*
Ratio of LA to TL (mg/mm)	0.23 ± 0.01	0.21 ± 0.01	0.30 ± 0.01*	0.29 ± 0.02*
Ratio of kidney to TL (mg/mm)	21.49 ± 0.98	20.03 ± 1.08	18.77 ± 0.32*	19.47 ± 0.47

Data are presented as mean ± SEM when normally distributed. *$p<0.05$ as compared with corresponding sham conditions; † $p<0.05$ as compared with WT mice under the hypoxia+SU5416 condition.

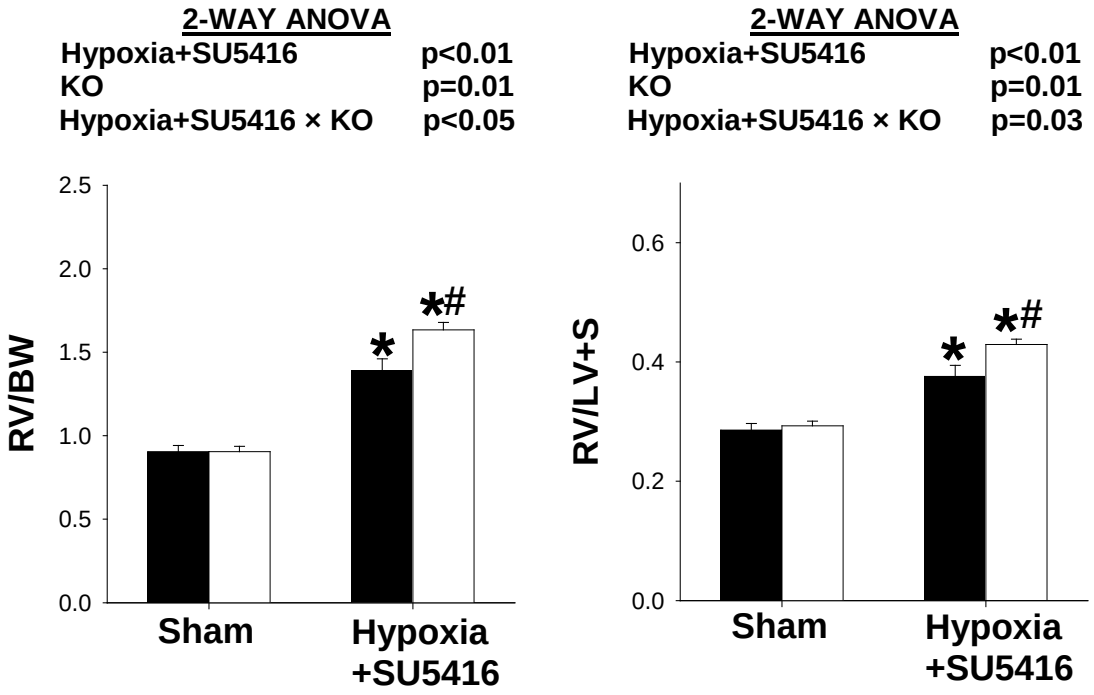

Figure 8. Global DDAH1 KO exacerbated hypoxia+SU5416-induced increase of RV hypertrophy. Hearts were collected. Right ventricle weight to body weight ratio and right ventricle weight to left ventricle + septum weight ratios were calculated from 10 to 22 samples in each group. Data were presented as mean ± SEM. * indicates p<0.05 comparing hypoxia+SU5416 to sham. # indicates P<0.05 comparing WT to KO.

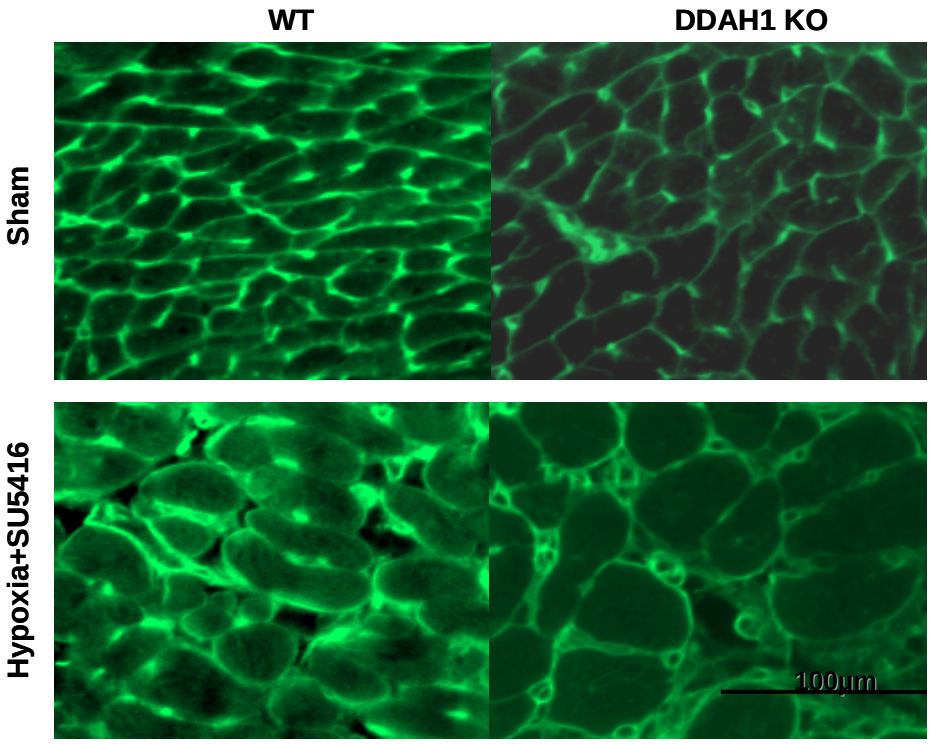

Figure 9. Representative images of RV cell size with WGA staining from wild type and global DDAH1 KO mice exposed to sham and hypoxia+SU5416 conditions.

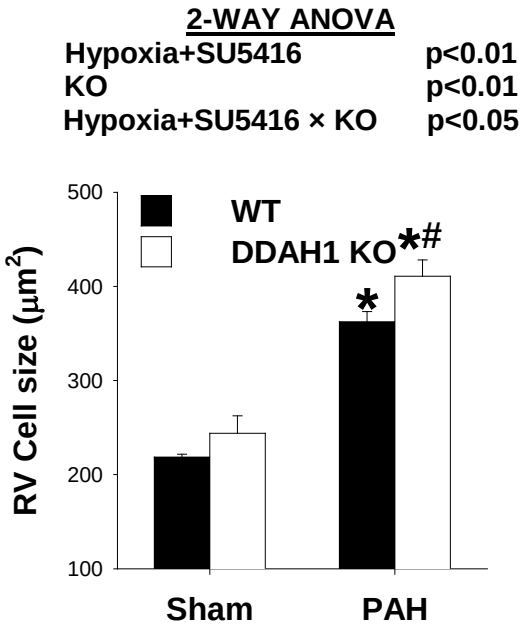

Figure 10. Global DDAH1 KO impact on hypoxia+SU5416 induced increases of RV cell size. Right ventricular tissue was fixed and stained with WGA for cardiomyocyte cell size from wild type and global DDAH1 KO mice. Cardiomyocyte cell size was calculated from 5 samples in each group. Data were presented as mean ± SEM. * indicates $p<0.05$ comparing hypoxia+SU5416 to sham. # indicates $P<0.05$ comparing WT to KO.

Global DDAH1 KO exacerbated hypoxia+SU5416-induced increases of RV fibrosis

To determined right ventricular fibrosis in global DDAH1 KO and wild type mice under control and hypoxia+SU5416 conditions, Sirius red staining was performed on 5 samples in each group. Representative pictures of RV staining were illustrated in Figure 11. There was no significant difference between global DDAH1 KO mice and wild type mice under control conditions. Hypoxia+SU5416 increased RV fibrosis to a greater degree in global DDAH1 KO mice as compared to wild type mice (6.17 ± 0.34 % in wild type hypoxia+SU5416 group versus 7.27 ± 0.20 % in global DDAH1 KO hypoxia+SU5416 group; $p<0.05$) (Figure12).

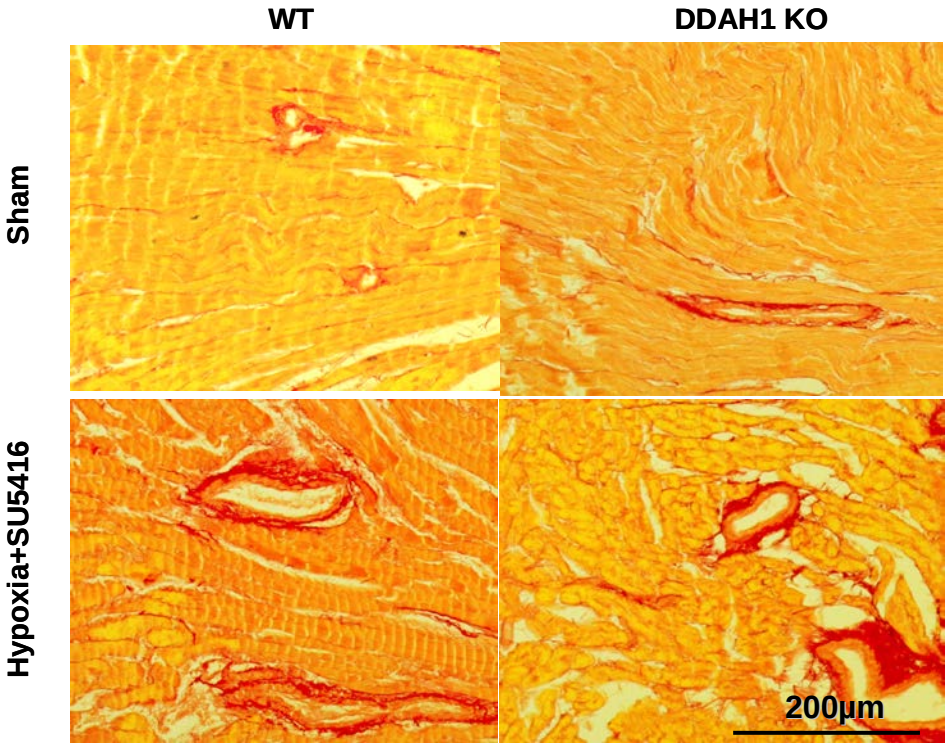

Figure 11. Sirius red stained cross-sections of right ventricles from wild type and global DDAH1 KO mice. The right ventricle cross-sections (20X) were stained with Sirius red from wild type and global DDAH1 KO mice under sham and hypoxia+SU5416 conditions.

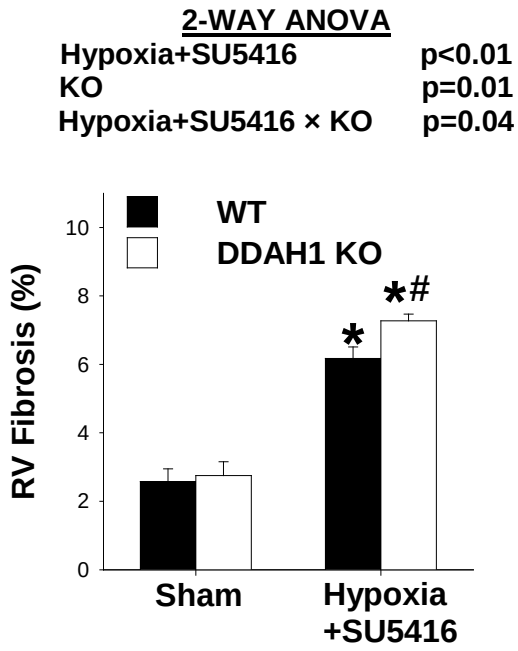

Figure 12. Global DDAH1 KO exacerbated hypoxia+SU5416-induced increase of RV fibrosis. Right ventricular sections were stained with Sirius red in wild type and global DDAH1 KO mice under sham and hypoxia+SU5416 conditions. The average percent of right ventricular fibrosis was calculated from 5 samples in each group. Data were presented as mean ± SEM. * indicates $p<0.05$ comparing hypoxia+SU5416 to sham. # indicates $P<0.05$ comparing WT to KO.

Global DDAH1 KO aggravated hypoxia+SU5416-induced pulmonary vascular remodeling and pulmonary fibrosis

To determine the effect of global DDAH1 KO on pulmonary vascular remodeling, we determined the percentage of non-muscularized (NM), partially muscularized (PM), and fully muscularized small arteries (FM) in wild type and global DDAH1 KO mice under sham conditions and 3 weeks after hypoxia+SU5416 (Figure 13 and 14). Hematoxylin stained histological characteristics of lung tissue with global DDAH1 KO and wild type mice were illustrated in Figure 13. The percentage of non-muscularized, partially muscularized and fully muscularized small arteries in lung tissues was not different between wild type mice and global DDAH1 KO mice under sham conditions (Figure 13 and 14). Exposure to hypoxia caused increases in fully muscularized small arteries in wild type and global DDAH1 KO mice (Figure 14). The increases were greater in the global DDAH1 KO mice ($p<0.05$). As expected, hypoxia also resulted in a decreased number of non-muscularized small arteries in both wild type and global DDAH1 KO mice (Figure 14).

In addition, pulmonary fibrosis was detected using Masson trichrome staining under sham conditions and 3 weeks post hypoxia+SU5416 (Figure 15). Pulmonary fibrosis was comparable between global DDAH1 KO mice and wild type mice under sham conditions (Figure 16). Hypoxia+SU5416 caused pulmonary fibrosis in both wild type mice and global DDAH1 KO mice, but increases were significantly greater in the global DDAH1 KO mice than in the wild type mice (5.35 ± 0.63 % in wild type hypoxia+SU5416 group versus 8.40 ± 1.0. % in global DDAH1 KO hypoxia+SU5416 group; $p<0.05$) (Figure 15 and 16).

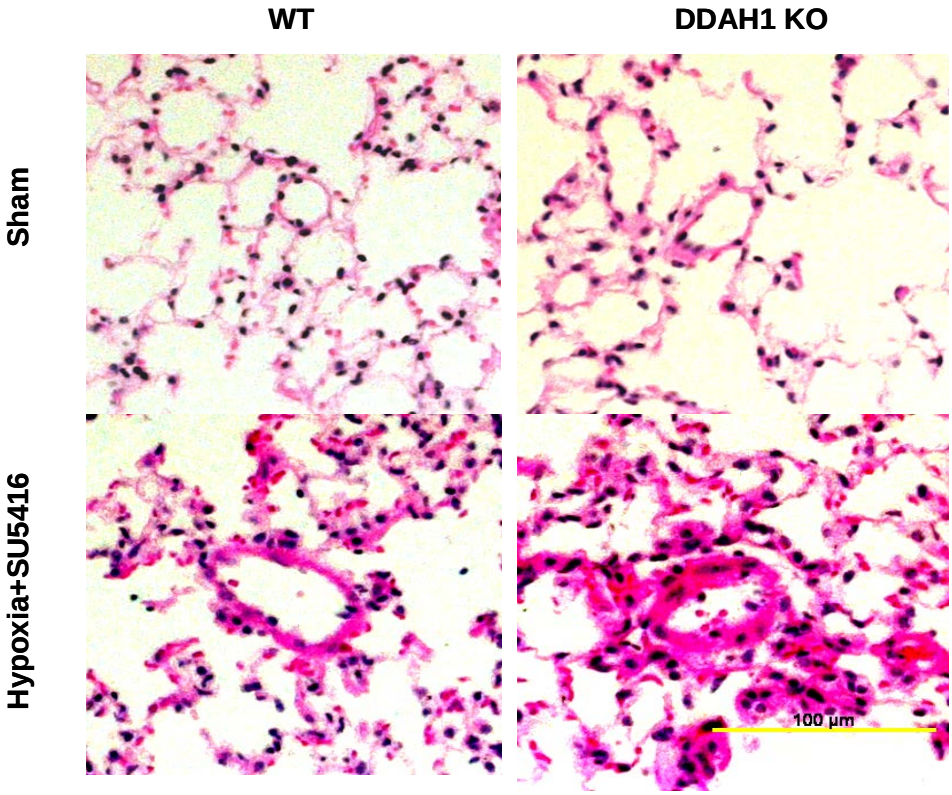

Figure 13. Representative images of pulmonary vascular remodeling. Lungs from wild type and global DDAH1 KO mice exposed to sham and hypoxia+SU5416 conditions were flushed, fixed in formalin, and stained using eosin-hemotoxylin for pulmonary vessel muscularization.

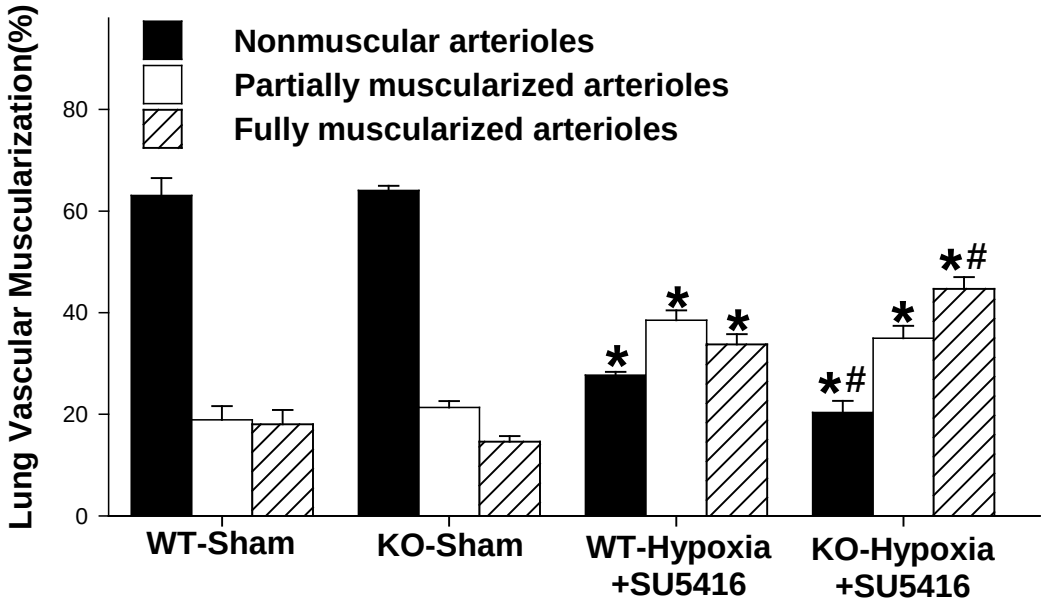

Figure 14. Global DDAH1 KO aggravated hypoxia+SU5416-induced pulmonary vascular remodeling. The average percent of non-muscularized, partially muscularized, and fully muscularized pulmonary arterioles were calculated from 5 samples in each group. Data were presented as mean ± SEM. * indicates $p<0.05$ comparing hypoxia+SU5416 to sham. # indicates $P<0.05$ comparing WT to KO.

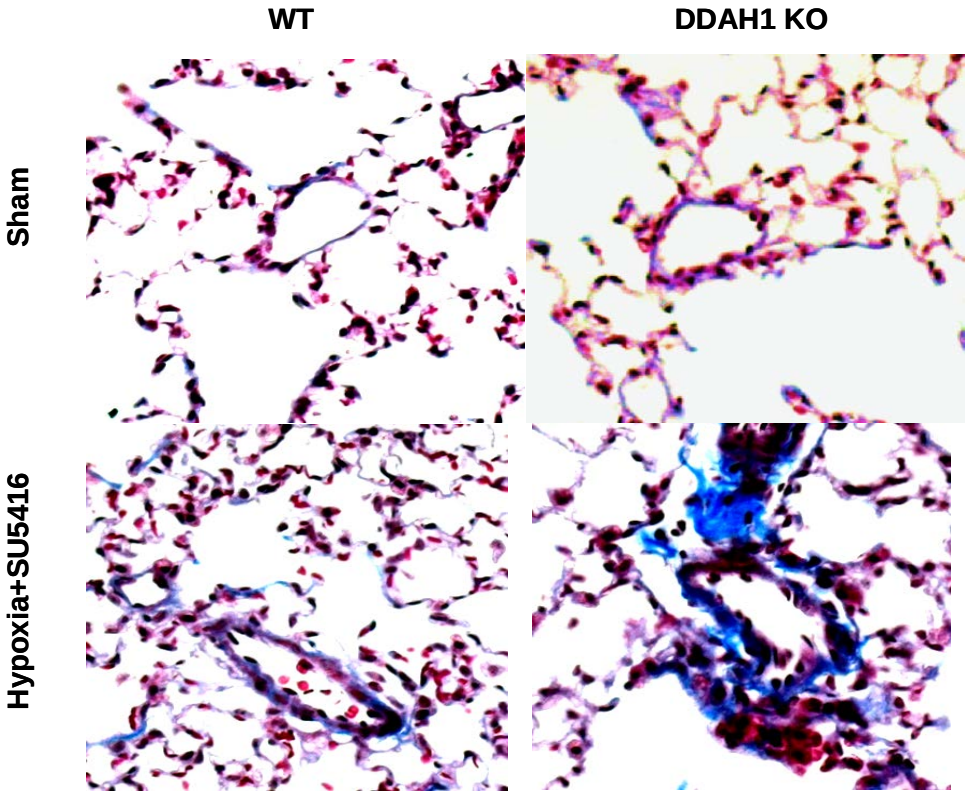

Figure 15. Representative images of lung fibrosis from wild type and global DDAH1 KO mice. Lungs from wild type and global DDAH1 KO mice exposed to sham or hypoxia+SU5416 conditions were flushed, fixed in formalin, and stained using trichrome stain for pulmonary fibrosis.

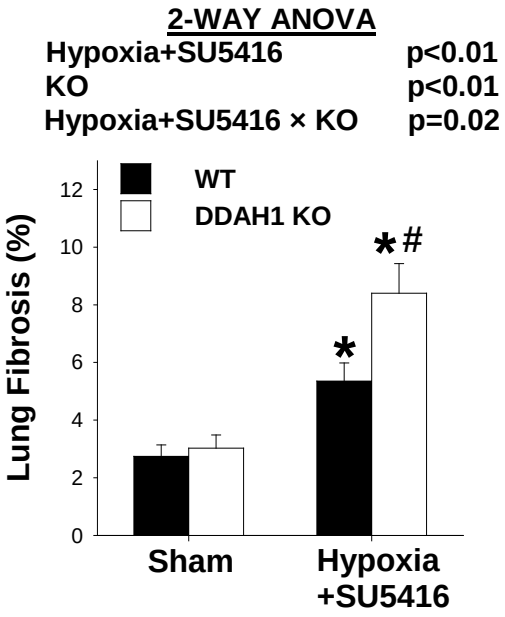

Figure 16. Global DDAH1 KO aggravated hypoxia+SU5416-induced pulmonary fibrosis. Lung sections were stained with trichrome in wild type and global DDAH1 KO mice under sham and hypoxia+SU5416 conditions. The average percent of lung fibrosis was calculated from 5 samples in each group. Data were presented as mean ± SEM. * indicates $p<0.05$ comparing hypoxia+SU5416 to sham. # indicates $P<0.05$ comparing WT to KO.

Hypoxia+SU5416 increased eNOS expression in wild type and global DDAH1 KO mice

Expression of DDAH1 and eNOS proteins were determined by Western blotting (Figure 17). Western blot demonstrated that lung DDAH1 expression was not detectable in global DDAH1 KO mice under sham conditions and after hypoxia+SU5416 as expected (Figure 17). Hypoxia+SU5416 caused no change in lung DDAH1 expression in wild type mice (Figure 17). Lung eNOS expression was not significantly different between wild type and global DDAH1 KO mice under sham conditions (Figure 17), while hypoxia+SU5416 increased lung eNOS expression in both wild type and global DDAH1 KO mice (0.47 ± 0.07 in wild type sham group versus 1.76 ± 0.33 in wild type hypoxia+SU5416 group; $p<0.05$) (0.51 ± 0.06 in global DDAH1 KO sham group versus 1.51 ± 0.13 in global DDAH1 KO hypoxia+SU5416 group; $p<0.05$) (Figure 17).

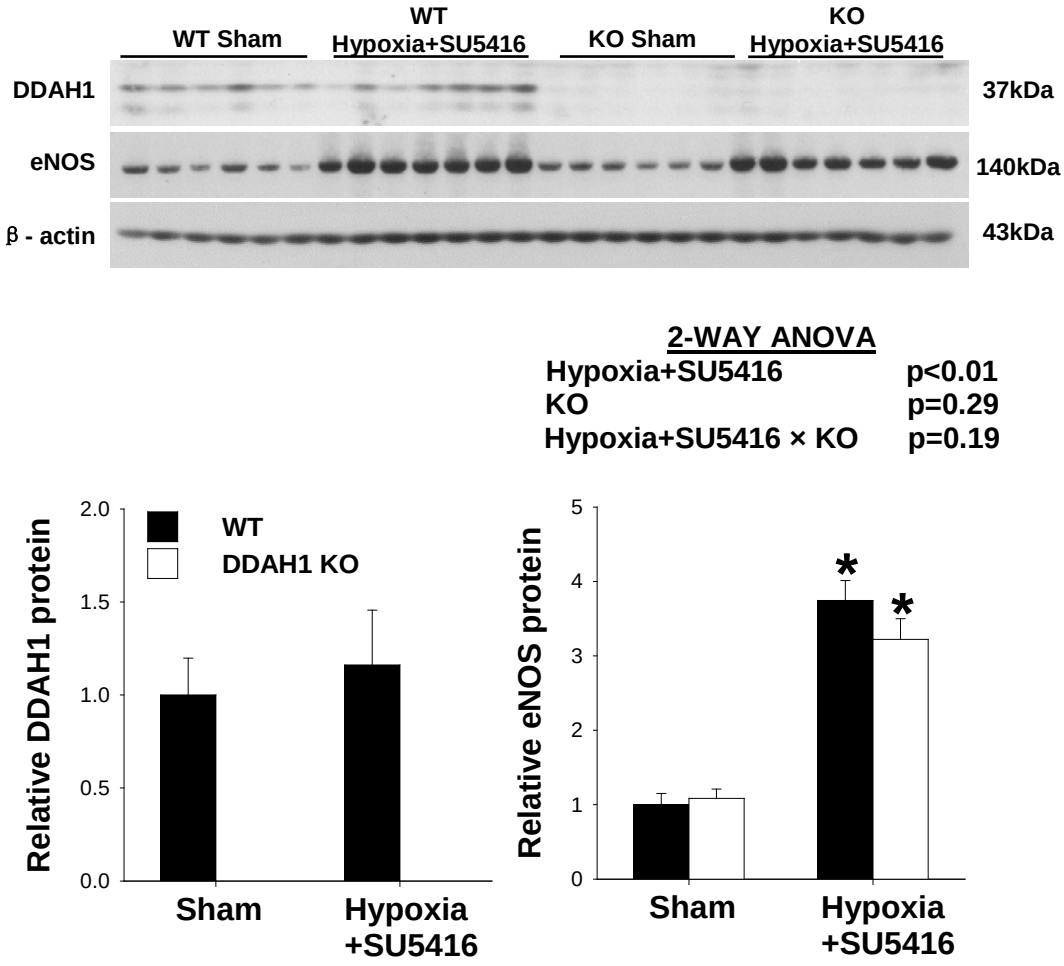

Figure 17. Hypoxia+SU5416 increased eNOS expression in wild type and global DDAH1 KO mice. Data were presented as mean ± SEM. * indicates p<0.05 comparing hypoxia+SU5416 to sham. # indicates P<0.05 comparing WT to KO.

Effects of hypoxia+SU5416 and global DDAH1 KO on DDAH activity

To determine global DDAH1 KO affect on DDAH activity under control and hypoxia+SU5416 conditions, lung DDAH activity was determined. Global DDAH1 KO almost abolished lung DDAH activity under control conditions and after hypoxia+SU5416 (Figure 18). Hypoxia+SU5416 caused decreased lung DDAH activity in wild type (27.65 ± 1.88 nmol/g/min in wild type sham group versus 16.64 ± 2.11 nmol/g/min in wild type hypoxia+SU5416 group; $p<0.05$), while slightly increasing DDAH activity in global DDAH1 KO mice (1.04 ± 0.69 nmol/g/min in global DDAH1 KO sham group versus 3.01 ± 0.83 nmol/g/min in global DDAH1 KO hypoxia+SU5416 group; $p<0.05$) (Figure 18). The lung DDAH activity was significantly different between wild type and global DDAH1 KO mice under both sham and hypoxia+SU5416 conditions (27.65 ± 1.88 nmol/g/min in wild type sham group versus 1.04 ± 0.69 nmol/g/min in global DDAH1 KO sham group; $p<0.05$) 16.64 ± 2.11 nmol/g/min in wild type hypoxia+SU5416 group versus 3.01 ± 0.83 nmol/g/min in global DDAH1 KO hypoxia+SU5416 group; $p<0.05$) (Figure 18).

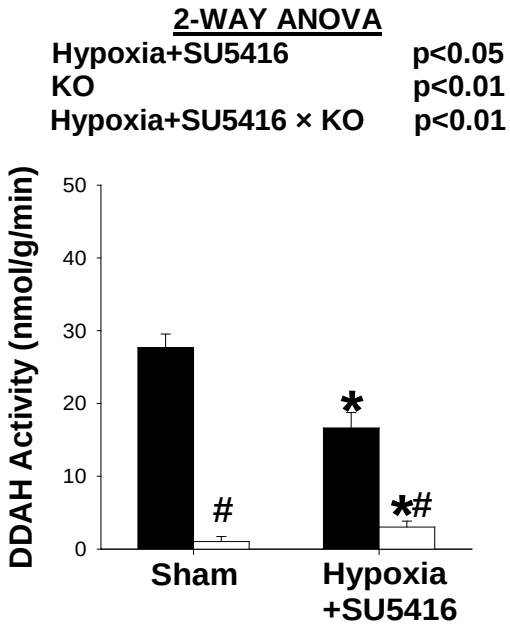

Figure 18. Effects of hypoxia+SU5416 and global DDAH1 KO on DDAH activity. Data were presented as mean ± SEM. * indicates p<0.05 comparing hypoxia+SU5416 to sham. # indicates P<0.05 comparing WT to KO

Global DDAH1 KO increased lung ADMA without affecting lung SDMA content under control and hypoxia+SU5416 conditions

To determine the effect of global DDAH1 KO on lung ADMA and SDMA content under control and hypoxia conditions, we determined the ADMA and SDMA content from the lung. Lung ADMA content was significantly increased in global DDAH1 KO mice under sham conditions and after hypoxia+SU5416 (55.01 ± 9.70 nmol/g in wild type sham group versus 92.05 ± 10.17 nmol/g in global DDAH1 KO sham group; $p<0.05$) (67.60 ± 9.27 nmol/g in wild type hypoxia+SU5416 group versus 92.83 ± 8.97 nmol/g in global DDAH1 KO hypoxia+SU5416 group; $p<0.05$) (Figure 19). Lung SDMA was not different in wild type mice or global DDAH1 KO mice under sham conditions and after hypoxia+SU5416 (Figure 19).

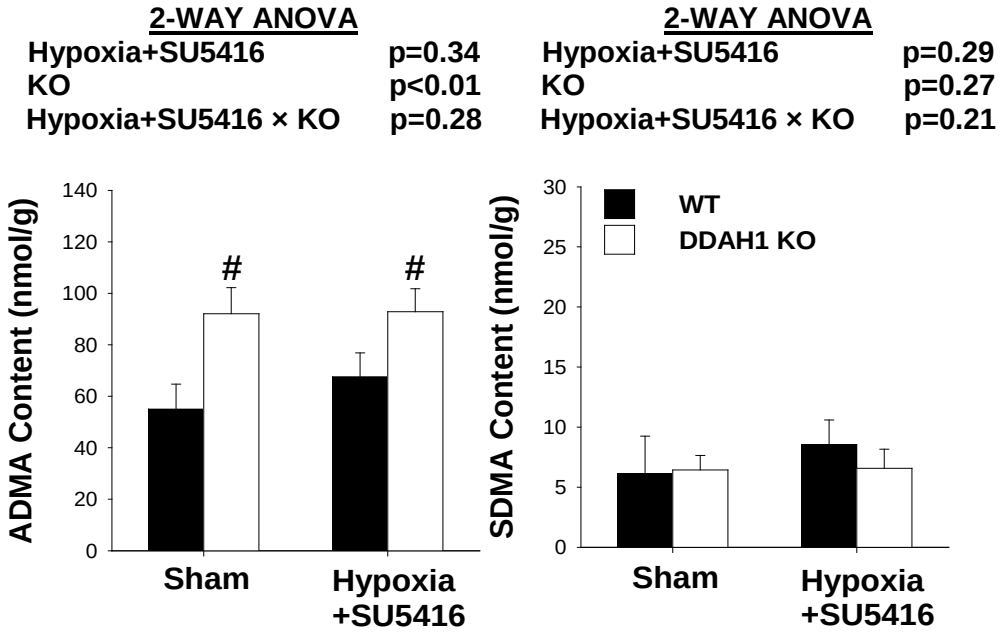

Figure 19. Global DDAH1 KO increased lung ADMA without affecting lung SDMA content under sham and hypoxia+SU5416 conditions. Lung ADMA and SDMA were determined using a high-through put liquid chromatographic-tandem mass spectrometric method. Data were presented as mean ± SEM. * indicates p<0.05 comparing hypoxia+SU5416 to control. # indicates P<0.05 comparing WT to KO

Global DDAH1 KO did not affect the expression of lung PRMT1, PRMT3, and CAT1

Western blot showed that lung PRMT1 and CAT1 expression were not altered by hypoxia+SU5416 or by global DDAH1 KO (Figure 20). Lung PRMT3 expression was significantly increased in response to hypoxia+SU5416 in both wild type (1.00 ± 0.06 in wild type sham group versus 1.34 ± 0.11 in wild type hypoxia+SU5416 group; $p<0.05$) and global DDAH1 KO mice (0.90 ± 0.06 in global DDAH1 KO sham group versus 1.21 ± 0.08 in global DDAH1 KO hypoxia+SU5416 group; $p<0.05$), but no difference was observed between WT and global DDAH1 KO mice (Figure 20).

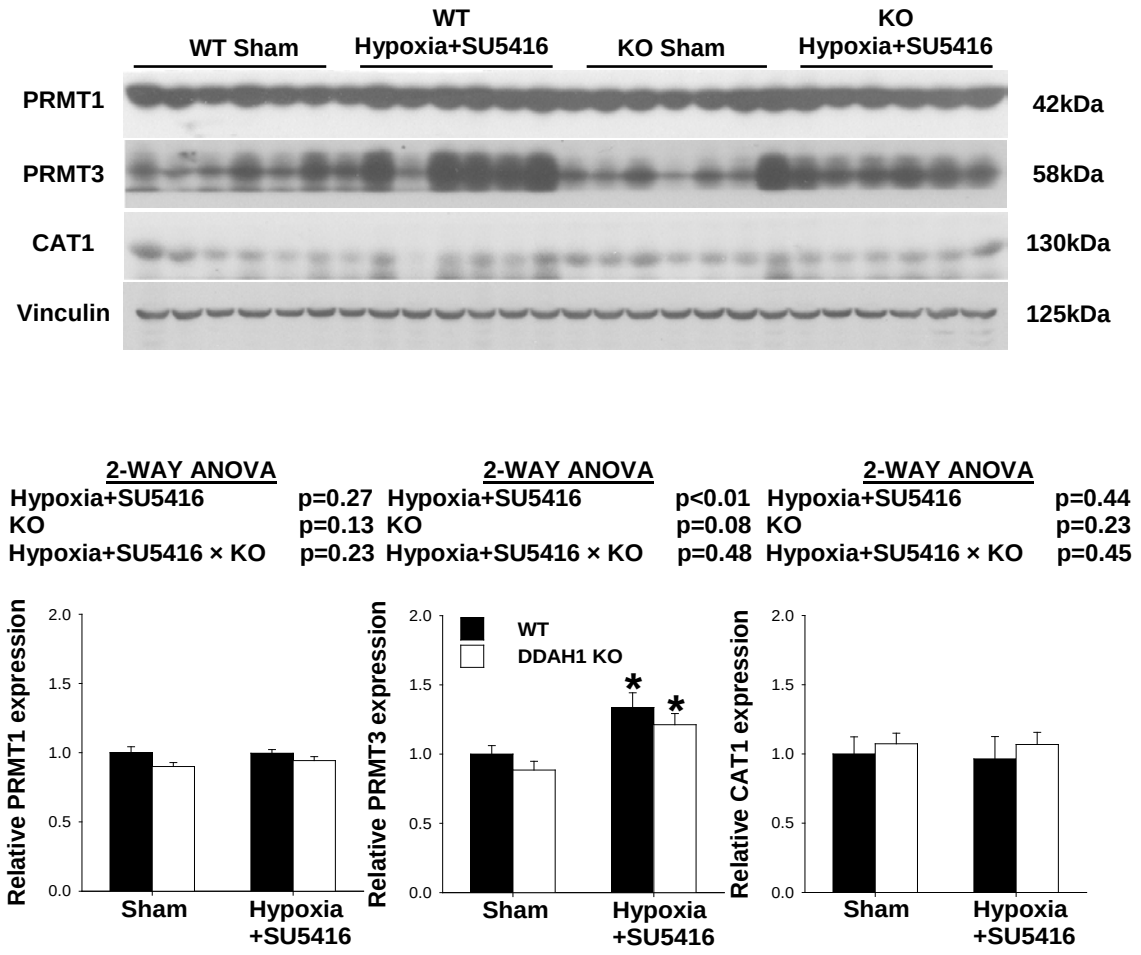

Figure 20. Global DDAH1 KO did not affect the protein expression of lung PRMT1, PRMT3, and CAT1. Data were presented as mean ± SEM. * indicates p<0.05 comparing hypoxia+SU5416 to sham. # indicates P<0.05 comparing WT to KO

Global DDAH1 KO cause accumulation of plasma ADMA under control and hypoxia+SU5416 conditions

Plasma ADMA content was significantly increased in global DDAH1 KO mice as compared with wild type mice under control conditions (0.62 ± 0.05 µmol in wild type sham group versus 1.25 ± 0.11 µmol in global DDAH1 KO sham group; $p<0.05$) and further elevated in response to hypoxia+SU5416 (0.86 ± 0.10 µmol in wild type hypoxia+SU5416 group versus 1.91 ± 0.20 µmol in global DDAH1 KO hypoxia+SU5416 group; $p<0.05$) (Figure 21). While hypoxia+SU5416 increased plasma ADMA content in wild type (0.62 ± 0.05 µmol in wild type sham group versus 0.86 ± 0.10 µmol in wild type hypoxia+SU5416 group; $p<0.05$), this increase was significantly greater in global DDAH1 KO mice (1.25 ± 0.11 µmol in global DDAH1 KO sham group versus 1.91 ± 0.20 µmol in global DDAH1 KO hypoxia+SU5416 group; $p<0.05$) (Figure 21). Plasma L-Arginine content was not significantly different between wild type and global DDAH1 KO mice under sham and hypoxia+SU5416 conditions (Figure 21). Hypoxia+SU5416 also induced no significant changes in L-Arginine content in wild type and global DDAH1 KO mice (Figure 21). The ratio of plasma ADMA to L-Arginine, a common indicator of systemic nitric oxide bio availability, was significantly increased in global DDAH1 KO mice under sham and after hypoxia+SU5416 in comparison to WT mice (Figure 21).

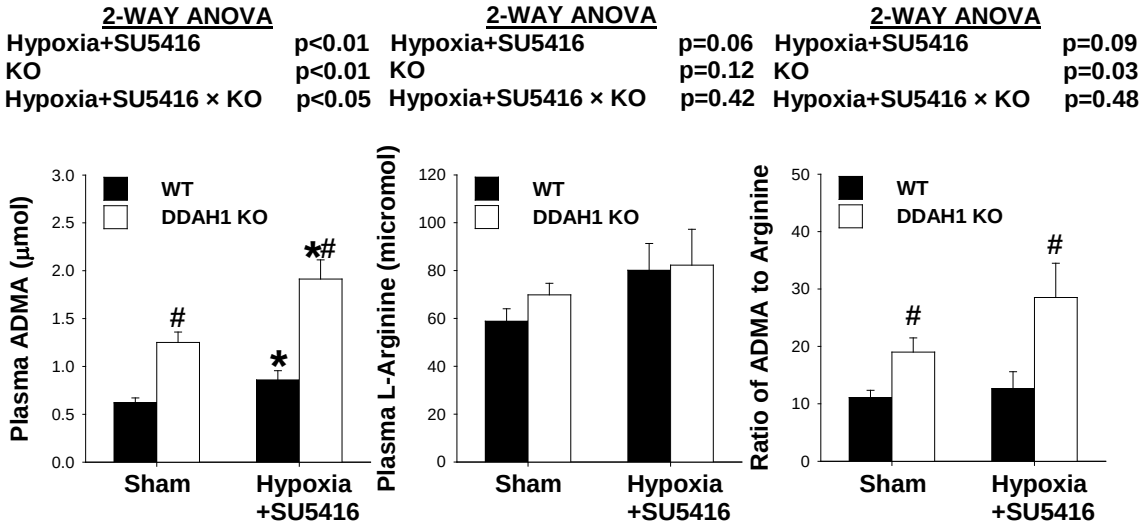

Figure 21. Global DDAH1 KO caused accumulation of plasma ADMA under sham and hypoxia+SU5416 conditions. Plasma ADMA and L-Arginine were determined by a high through put chromatographic-tandem mass spectrometric method. Data were presented as mean ± SEM. * indicates p<0.05 comparing hypoxia+SU5416 to sham. # indicates P<0.05 comparing WT to KO

Global DDAH1 KO increased plasma L-NMMA accumulation under control conditions and in response to hypoxia+SU5416

Plasma L-NMMA content was significantly higher in global DDAH1 KO mice than WT mice under sham conditions (0.18 ± 0.02 μmol in wild type sham group versus 0.69 ± 0.14 μmol in global DDAH1 KO sham group; $p<0.05$) and further increased in response to hypoxia+SU5416 (0.22 ± 0.05 μmol in wild type hypoxia+SU5416 group versus 0.97 ± 0.06 μmol in global DDAH1 KO hypoxia+SU5416 group; $p<0.05$). Hypoxia+SU5416 increased plasma L-NMMA content in global DDAH1 KO mice (from 0.69 ± 0.14 μmol in global DDAH1 KO sham group to 0.97 ± 0.06 μmol in global DDAH1 KO hypoxia+SU5416 group; $p<0.05$) (Figure 22). Plasma L-Arginine content was not significantly different between wild type and global DDAH1 KO mice under sham or hypoxia+SU5416 conditions (Figure 22). Hypoxia+SU5416 also caused no changes in L-Arginine content wild type or global DDAH1 KO mice (Figure 22). The ratio of plasma ADMA to L-arginine was significantly increased in global DDAH1 KO mice under sham and after hypoxia+SU5416 (Figure 22).

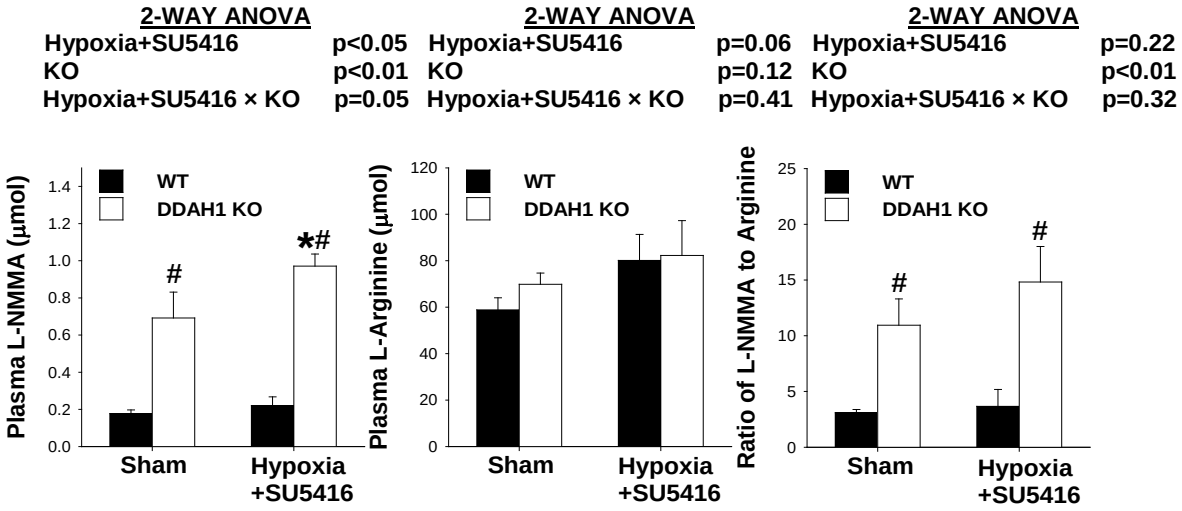

Figure 22. Global DDAH1 KO increased plasma L-NMMA accumulation under sham conditions and in response to hypoxia+SU5416. Plasma L-NMMA and L-Arginine were determined by a high through put chromatographic-tandem mass spectrometric method. Data were presented as mean ± SEM. * indicates p<0.05 comparing hypoxia+SU5416 to sham. # indicates P<0.05 comparing WT to KO

Global DDAH1 KO had no effect on hypoxia+SU5416 induced plasma SDMA contents

Plasma SDMA content was determined by high through put chromatographic-tandem mass spectrometric method. Plasma SDMA content was not significantly different between wild type mice and global DDAH1 KO mice under sham and hypoxia+SU5416 conditions but significantly increased in both wild type (0.17 ± 0.01 µmol in wild type sham group versus 0.28 ± 0.04 µmol in wild type hypoxia+SU5416 group; $p<0.05$) and global DDAH1 KO mice after hypoxia+SU5416 (0.19 ± 0.02 µmol in global DDAH1 KO sham group versus 0.38 ± 0.05 µmol in global DDAH1 KO hypoxia+SU5416 group; $p<0.05$) (Figure 23). This indicates that DDAH1 does not regulate plasma SDMA levels.

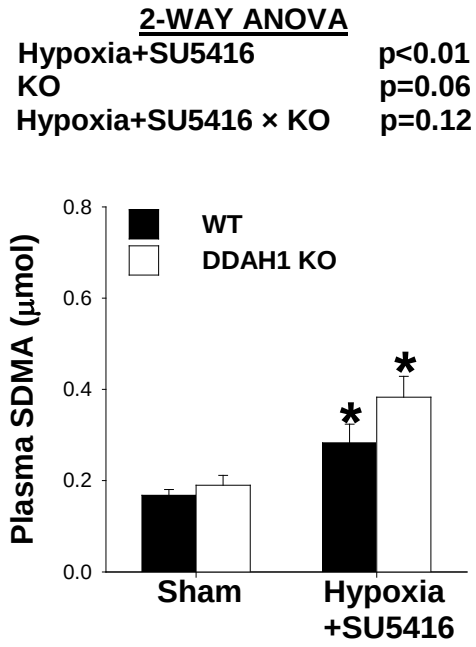

Figure 23. Global DDAH1 KO had no effect on hypoxia+SU5416-induced plasma SDMA contents. Plasma SDMA content was determined by a high through put chromatographic-tandem mass spectrometric method. Data were presented as mean ± SEM. * indicates p<0.05 comparing hypoxia+SU5416 to sham. # indicates P<0.05 comparing WT to KO

4.2. Effect of cardio DDAH1 KO on hypoxia+SU5416-induced PAH and RV hypertrophy

Cardio-DDAH1 KO has no effect of RV hypertrophy under sham conditions but exacerbates hypoxia+SU5416-induced RV hypertrophy

Body weight, RV weight, and LV weight (LV + Septum) were measured to examine RV hypertrophy in wild type and cardio-DDAH1 KO mice under sham and hypoxia+SU5416 conditions. RV to body weight and ratio of RV to LV (LV + Septum) weight were not significantly different between wild type and cardio-DDAH1 KO mice under sham conditions (Table 4 and Figure 24). However, cardio-DDAH1 KO significantly exacerbated hypoxia+SU5416-induced increases of RV hypertrophy as indicated by the ratio of RV to body weight (1.82 ± 0.08 mg/g in wild type hypoxia+SU5416 group versus 2.26 ± 0.12 mg/g in KO hypoxia+SU5416 group; $p<0.05$) and RV to LV (LV + Septum) weight (0.33 ± 0.01 mg/g in wild type hypoxia+SU5416 group versus 0.37 ± 0.02 mg/g in KO hypoxia+SU5416 group; $p<0.05$). Interestingly, the RV systolic pressure and RV dp/dtmax were not significantly different between wild type and cardio-DDAH1 KO mice after hypoxia+SU5416 (Figure 27 and 28). RV cell size, another indicator of hypertrophy, was determined by WGA staining. Histological analysis indicated that hypoxia+SU5416 caused a significant increase of RV cell size in both wild type and cardio-DDAH1 KO mice but the increase of RV cell size was significantly greater in cardio-DDAH1 KO mice (343.79 ± 9.76 μm^2 in wild type hypoxia+SU5416 group versus 409.69 ± 21.70 μm^2 in KO hypoxia+SU5416 group) (Figure 25 and 26).

Table 4. Anatomic data for WT and cardio-DDAH1 KO mice under sham and hypoxia+SU5416 conditions

Parameters	**WT-Sham**	**CardioDDAH1 KO-Sham**	**WTHypoxia +SU5416**	**Cardio-DDAH1 KOHypoxia+SU5416**
Number of mice	8	8	11	9
Bodyweight (g)	27.78 ± 1.64	28.80 ± 2.67	27.24 ± 0.72	25.10 ± 1.00†
Tibia length (mm)	17.46 ± 0.12	17.57 ± 0.24	17.83 ± 0.05	17.73 ± 0.11*
RV weight (mg)	26.95 ± 2.03	30.19 ± 2.52	49.12 ± 1.66*	56.89 ± 3.63*†
LV + septum (mg)	133.24 ± 11.60	131.93 ± 14.22	148.72 ± 4.99	153.61 ± 7.29
Ratio of RV to LV + septum	0.20 ± 0.08	0.24 ± 0.01	0.33 ± 0.01*	0.37 ± 0.02*†
Lung mass (mg)	140.36 ± 7.81	138.23 ± 10.98	191.23 ± 4.18*	190.27 ± 13.48*
Right atria (mg)	3.00 ± 0.25	3.21 ± 0.36	4.44 ± 0.27*	9.10 ± 3.39*
Left atria weight (mg)	5.35 ± 0.67	5.23 ± 0.74	6.24 ± 0.43	6.83 ± 0.59
Kidney weight (mg)	368.76 ± 29.59	435.41 ± 53.69	320.46 ± 10.29*	326.24 ± 24.43*
Ratio of RV to BW (mg/g)	0.97 ± 0.05	1.06 ± 0.05	1.82± 0.08*	2.26 ± 0.12*†
Ratio of LV to BW (mg/g)	4.75 ± 0.18	4.54 ± 0.16	5.49 ± 0.22*	6.12 ± 0.21*†
Ratio of lung to BW (mg/g)	5.14 ± 0.34	4.88 ± 0.20	7.07 ± 0.22*	7.52 ± 0.32*
Ratio of RA to BW (mg/g)	0.11 ± 0.01	0.11 ± 0.01	0.17 ± 0.01*	0.37 ± 0.14*
Ratio of LA to BW (mg/g)	0.19 ± 0.02	0.18 ± 0.02	0.23 ± 0.02*	0.27 ± 0.02*
Ratio of kidney to BW (mg/g)	13.19 ± 0.43	14.82 ± 0.62	11.85 ± 0.45*	12.92 ± 0.78*
Ratio of RV to TL (mg/mm)	1.55 ± 0.12	1.71 ± 0.13	2.76 ± 0.09*	3.20 ± 0.20*†
Ratio of LV to TL (mg/mm)	7.66 ± 0.70	7.45 ± 0.74	8.35 ± 0.29	8.67 ± 0.42
Ratio of lung to TL (mg/mm)	8.04 ± 0.44	7.83 ± 0.54	10.73 ± 0.25*	10.74 ± 0.79*
Ratio of RA to TL (mg/mm)	0.17 ± 0.01	0.18 ± 0.02	0.25 ± 0.01*	0.51 ± 0.19*†
Ratio of LA to TL (mg/mm)	0.31 ± 0.04	0.30 ± 0.04	0.35 ± 0.02	0.39 ± 0.03
Ratio of kidney to TL (mg/mm)	21.18 ± 1.78	24.56 ± 2.80	17.97 ± 0.57*	18.39 ± 1.37*

Data are presented as mean ± SEM when normally distributed. *$p<0.05$ as compared with corresponding sham conditions; † $p<0.05$ as compared with WT mice under the hypoxia+SU5416 condition

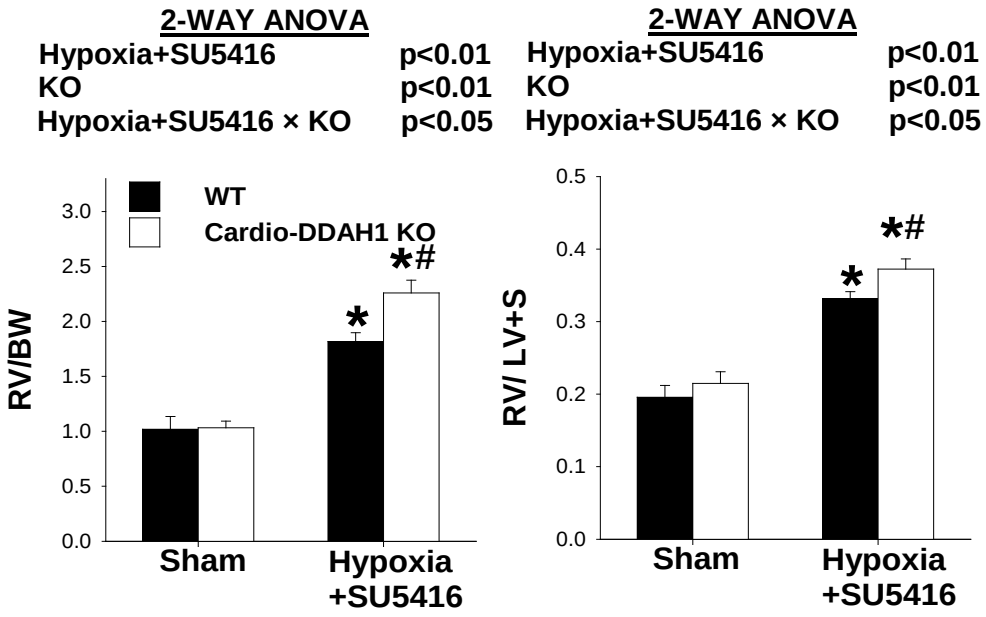

Figure 24. Cardio-DDAH1 KO exacerbated hypoxia+SU5416-induced increase of RV hypertrophy. After 3 weeks exposure to hypoxia+SU5416 or sham conditions, hearts were collected. Right ventricle weight to body weight ratio, right ventricle weight to left ventricle + septum weight were calculated from 8 to 11 samples in each group. Data were presented as mean ± SEM. * indicates $p<0.05$ comparing hypoxia+SU5416 to sham. # indicates $P<0.05$ comparing WT to cardio-DDAH1 KO.

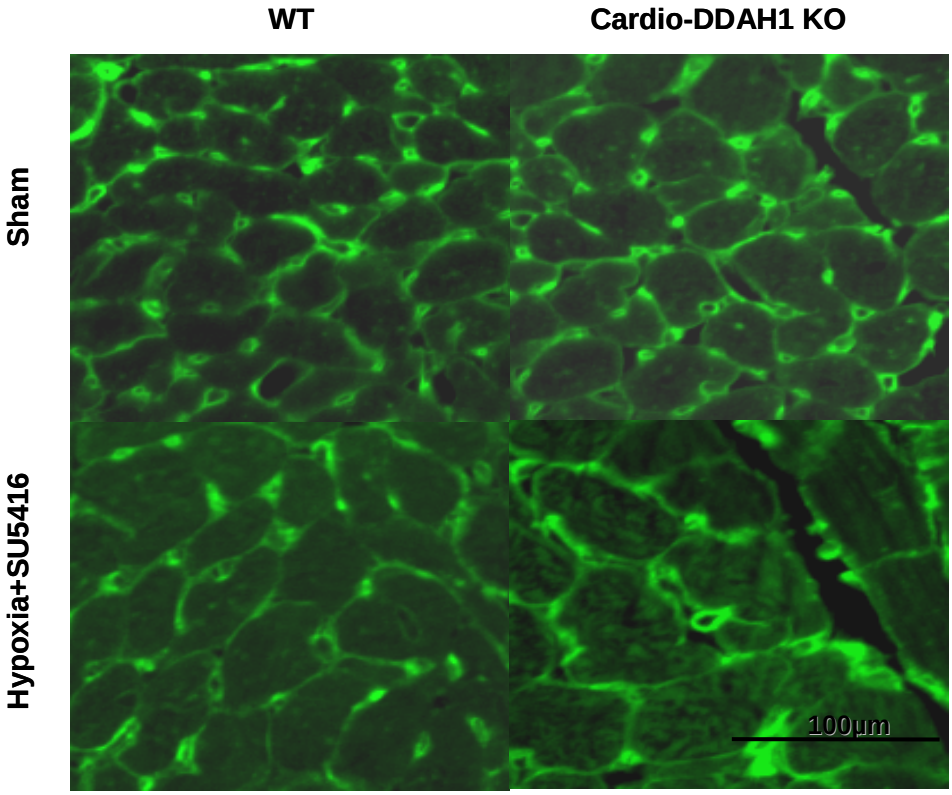

Figure 25. Representative images of RV cell size with WGA staining from wild type and cardio-DDAH1 KO mice exposed to sham and hypoxia+SU5416 conditions.

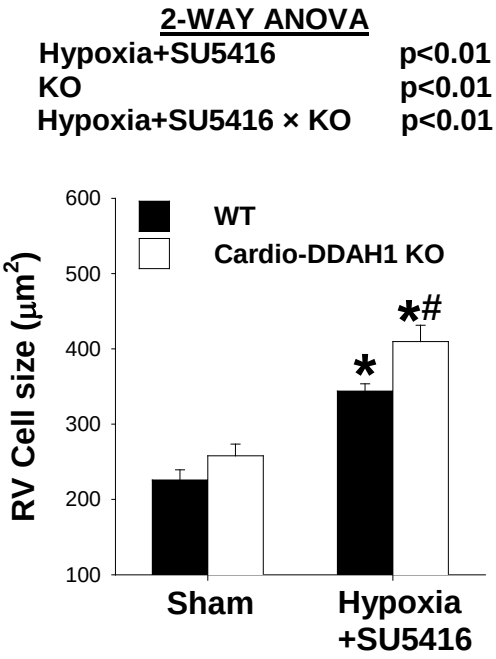

Figure 26. Cardio-DDAH1 KO exacerbated hypoxia+SU5416-induced increase of RV cell size. Right ventricular tissue from wild type and cardio-DDAH1 KO mice was fixed and stained with WGA for cardiomycyte cell size. Cardiomycyte cell size was calculated from 5 samples in each group. Data were presented as mean ± SEM. * indicates p<0.05 comparing hypoxia+SU5416 to sham. # indicates P<0.05 comparing WT to cardio-DDAH1 KO.

Cardio-DDAH1 KO exacerbated hypoxia+SU5416-induced increase of RV hypertrophy but had no significant effect on RV pressure

To determine whether cardio specific DDAH1 influences PAH development, we examined the effect of cardio-DDAH1 KO on hypoxia+SU5416-induced PAH in mice. RV systolic pressure, RV end diastolic pressure, RV dp/dtmax, and RV dp/dtmin were not different between wild type and Cardio-specific DDAH1 KO mice under sham condition (Table 5 and Figure 27 and 28). The RV systolic pressure and RV dp/dtmax were also not significantly different between wild type and cardio-DDAH1 KO mice after hypoxia+SU5416 (Table 4, Figure 27, and 28). Hypoxia+SU5416 increased RV systolic pressure and RV dp/dtmax in both wild type (20.89 ± 0.84 mmHg in wild type sham group versus 38.53 ± 1.45 mmHg in wild type hypoxia+SU5416 group; $p<0.05$) and cardio-DDAH1 KO mice (20.65 ± 0.70 mmHg in cardio-DDAH1 KO sham group versus 40.34 ± 5.06 mmHg in cardio-DDAH1 KO hypoxia+SU5416 group; $p<0.05$). Cardio-DDAH1 KO mice exhibited no significant difference in RV diastolic pressure as compared with wild type mice under both sham and hypoxia+SU5416 conditions (Figure 27).

Table 5. Hemodynamic data for WT and cardio-DDAH1 KO mice under sham and hypoxia+SU5416 conditions

Parameters	**WT Sham**	**Cardio-DDAH1 KO Sham**	**WT Hypoxia+SU5416**	**Cardio-DDAH1 KO Hypoxia+SU5416**
Number of mice	6	7	8	5
Heart rate (beat/min)	541.45±13.55	548.65±9.86	491.39±7.04*	477.20±9.83*
RV systolic pressure (mmHg)	20.46±0.85	20.65±0.70	37.81±1.43*	39.94±3.94*
RV end diastolic pressure (mmHg)	1.02±0.21	1.34±0.27	1.80±0.39	2.20±1.00
RV dp/dt max (mmHg/s)	1838.04±140.56	1940.92±145.08	2437.52±114.21*	2488.26±95.38*
RV dp/dt min (mmHg/s)	-1645.03±121.39	-1811.87±153.07	-2303.46±86.61*	-2327.43±123.31*

Data are presented as mean ± SEM when normally distributed. *$p<0.05$ as compared with corresponding sham conditions; † $p<0.05$ as compared with WT mice under the hypoxia+SU5416 condition.

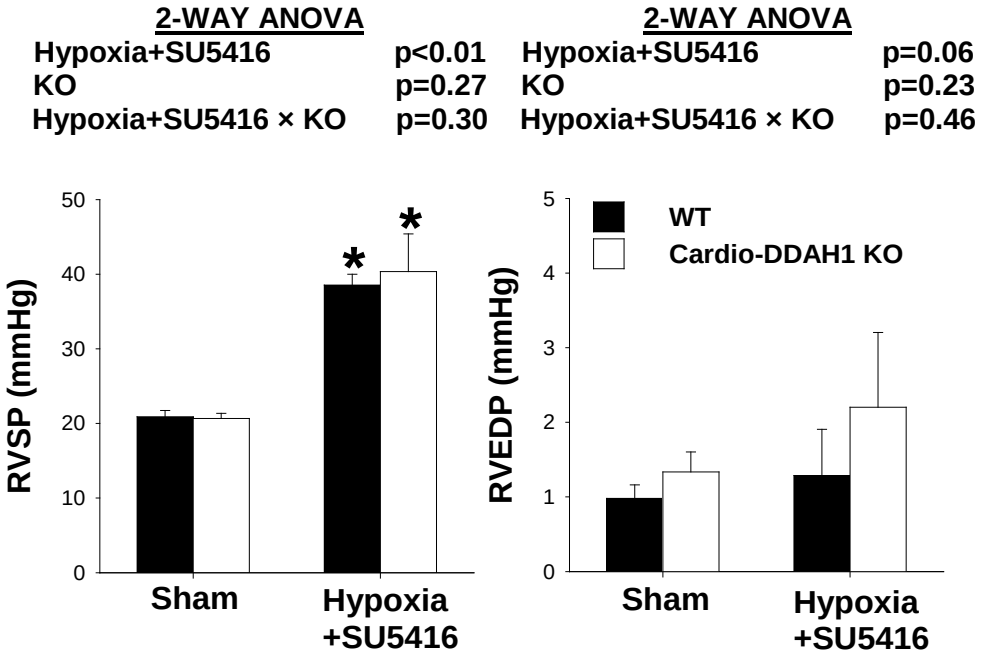

Figure 27. Cardio-DDAH1 KO had no significant effect on hypoxia+SU5416-induced RV pressure. To measure RV systolic pressure and RV diastolic pressure, RV catheterization was performed. Data were presented as mean ± SEM. * indicates p<0.05 comparing hypoxia+SU5416 to sham. # indicates P<0.05 comparing WT to KO

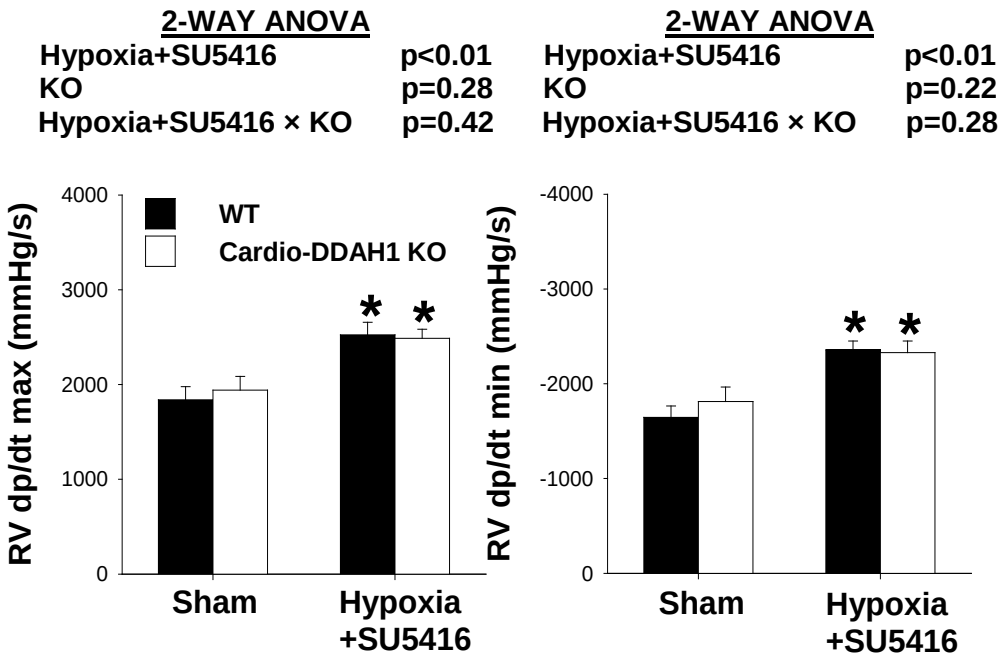

Figure 28. Cardio-DDAH1 KO had no significant effect on hypoxia+SU5416-induced RV contractility. Data were presented as mean ± SEM. * indicates p<0.05 comparing hypoxia+SU5416 to sham. # indicates P<0.05 comparing WT to KO.

Cardio-DDAH1 KO did not affect hypoxia+SU5416-induced RV fibrosis

Sirius red staining was used to determine right ventricular fibrosis in wild type and under sham and hypoxia+SU5416 conditions (n=5 samples each group. Representative pictures of RV staining are shown in Figure 29. While hypoxia+SU5416 increased RV fibrosis in wild type and cardio-DDAH1 KO mice (2.89 ± 0.34 % in wild type sham group versus 5.97 ± 0.34 % in wild type hypoxia+SU5416 group and 2.98 ± 0.25 % in KO sham group versus 6.98 ± 0.88 % in KO hypoxia+SU5416 group; $p<0.05$). No significant difference in fibrosis was observed between cardio-DDAH1 KO mice and wild type mice under sham or hypoxia+SU5416 conditions.

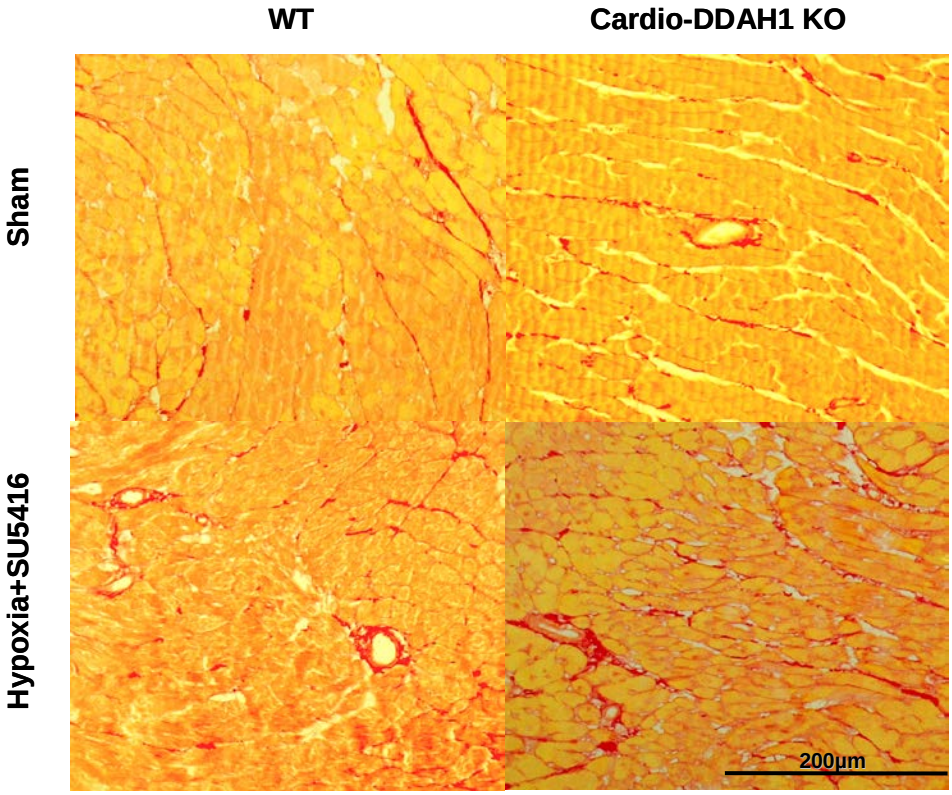

Figure 29. Representative images of RV fibrosis. Right ventricle cross-sections (20X) were stained with Sirius red from wild type and cardio-DDAH1 KO mice under sham and hypoxia+SU5416 conditions.

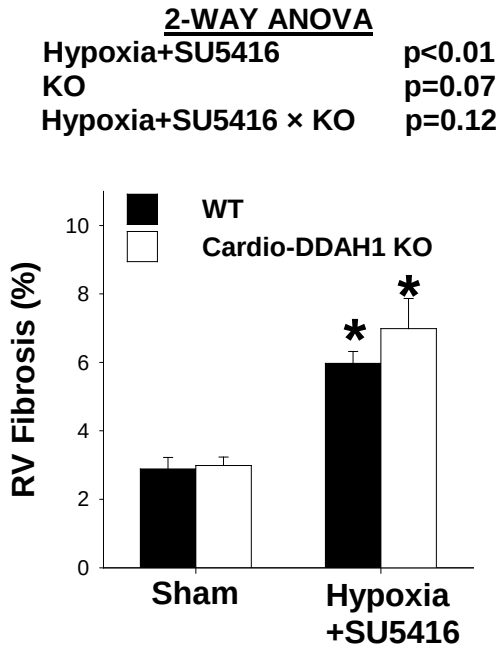

Figure 30. Cardio-DDAH1 KO did not affect hypoxia+SU5416-induced RV fibrosis. RV sections from wild type and cardio-DDAH1 KO mice under sham and hypoxia+SU5416 conditions were stained with Sirius red. The average percent of right ventricular fibrosis was calculated from 5 samples in each group. Data were presented as mean ± SEM. * indicates $p<0.05$ comparing hypoxia+SU5416 to sham. # indicates $P<0.05$ comparing WT to KO.

Cardio-DDAH1 KO did not affect hypoxia+SU5416-induced pulmonary vascular remodeling

To determine the effect of cardio-DDAH1 KO on pulmonary vascular remodeling, the percentages of non-muscularized (NM), partially muscularized (PM), and fully muscularized small arteries (FM) were determined in wild type and cardio-DDAH1 KO mice under control and hypoxia+SU5416 conditions. The lung sections were stained with hematoxylin (n=5 samples from each group (Figure 31). The percentage of non-muscularized, partially muscularized and fully muscularized small arteries in lung tissue was not different between wild type and cardio-DDAH1 KO mice under sham conditions (Figure 31 and 32). Hypoxia+SU5416 decreased the number of non muscularized small arteries and increased the number of partially muscularized and fully muscularized small arteries in both wild type and cardio-DDAH1 KO mice (Figure 32). There was no significant difference between wild type and cardio-DDAH1 KO mice under hypoxia+SU5416 conditions (Figure 32).

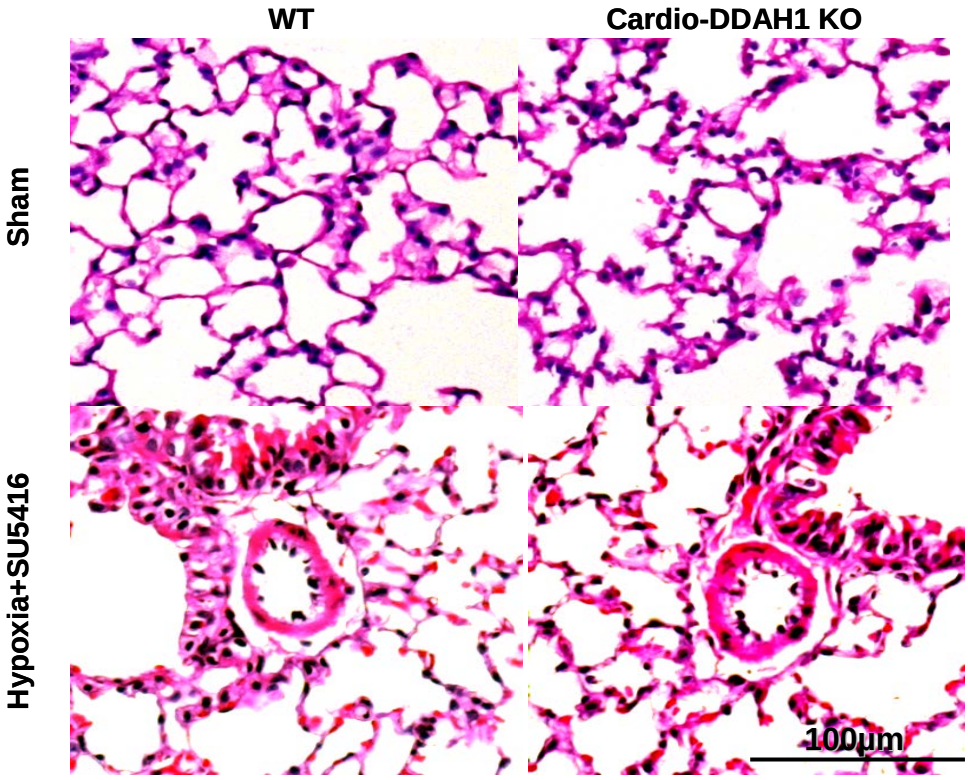

Figure 31. Representative images of pulmonary vascular remodeling. Lungs from wild type and cardio-DDAH1 KO mice exposed to sham and hypoxia+SU5416 conditions were flushed, fixed in formalin, and stained using eosin-hemotoxylin for pulmonary vessel muscularization

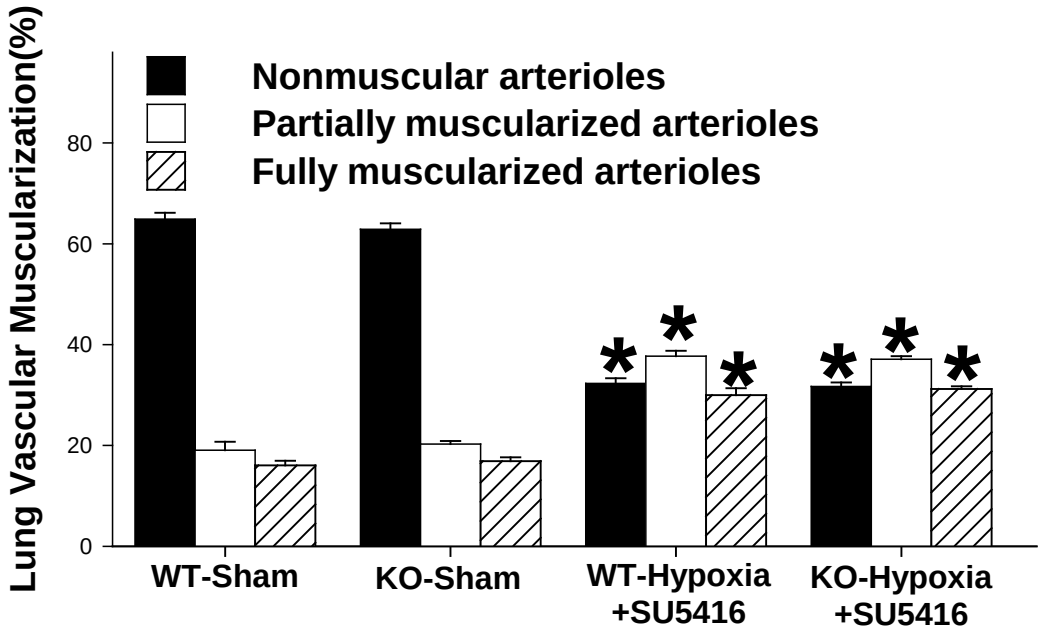

Figure 32. Cardio-DDAH1 KO did not affect hypoxia+SU5416-induced pulmonary vascular remodeling. The average percent of non-muscularized, partially muscularized, and fully muscularized pulmonary arterioles were calculated from 5 samples in each group. Data were presented as mean ± SEM. * indicates $p<0.05$ comparing hypoxia+SU5416 to sham. # indicates $P<0.05$ comparing WT to cardio-DDAH1 KO.

Cardio-DDAH1 KO did not affect plasma ADMA, L-NMMA, and SDMA

Plasma ADMA, L-NMMA and SDMA content were determined by high through put chromatographic-tandem mass spectrometric method in wild type and cardio-DDAH1 KO mice under control and hypoxia+SU5416 conditions. Cardio-DDAH1 KO did not significantly alter plasma ADMA, L-NMMA, and SDMA content under sham or hypoxia+SU5416 conditions in compared to WT mice (Figure 33).

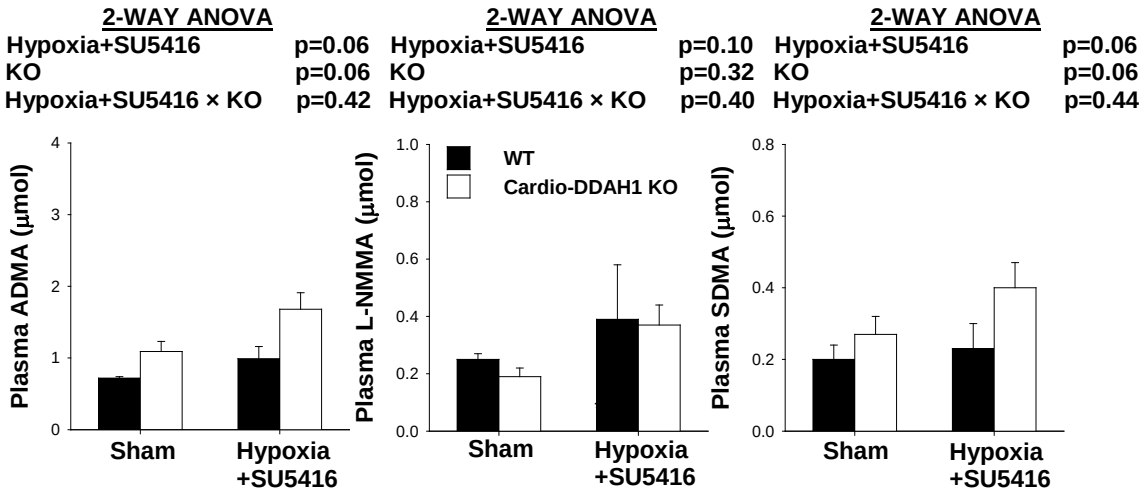

Figure 33. Cardio-DDAH1 KO did not significantly increase plasma ADMA, L-NMMA, and SDMA. Plasma ADMA, L-NMMA, and SDMA contents were determined by a high through put chromatographic-tandem mass spectrometric method. Data were presented as mean ± SEM. * indicates p<0.05 comparing hypoxia+SU5416 to sham. # indicates P<0.05 comparing WT to cardio-DDAH1 KO

5. Discussion

PAH increases the workload in the right ventricle, causing RV hypertrophy that eventually develops into right heart failure. DDAH1 regulates NO-cGMP signaling in part by degrading the NOS inhibitor ADMA. Because NO-cGMP signaling is important in both pulmonary vessels and in cardiomyocyte physiology, and DDAH1 is expressed in both of these tissues, it is difficult to distinguish whether DDAH1 regulation of PAH and subsequent RV hypertrophy is due to lung specific DDAH1 effects or through cardiomyocyte DDAH1 influence on the heart. Therefore, cardiomyocyte specific disruption of DDAH1 was used to determine cardiomyocyte DDAH1 impact on RV hypertrophy that occurs in response to PAH. Because DDAH1 KO in cardiomyocytes did not increase systemic ADMA levels, it determines the specific impact of cardiac DDAH1 on RV hypertrophy by comparing the response of wild type and cardio-DDAH1 KO hearts to similar degrees of PAH. Together, using of global and cardio-specific DDAH1 KO provides new insight into the specific pulmonary and cardiac roles of DDAH1 in cardiovascular response to the stress imposed by PAH.

Our data indicate that genetic disruption of global DDAH1 has no observable influence on pulmonary structure or right ventricular hemodynamics under basal conditions, but significantly exacerbates muscularization of pulmonary arteries, RV hypertrophy, lung fibrosis, and pulmonary vascular resistance (as indicated by increase right ventricular pressure) in response to hypoxia+SU5416. Global DDAH1 KO caused significant increases of NOS inhibitors ADMA and L-NMMA in the plasma under sham conditions. hypoxia+SU5416 further elevates the levels of these NOS inhibitors in global DDAH1 KO mice as compared to WT mice. Chronic hypoxia+SU5416 resulted in decreased DDAH1

activity and increased ADMA content in wild type mice, in agreement with the proposal that diminished DDAH1 activity in PAH promotes ADMA accumulation. However, cardio-DDAH1 KO aggravated hypoxia+SU5416-induced increase of RV hypertrophy under apparently similar levels of PAH, indicated by ratios of RV to BW and RV to LV + S and without significantly higher levels of plasma. This suggests that distribution of DDAH1 in cardiomyocytes protects the heart against RV hypertrophy. Collectively, these findings indicate that DDAH1 plays an important role in protecting both the lung and heart from the development of PAH under hypoxia+SU5416 conditions.

Impaired NO signaling is believed to play a role in development of PAH (109, 111). NO plays a vital role in endothelial smooth muscle cell coupling (26, 27) and pulmonary vascular tone (111, 112), inhibits platelet aggregation (113) and reduces leukocyte adhesion to vascular endothelium (114, 115). These events may be important early in PAH pathogenesis, which is believed to involve vasoconstriction (116, 117) and vascular inflammation (118, 119). NO also can reduce vascular smooth muscle cell proliferation (120), migration (121), and collagen synthesis (122). Conversely, endogenous NOS inhibitors ADMA and L-NMMA (17, 45) promote oxidative stress (123, 124), smooth muscle cell proliferation (125), and fibrosis (126), suggesting maintaining NO signaling is important for attenuating the vascular remodeling that is a hallmark of established PAH. Importantly plasma ADMA is commonly elevated in animal PAH models (7) and human PAH of various etiologies (127-130), while expression or activity of DDAH1 is reduced (7). Consistent with DDAH1 playing the major role in ADMA removal (6), ADMA levels were nearly doubled in the lungs and plasma of DDAH1 KO mice as compared to WT

mice. However, this did not induce any observable signs of PAH under basal conditions, even though ADMA levels in DDAH KO mice under basal conditions were significantly higher than in hypoxic WT mice. This finding indicates that DDAH1 deficiency and chronically increased systemic ADMA does not independently induce PAH. The finding that DDAH1 KO mice exhibit significantly elevated pulmonary peripheral artery muscularization, pulmonary fibrosis, RV pressure, and RV hypertrophy in response to hypoxia+SU5416 however, suggests that DDAH1 activity, likely through degradation of ADMA and preserving NO signaling, does attenuate PAH induced by additional pulmonary stress. While our findings clearly indicate that DDAH1 deletion does not induce pulmonary hypertension in the relatively sterile, unstressed, basal conditions of this experiment, it seems plausible, based on the exacerbated response to hypoxia+SU5416, that chronic DDAH1 deficiency could increase risk of PAH development in environmental conditions that introduce more pulmonary stress (i.e. environmental toxins, infection, etc).

While the most obvious protective role of DDAH1 is degrading ADMA, DDAH1 has demonstrated several ADMA independent effects which could also influence PAH. For instance, DDAH1 can promote endothelial cell proliferation through activation of ras and Akt (16). Akt activity is also important for eNOS activity (131), so this may be an additional mechanism of increasing NO formation. While promoting endothelial cell proliferation may help repair damaged endothelium and preserve normal vessel architecture in the early stages of this disease, disorganized endothelial cell proliferation can also exacerbate PAH progression through formation of plexiform lesions (132). In addition, Akt activation promotes smooth muscle cell proliferation that promotes small

artery occlusion (133). Thus, ADMA dependent and independent actions of DDAH1 may have different impacts on PAH pathology depending upon the cell type involved and stage of PAH development.

Because of the important role of NO signaling in attenuating PAH, and because DDAH1 activity is often reduced in this condition, over-expression of DDAH1 might be expected to attenuate PAH. Transgenic DDAH1 over-expressing mice have been produced, and these mice exhibit reduced ADMA levels, and lower systemic vascular resistance (39). In a 2 week hypoxia-induced PAH model, DDAH1tg mice exhibited less vascular remodeling, reversal of pulmonary cGMP reduction, and complete prevention of RV hypertrophy (134). A separate study however, demonstrated that while DDAH1tg mice exhibited improved vasodilation under hypoxia for 3 hours, PAH development was no different from WT mice after 4 weeks hypoxia (135). It is possible that the protective effects of increased DDAH1 are only manifested early in the disease, or that other factors override the protective effects of DDAH1 over-expression during extended hypoxia. Interestingly, our study showed that DDAH1 activity at 3 weeks of hypoxia+SU5416 is reduced approximately 30% in WT mice even though DDAH1 protein levels did not change, indicating the reduced DDAH activity is a result of reduced DDAH1 quality. Previous studies have also shown that DDAH1 activity is inhibited post-translationally by oxidative stress (68) or inflammatory factors (48). Thus, DDAH1 protein levels do not necessarily indicate DDAH1 activity, indicating that maintaining DDAH1 activity as well as DDAH1 expression is likely important for preserving NOS function in PAH.

Our data showing that lung DDAH1 activity was reduced in WT mice by hypoxia+SU5416, and that global (6) or endothelial specific (15) deletion of DDAH1 increases plasma ADMA levels, supports the concept that a reduction in DDAH1 activity contributes to increased ADMA levels. However, plasma ADMA levels were still elevated by hypoxia in DDAH1 KO mice, suggesting additional mechanisms also contribute to elevated ADMA. Expression of the arginine methyl transferase, PRMT3, was increased by hypoxia in both WT and DDAH1 KO mice, and increased arginine methylation may result in further amplified ADMA levels in absence of DDAH1 activity. Because ADMA is derived from proteolysis of proteins containing methylated arginines, increased protein catabolism associated with tissue remodeling may also contribute to increased ADMA. There is also evidence that elevations in systemic ADMA contributes to chronic kidney disease (45), so renal excretion of ADMA might also be impaired in this model, further exacerbating the already elevated plasma ADMA levels.

In addition to attenuating systemic ADMA accumulation and vascular remodeling in the lungs, our data also suggest DDAH1 exerts anti-hypertrophic effects within cardiomyocytes, as indicated by the greater hypertrophy observed in cardio-specific DDAH1 KO mice under apparently equivalent pulmonary arterial pressures. The specific mechanism of DDAH1 protection against cardiomyocyte hypertrophy is currently unknown. Based upon previous studies showing protection against pressure overload induced LV hypertrophy by sildenafil (99, 136) or tetrahydrobiopterin (137), DDAH1 removal of cardiomyocyte ADMA might be expected to exert similar anti-hypertrophic effects by preserving NO synthesis and cGMP production. Right heart failure is a

significant cause of mortality in PAH patients (138), so identifying the specific mechanisms by which DDAH1 protects against RV hypertrophy will be important.

6. Conclusion

Novelty and Significance: Increased ADMA levels and reduced DDAH activity are associated with several cardiovascular diseases, including pulmonary hypertension, but whether these factors cause or contribute to PAH development was not clear.

What Is New? Global and cardiac specific DDAH1 knockout mice were used to examine the impact of DDAH1 in hypoxia+SU5416 induced pulmonary hypertension and right ventricular hypertrophy.

What Is Relevant? Global DDAH1 deletion and chronically increased ADMA did not cause PAH under basal conditions, but exacerbated vascular remodeling and PAH induced by hypoxia+SU5416. Cardiomyocyte DDAH1 attenuated right ventricular hypertrophy without influencing lung remodeling and pulmonary arterial pressure.

7. Summary

Pulmonary arterial hypertension (PAH) is a progressive disease with a very poor prognosis. Recent studies have demonstrated that PAH is associated with diminished nitric oxide (NO) bioavailability, increased level of endogenous nitric oxide synthase (NOS) inhibitor Asymmetric dimethylarginine (ADMA), and decreased lung dimethylarginine dimethylaminohydrolse (DDAH) activity. DDAH1 is essential for degradation of ADMA and for optimal vascular endothelial nitric oxide production, but the impact of DDAH1 in PAH development and subsequent right ventricular (RV) hypertrophy is not clear. The objective of this study is to determine the impact of global DDAH1 gene knockout (KO) and cardiomyocyte restricted DDAH1 gene KO (Cardio-DDAH1 KO) on hypoxia+SU5416 induced PAH development and RV hypertrophy.

Chronic hypoxia and SU5416 result in reduced lung DDAH activity, increased circulating ADMA content, and PAH in wild type mice. Using global DDAH1 KO mice, we demonstrate that DDAH1 KO increases lung and circulating ADMA levels, but this does not cause PAH development in mice under control conditions. However, DDAH1 KO significantly exacerbates chronic hypoxia+SU5416-induced PAH, as indicated by significantly increased RV pressure, more RV hypertrophy, and enhanced pulmonary vascular remodeling in DDAH1 KO mice as compared to wild type mice. In addition, cardiomyocyte specific DDAH1 KO did not exacerbate hypoxia+SU5416-induced increases in RV pressure or lung vascular remodeling, but significant exacerbated hypoxia+SU5416-induced RV hypertrophy in comparison to wild type littermates, indicating that DDAH1 distributed in cardiomyocytes protects against RV hypertrophy independent of increased pulmonary artery pressure.

Collectively, our data indicate that DDAH1 plays an important role in protection against hypoxia+SU5416-induced PAH and RV hypertrophy by attenuating maladaptive pulmonary remodeling and through cardiomyocyte specific anti-hypertrophic effects in the heart.

CHAPTER 2

Effect of adenosine monophosphate-activated protein kinase (AMPK) alpha 2 gene deletion on pulmonary arterial hypertension in mice

1. Introduction

Pulmonary arterial hypertension (PAH) is a life-threatening disease characterized by progressively increasing pulmonary vascular resistance, right heart failure and death. Increased lung vascular smooth muscle cell (VSMC) growth and proliferation is a key cellular event that leads to pathological pulmonary vascular remodeling and right ventricular hypertrophy or failure.

Adenosine monophosphate-activated protein kinase (AMPK) is a heterotrimeric protein complex consisting of a catalytic subunit α (either α1 or α2), and 2 regulatory subunits (β and γ). In response to increased cellular AMP content under metabolic or other stress conditions, AMPK is quickly activated to maintain cellular energy homeostasis (139, 140). AMPK activation reduces energy-consuming processes such as protein translation by inhibiting the mTOR signaling pathway and increasing energy production by enhancing glucose uptake and glycolysis etc (139, 140). Recent studies indicate that AMPK activation may play an important role in attenuating PAH and right ventricular hypertrophy. Igata et al reported that 5-aminoimidazole-4-carboxamide ribonucleoside (AICAR), an activator of AMPK, inhibits human VSMC proliferation (141). AMPK

activation was also shown to inhibit rat VSMC proliferation (142) and limit VSMC protein synthesis under conditions of thromboxane receptor activation (143). In addition, a recent study suggests that mTOR complex 2 promotes VSMC proliferation and survival in part through down-regulation of AMPK (144). While AMPKα1 appears to be the dominant catalytic isoform in smooth muscle cells, several recent studies demonstrated that AMPKα2 (but not AMPKα1) plays the essential role in attenuating vascular smooth muscle cell growth and proliferation (145, 146). Moreover, studies have demonstrated that activation of AMPK is important in attenuating cardiac hypertrophy and heart failure development (147-152). Our previous studies have demonstrated that AMPKα2 plays an important role in attenuating cardiomyocyte hypertrophy and left ventricular failure (147, 150, 151).

Based on the findings that AMPKα2 attenuates VSMC proliferation and cardiomyocyte hypertrophy (145-148), we reasoned that AMPKα2 might play a role in attenuating hypoxia-induced PAH and right ventricular hypertrophy. Consequently, the effect of AMPKα2 gene knockout on hypoxia induced PAH in mice was studied.

2. Materials and Methods

AMPKα2 knockout (KO) mice

AMPK α2 mice and control wild type mice used in the present study are described previously (147, 150 153). This study was approved by the Institutional Animal Care and Use Committee of University of Minnesota.

Hypoxia and Sugen5416-induced PAH in mice

Male mice ages 3-5 months were exposed to hypobaric hypoxia (154). Briefly, the pressure in the hypobaric chamber was decreased progressively from 0.8 atm (16.9% oxygen) on day 1 to 0.5 atm (10.5% oxygen) after day 7 for adaptation and was maintained at 10.5% oxygen for 2 more weeks as illustrated in Figure 1A. The chamber was opened once every week for cleaning, feeding, and injection. The mice in the hypoxia group received subcutaneous weekly injection of Sugen-5416 (25mg/kg, R&D Systems) (155). After hypoxic exposure for total 3 weeks, determination of RV pressure and hypertrophy was performed as described. The mice in sham group were kept in normobaric conditions for 3 weeks.

Measurements of RV hemodynamics

At the end of the study protocol, mice were anesthetized with 2% isoflurane. Mice were intubated with a 20-gauge Teflon tube attached to a MiniVent type 845 mouse ventilator (Hugo Sachs Elektronik) (ventilator settings: breathing frequency, 80 breaths per minute; pressures, 9/0 cm H_2O; inspiratory/expiratory ratio, 1:1). RV hemodynamics were determined at open-chest by a 1.2-F pressure catheter (Scisense Inc, Ontario Canada) (156, 157).

Sample Preparation

After the final hemodynamic assessment, the mice were euthanized by exsanguination. Before sample collection, the lungs were perfused with 6 ml of Calcium and magnesium free phosphate buffered saline through the right ventricle. The upper right lobe of lung was inflated through the trachea and then fixed in 10% buffered formalin for histological analysis. The other lung tissue was harvested and stored in -80°C freezer for biochemical analysis. The wet weights of RV and left ventricle (LV) + septum (S) were weighed and the ratios of RV weight to LV + S were determined (157)

Histological staining, evaluation of lung vascular muscularization, lung fibrosis and RV fibrosis

For histological staining, tissues were sectioned to 5μm. The relative pulmonary vascular muscularization was determined by H&E staining. Briefly, 60 intra-acinar arteries (50-200 μm) were examined per mouse. Intra-acinar arteries with a complete medial coat of muscle were categorized as Fully Muscular (FM) arteries. Intra-acinar arteries with only a crescent of muscle were defined as partially muscular (PM) arteries. Intra-acinar arteries with no apparent muscle were defined as nonmuscular (NM) arteries as previously described (155, 157).

RV sections were stained with Sirius Red (Sigma) for detection of fibrosis. Lung fibrosis was stained using Modified Masson's Trichrome Stain Kit (Scy Tek laboratories). The percent volume fibrosis for lung and ventricular fibrosis was determined using the method described previously (156, 158). Lung sections were also stained with monoclonal antibody to identify leucocytes using an antibody against CD45. Briefly, tissue sections were deparaffinized and rehydrated in PBS. The sections were incubated with 3% H_2O_2 in PBS for 20 minutes, followed by 3% BSA solution for 1 hour. Sections were then incubated with corresponding monoclonal primary antibody (1:400) overnight at 4^{o}C, followed by incubation with avidin/biotin peroxidase-linked secondary antibody (1:1000) (Invitrogen). Staining was visualized using an avidin/biotin peroxidase-linked detection system (Vector Laboratories, Burlingame, CA).

Western Blots and Chemical Analysis

Protein extracts from different groups of lung were fractionated on a polyacrylamide gel, transferred to nitrocellulose membranes, and probed with various antibodies. Total AMPK activity of lung tissues was measured as previously described (147).

Data and Statistical Analysis

All values were expressed as mean ± standard error. Data from two groups was compared with an unpaired t-test. Two-way ANOVA was used to test for differences between KO and wild type animals under sham conditions and after hypoxia+SU5416-induced PAH. Post hoc pairwise comparisons were made using the Fisher least significant difference test. Statistical significance was defined as $p<0.05$.

3. Results

AMPKα2 KO had no detectable effect on RV pressure and RV hypertrophy

The bodyweight was monitored weekly as presented in Figure 1B. The result indicates that hypoxia caused a significant but similar reduction of bodyweight in both wild type and AMPKα2 KO mice. We assessed RV pressure as a surrogate of the pulmonary arterial pressure in each group. RV systolic pressure, RV end-diastolic pressure, RV dp/dtmax, RV dp/dtmin and heart rate were not different between AMPKα2 KO mice and wild type controls under sham conditions (Figure 1C-H). AMPKα2 KO also had no detectable effect on RV hypertrophy under sham conditions as indicated by the similar ratio of RV weight to LV (LV+ septum) weight between AMPKα2 KO mice and wild type mice, as well as comparable RV weight, and RV weight ratios to bodyweight, or tibial length (Figure 2B,).

AMPKα2 KO aggravated the hypoxia+SU5416-induced increase of RV pressure

Interestingly, AMPKα2 KO significantly exacerbated hypoxia-induced increases of RV systolic pressure (Figure 1D), RV dp/dtmax, (Figure 1F), and RV dp/dtmin (Figure 1G). AMPKα2 KO did not affect RV diastolic pressure and heart rate in mice after chronic hypoxia+SU5416 (Figure 1E and H).

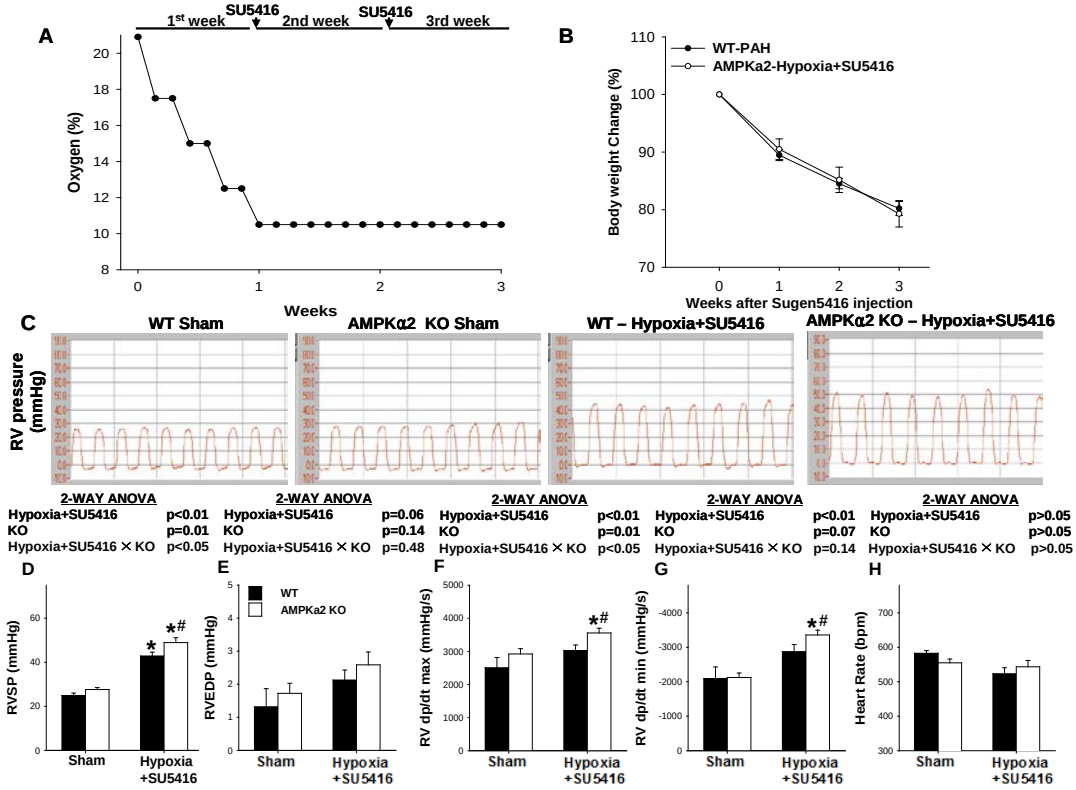

Figure 1. AMPKα2 knockout aggravated the hypoxia+SU5416-induced increase of RV pressure. Wild type or AMPKα2 KO mice were exposed to normoxic conditions or hypoxia+SU5416 treatment for 3 weeks (A), and the change (%) of body weight were determined (B). RV pressure measurements were obtained by catheterization of the right ventricle. Reprentative RV pressure tracings from wild type and AMPK α2 KO mice exposed to sham or hypoxia+SU5416 conditions are shown in (C) Right ventricular systolic pressure (D), right ventricular end-diastolic pressure (E), right ventricular dp/dtmax (F), right ventricular dp/dtmin (G), heart rate (H) were calculated from 7-9 mice in each group. * indicates $p<0.05$ comparing hypoxia+SU5416 to sham. # indicates $p<.05$ comparing WT to KO.

AMPKα2 KO exacerbated the hypoxia+SU5416-induced increase of RV hypertrophy and fibrosis

Consistent with the greater increase of RV systolic pressure in AMPKα2 KO mice after hypoxia+SU5416, AMPKα2 KO mice exhibited greater increase in RV to body weight ratio (1.45 ± 0.06mg/g in wild type hypoxia+SU5416 group versus 1.72 ± 0.07mg/g in KO hypoxia+SU5416 group; $p<0.05$) (Figure 2A) and RV to LV + septum ratio (0.39 ± 0.01 in wild type hypoxia+SU5416 versus 0.45 ± 0.02 in KO hypoxia+SU5416; $p<0.05$) (Figure 2B) after hypoxia+SU5416, indicating that AMPKα2 KO exacerbated hypoxia-induced RV hypertrophy. Histological analysis indicated that hypoxia increased RV fibrosis to a greater degree in AMPKα2 KO mice compared to wild type mice (5.67 ± 0.54 % in wild type mice versus 7.35 ± 0.43 % in AMPKα2 KO mice; $p<0.05$) (Figure 2E and F).

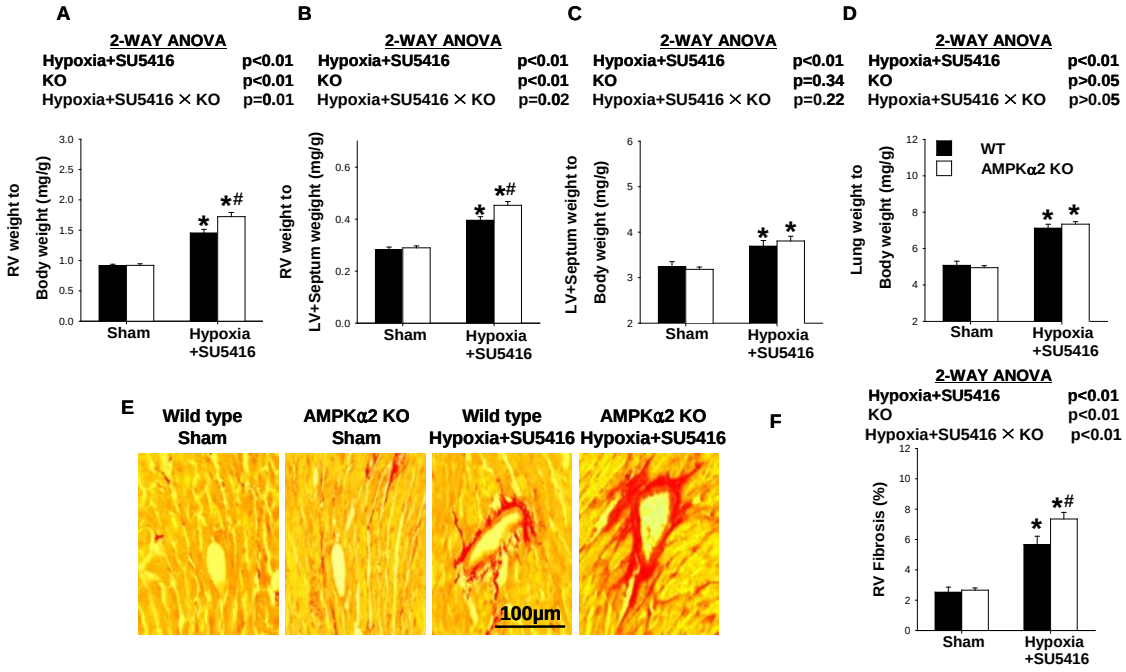

Figure 2. AMPKα2 KO exacerbated the hypoxia+SU5416-induced increase of RV hypertrophy and fibrosis. After 3 week exposure to hypoxic+SU5416 or sham conditions, hearts and lungs were collected. Right ventricle weight to body weight ratio (A), right ventricle weight to left ventricle + septum weight (B), left ventricle weight septum to body weight ratio (C), and lung weight to body weight ratio (D). For analysis of right ventricular fibrosis, right ventricular tissue was fixed and stained with Sirius red reagent (E). Percent fibrotic tissue was calculated from 5 samples in each group (F). * indicates $p<0.05$ comparing hypoxia+SU5416 to sham. # indicates $p<.05$ comparing WT to KO.

AMPKα2 KO exacerbated hypoxia+SU5416-induced pulmonary vascular remodeling

To determine the effect of AMPKα2 KO on pulmonary vascular remodeling, we determined the percentage of non-muscularized (NM), partially muscularized (PM), and fully muscularized small arteries (FM) in wild type mice and AMPKα2 KO mice under sham conditions and 3 weeks after hypoxia+SU5416 (Figure 3A and B). Under control conditions, the percentage of nonmuscularized, partially muscularized and fully muscularized small arteries in lung tissues was not different between wild type mice and AMPKα2 KO mice (Figure 3A and B). Exposure to hypoxia+SU5416 caused increases in fully muscularized small arteries in wild type and AMPKα2 KO mice (Figure 3B). The increases were greater in the AMPKα2 KO mice ($p < 0.05$)(Figure 3B). As expected, hypoxia also resulted in decreased non-muscularized small arteries in wild type and AMPKα2 KO mice (Figure 3B). Again, the loss of non-muscularized small arteries was greater in AMPKα2 KO mice ($p < 0.05$)(Figure 3B).

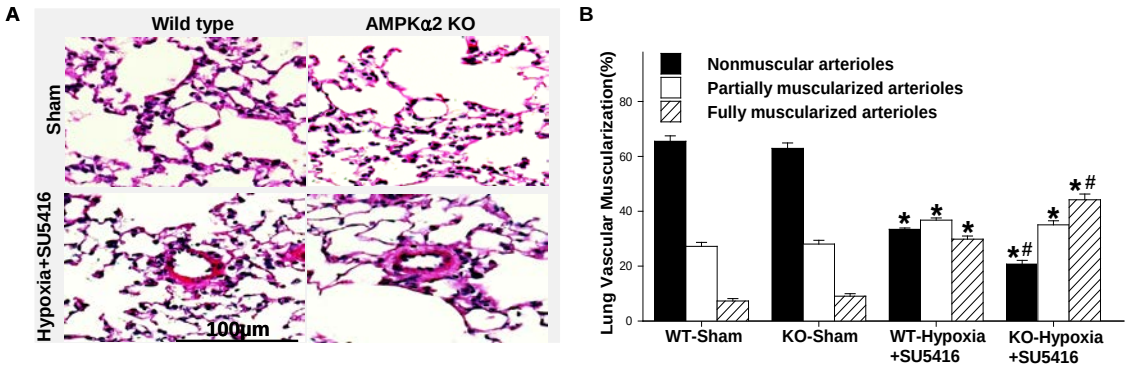

Figure 3. AMPKα2 KO exacerbated hypoxia+SU5416-induced pulmonary vascular remodeling and fibrosis. Lungs from wild type and AMPKα2 KO mice exposed to sham or hypoxia+SU5416 conditions were flushed, fixed in formalin, and stained using eosin-hemotoxylin for analysis of pulmonary vessel muscularization. Representative images are shown in (A) and average percent of non-muscularized, partially muscularized, and completely muscularized pulmonary arterioles were calculated from 5 samples in each group (B). * indicates $p<0.05$ comparing hypoxia+SU5416 to control. # indicates $p<.05$ comparing WT to KO.

AMPKα2 KO significantly exacerbated the hypoxia+SU5416-induced lung fibrosis

Fibrosis was detected by Masson trichrome staining under sham conditions and 3 weeks post hypoxia+SU5416. Lung fibrosis was comparable between AMPKα2 KO mice and wild type under sham conditions. Hypoxia+SU5416 caused lung fibrosis in both wild type mice and AMPKα2 KO mice, but the increase was significantly greater in the AMPKα2 KO mice than in the wild type mice ($p < 0.05$) (Figure 4A and B). In addition, Western blotting showed that hypoxia+SU5416 caused significantly more increase of lung collagen-III protein content in AMPKα2 KO mice than in wild type mice (Figure 4C and D).

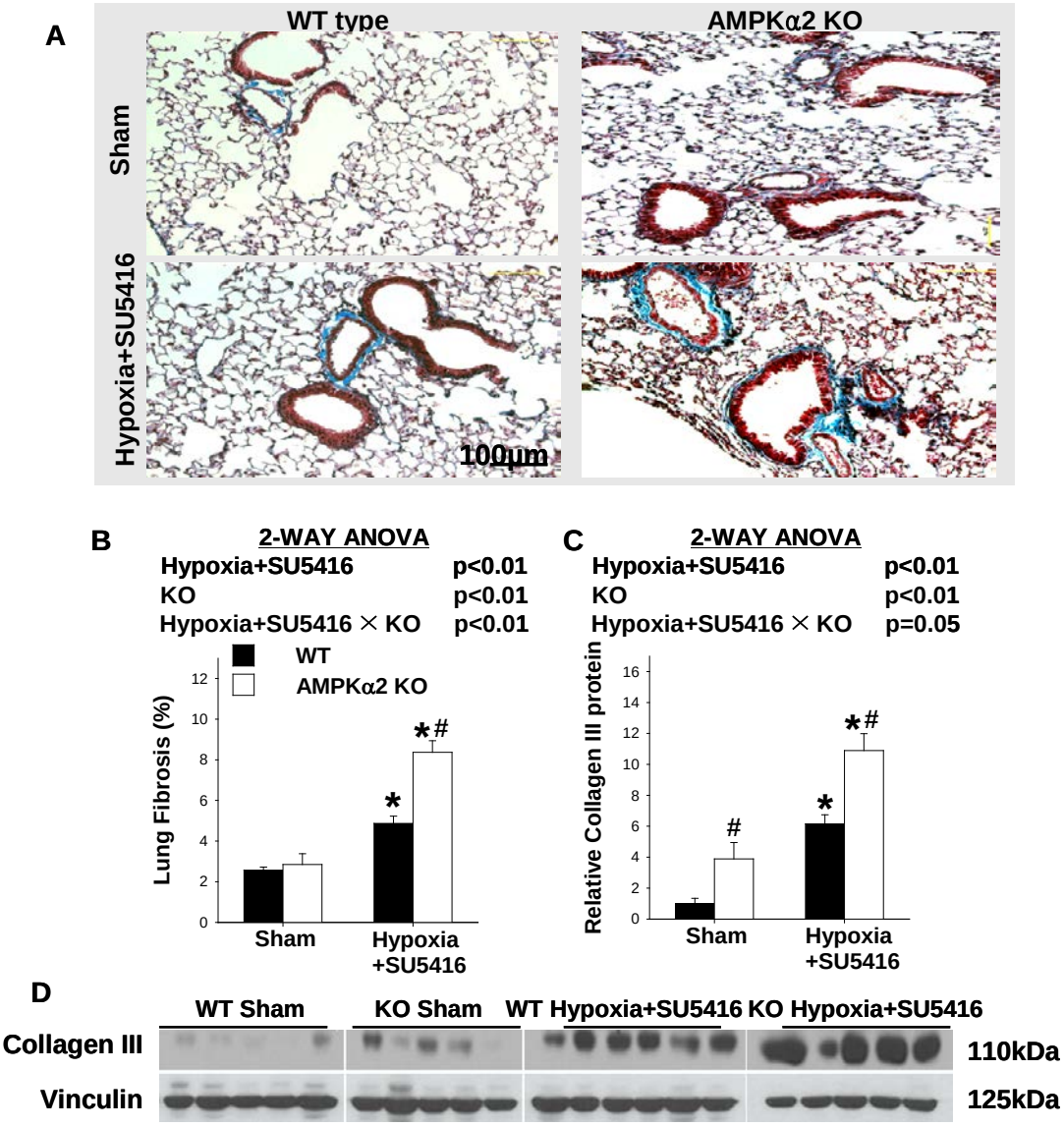

Figure 4. AMPKα2 KO exacerbated the hypoxia+SU5416-induced lung fibrosis. Lungs from wild type and AMPKα2 KO exposed to sham or hypoxia+SU5416 conditions were collected and fixed and analyzed for fibrosis using Trichrome stain. Representative images are shown in (A). Average percent lung fibrosis was calculated (B). Lungs were also analyzed by western blot for expression of type III collagen or vinculin (as a loading control) (D). Expression levels of the indicated proteins were analyzed by densitometry

from 5 animals in each group (C). * indicates $p<0.05$ comparing hypoxia+SU5416 to sham. # indicates $p<.05$ comparing WT to KO.

AMPKα2 KO exacerbated hypoxia+SU5416-induced pulmonary inflammation and increased lung VCAM-1 expression

Histological analysis did not reveal any noticeable increase of lung leukocyte infiltration in AMPKα2 KO mice under sham condition. Hypoxia+SU5416 caused lung leucocyte accumulation (as indicated by the staining of CD45) in both wild type mice and AMPKα2 KO mice, but the increase was significant greater in the AMPKα2 KO mice than in the wild type mice (Figure 5A and C), suggesting AMPKα2 plays a role in limiting hypoxia+SU5416-induced pulmonary inflammation.

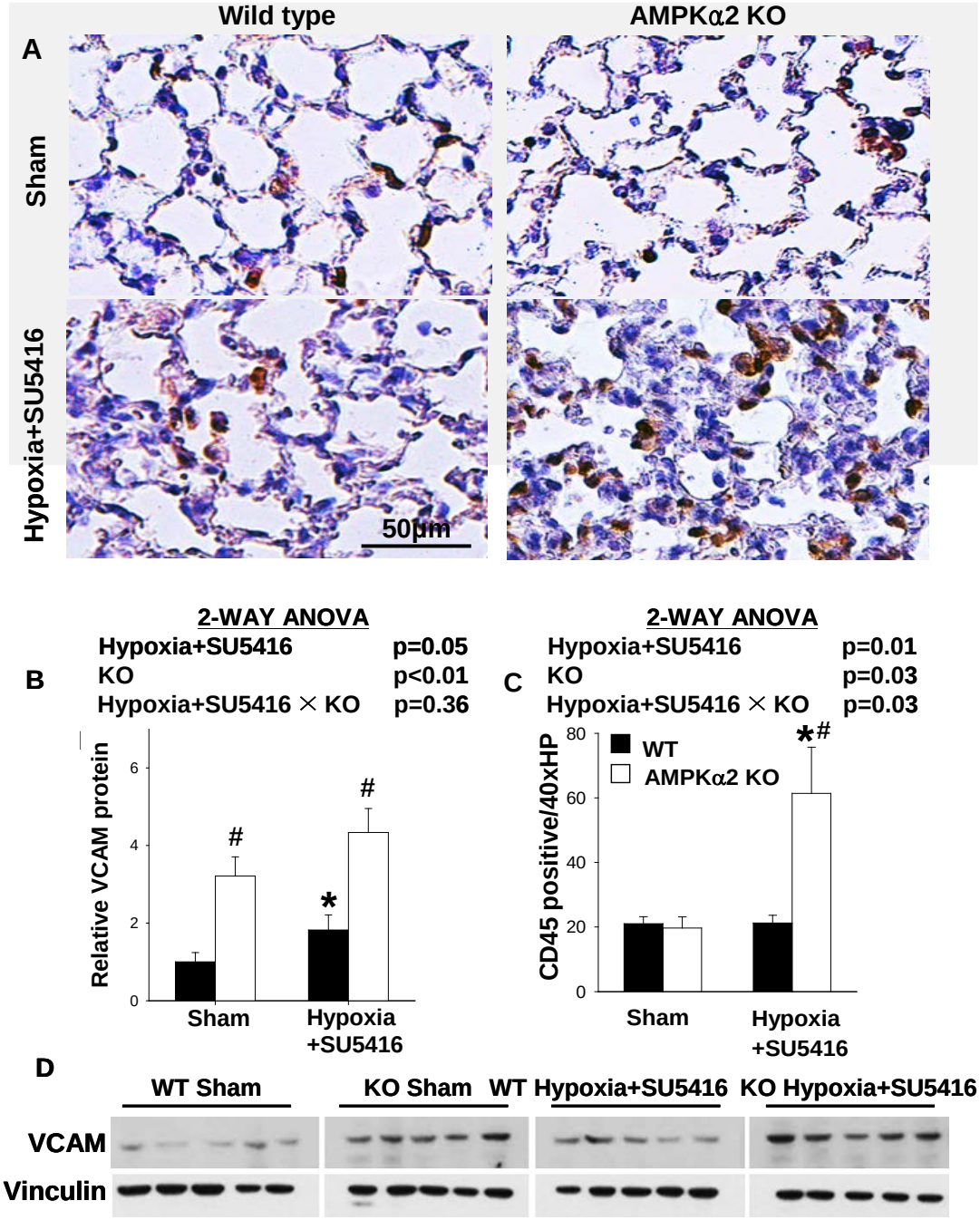

Figure 5. AMPKα2 KO exacerbated hypoxia+SU5416-induced pulmonary inflammation. Lungs from wild type and AMPKα2 KO exposed to sham or hypoxia+SU5416 conditions were collected and fixed and stained CD45 for leucocytes. Representative images are shown in (A). Count of leucocytes was calculated (C). Lungs were also analyzed by

western blot for expression of VCAM-1 (vinculin as a loading control) (D). Expression levels of VCAM-1 were analyzed by densitometry (C). * indicates $p<0.05$ comparing hypoxia+SU5416 to sham.

Effect of AMPKα2 KO on lung AMPK activity

Western blot showed that AMPKα2 KO abolished lung AMPKα2 expression as expected. Interestingly, AMPKα2 KO resulted in up-regulation of lung AMPKα1 expression under both sham conditions and after hypoxia+SU5416. Hypoxia+SU5416 caused no change of lung AMPKα2 expression in wild type mice but significant increased lung AMPKα1 expression in both wild type and AMPKα2 KO mice (Figure 6A – C), consistent with the notion that AMPKα1 is highly inducible (9)**.** Total AMPK activity was also determined (Figure 6D). To our surprise, lung AMPK activity did not decrease, but significantly increased in AMPKα2 KO mice under both sham conditions and after hypoxia+SU5416 (Figure 6D), suggesting increased AMPKα1 can maintain and even increase overall AMPK activity in absence of AMPKα2.

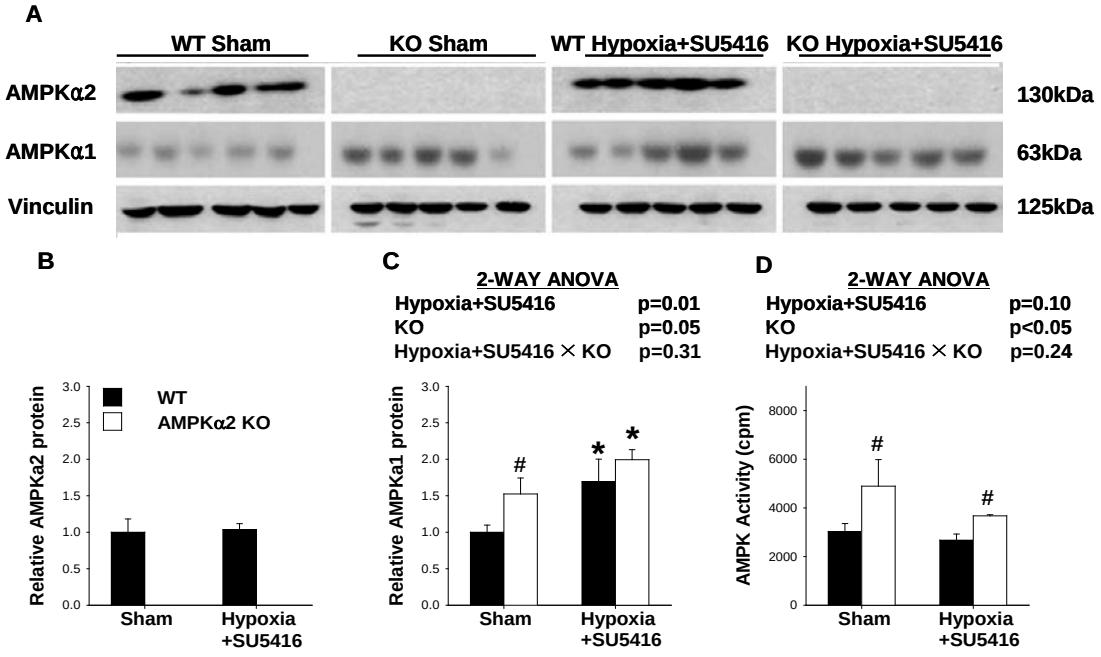

Figure 6. AMPK α2 KO did not decrease lung AMPK activity. Lungs from wild type and AMPKα2 KO exposed to sham or hypoxia+SU5416 conditions were collected and analyzed by western blot for expression of AMPKα2, AMPKα1 and vinculin (A). Expression levels of the indicated proteins were analyzed by densitometry (B and C). Total AMPK kinase activity was measured by immuno-precipitation of AMPK from lung lysates and incorporation of radioactivity from [^{32}P]ATP into SAMs peptide (D) (n=5 each group). * indicates $p<0.05$ comparing hypoxia+SU5416 to sham. # indicates $p<.05$ comparing WT to KO.

AMPKα2 KO significantly increased lung p70S6K and p-S6.

Because previous studies demonstrated that AMPK regulates activity of the p70SK/S6 signaling pathway that drives smooth muscle and cardiomyocyte hypertrophy, we further determined the expressions of total and phosphorylated p70S6K and S6 in lung tissues. The results showed that hypoxia+SU5416 caused significant increases of lung p-70S6K and p-S6 protein in AMPKα2 KO mice (Figure 7A - C).

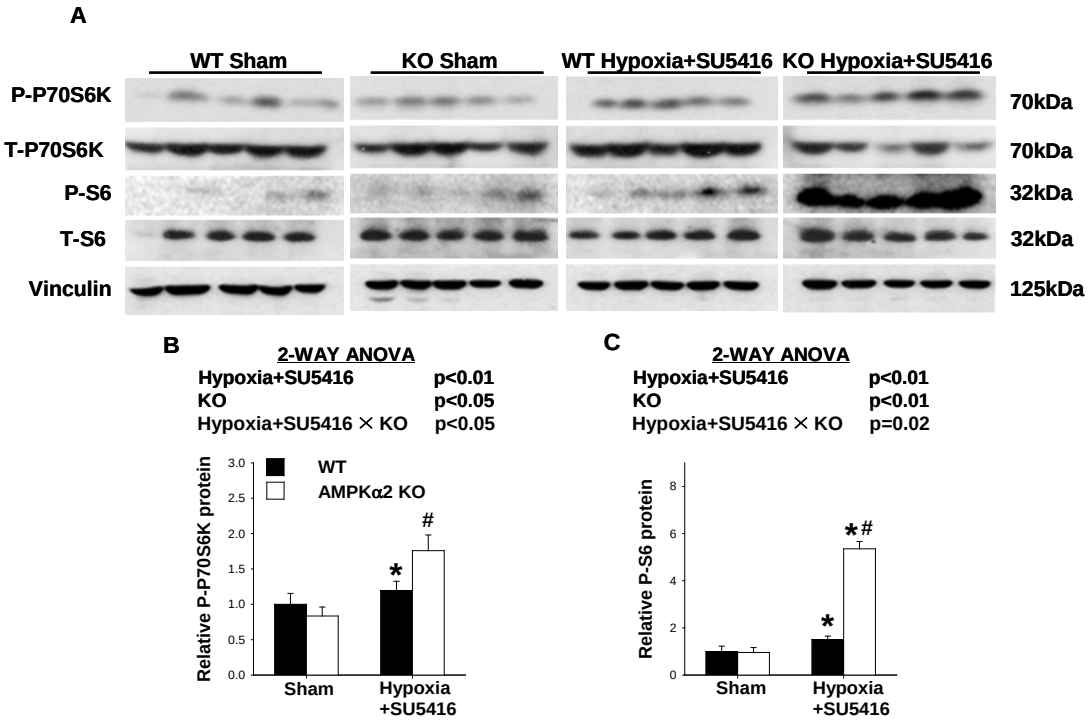

Figure 7. AMPKα2 KO up regulated phosphorylation of pulmonary mTOR complex 1 and its downstream targets in mice after hypoxia+SU5416. Lungs from wild type and AMPKα2 KO exposed to sham or hypoxia+SU5416 conditions were collected and analyzed by western blot for phosphorylated and total p70S6k, and S6 ribosomal protein, as well as vinculin as a loading control (A). Expression levels of the indicated proteins were analyzed by densitometry (B and C). * indicates $p<0.05$ comparing hypoxia+SU5416 to control. # indicates $p<.05$ comparing WT to KO.

4. Discussion

This study demonstrates for the first time that AMPKα2 plays an important role in attenuating development of PAH and right ventricular hypertrophy, at least in the Sugen/hypoxia model. Our data indicate that genetic disruption of AMPKα2 has no observable influence on pulmonary structure or right ventricular hemodynamics under basal conditions, but significantly exacerbates muscularization of pulmonary arteries, lung fibrosis, and pulmonary vascular resistance (as indicated by increased RV pressure) in response to hypoxia+SU5416. The development of PAH in AMPKα2 KO mice was associated with significant up-regulation of lung p70S6k activity, as well as increased expression of VCAM-1. This suggests that deletion of AMPKα2 promotes pro-growth and inflammatory signaling pathways. The maladaptive response to hypoxia+SU5416 in AMPKα2 KO mice occurred despite up-regulation of AMPKα1 and increased overall levels of AMPK activity. This suggests that AMPKα2 protects against the development of PAH independent of the total lung AMPK activity.

Pulmonary arterial hypertension is associated with pulmonary VSMC proliferation. Recent evidence suggests that VSMC proliferation is regulated by AMPK. For example, AMPK activation was shown to inhibit growth factor-induced VSMC proliferation through up-regulation of cell cycle inhibitors (141, 142), and block cell migration by preserving expression of cell-cell adhesion molecule cadherin (145). In addition, there is evidence that mTOR signaling, which is inhibited by AMPK, plays an important role in hypoxia and growth factor-induced VSMC proliferation (157, 158). We report that AMPKα2 disruption up-regulates phosphorylation of pulmonary mTOR complex 1 targets p70s6k^{Thr389}, up-regulates phosphorylation of ribosomal protein S6^{Ser235}, and increases pulmonary

arteriole muscularization in response to hypoxia+SU5416. This is consistent with a role for AMPKα2 in limiting VSMC proliferation, in part, by down-regulating mTOR activity.

AMPKα2 may also play a direct role in limiting lung inflammation. We found that VCAM-1 expression is elevated in AMPKα2 KO lungs under basal conditions and even further up-regulated in response to hypoxia+SU5416. VCAM-1 is a cell adhesion molecule expressed on vascular endothelial cells, usually in response to inflammatory cytokines such as TNFα and Il-1β. VCAM-1 promotes tight adhesion of leukocytes to the vessel wall, and plays an important role in recruitment of circulating monocytes to sites of tissue injury. In hypoxia+SU5416-induced PAH, a prolonged inflammatory response appears mostly as a consequence of a pro-inflammatory microenvironment within and surrounding the pulmonary arteries (159). While increased VCAM-1 expression in AMPKα2 KO lungs did not cause an observable influx of leucocytes under basal conditions, pulmonary vessels of AMPKα2 KO mice appear to be predisposed to increased leukocyte adhesion during hypoxic stress, as suggested by the high number of CD45 positive cells observed in AMPKα2 KO lungs after exposure to hypoxia+SU5416. In further support of AMPK regulation of vascular inflammation, metformin, an activator of AMPK, down-regulated activity of the inflammatory mediator NF-κβ (160) and reduced VCAM expression in endothelial cells (161).

AMPKα2 KO also exacerbated pulmonary fibrosis in response to hypoxia+SU5416. This finding can be interpreted together with the observation that VCAM-1 expression was elevated under basal conditions and that fibrosis in the lung was most evident surrounding pulmonary vessels. It implies that AMPKα2 disruption promotes a proliferative, pro-inflammatory micro-environment in and around the pulmonary

vasculature, that may elevate basal fibroblast proliferation or collagen synthesis. It is also possible that increased VCAM-1 expression in AMPKα2 KO promotes the recruitment of recently described monocyte-derived mesenchymal cells that synthesize collagen and contribute to vascular remodeling in hypoxia (162, 163). The increased collagen synthesis and VCAM-1 expression in AMPKα2 KO mice under control conditions suggests that these mice may be predisposed to vascular remodeling and fibrosis of PAH in response to additional stress, such as Sugen/hypoxia.

The greater development of PAH in AMPKα2 KO mice, despite increased AMPKα1 expression and no reduction of overall AMPK activity suggests AMPKα2 plays a critical role in adaptation to hypoxic stress that is not compensated for by increased AMPKα1 expression. While puzzling at first glance, these findings are consistent with recent studies identifying a specific role for AMPKα2, but not AMPKα1, in VSMC proliferation and vascular remodeling. For instance, Song et al. demonstrated that while AMPKα1 accounts for approximately 90% of total AMPKα subunits in mouse VSMCs, deletion of AMPKα2, but not AMPKα1 reduced expression of the cell cycle inhibitor p27 and enhanced VSMC proliferation[8]. AMPKα2 KO but not AMPKα1 KO, also promoted VSMC migration (145). On the other hand, AMPKα1 has distinct roles compared to AMPKα2 in myogenesis (168), regulation of the cystic fibrosis transmembrane conductance regulator in epithelial cells (169), and targeting Na/K-ATPase endocytosis in response to hypoxia (170). Thus, AMPKα1 and AMPKα2 likely exhibit both distinct and overlapping functions. Our findings demonstrate for the first time that AMPKα2 plays an important role in attenuating Sugen/hypoxia-induced PAH.

Not surprisingly, hypoxia+SU5416-induced RV hypertrophy was exacerbated in AMPKα2 KO mice. Increased RV hypertrophy in the AMPKα2 KO mice is likely due not only to increased RV systolic afterload caused by worse PAH, but also may be attributed to loss of the anti-hypertrophic influence of AMPKα2 in cardiomyocytes. Indeed, our previous study demonstrated that AMPKα2 KO mice exhibit elevated mTORC1 signaling and develop greater hypertrophy and heart failure in response to the same systolic pressure overload as compared to wild type mice (147). AMPK also attenuated phenylephrine-induced cardiomyocyte hypertrophy in vitro (152). While our combined studies indicate AMPKα2 not only attenuates RV hypertrophy through reducing afterload (by decreased lung vascular remodeling) and direct attenuated cardiomyoycte hypertrophy, we are unable to determine how much the increased right ventricular hypertrophy in AMPKα2 KO mice can be attributed to increased pulmonary vascular resistance or to increased sensitivity of cardiomyocytes to hypertrophic stimuli. In addition, while evidence suggests that AMPKα2 KO promotes VSMC proliferation, a key event in development of PAH, the involvement and cooperation of multiple cell types in progression of PAH make it difficult to identify which specific cellular response (i.e. VSMC proliferation, inflammation, fibrosis) aggravated by AMPKα2 disruption is most responsible for exacerbating PAH in global AMPKα2 KO mice.

5. Conclusion

What Is New?

AMPKα2 knockout exacerbated hypoxia+SU5416-induced pulmonary hypertension, lung vascular remodeling and right ventricular hypertrophy in mice. This protective role of AMPKα2 against pulmonary hypertension appears independent of total lung AMPK activity.

What Is Relevant?

This study demonstrates that proper AMPKα2 signaling is important in protecting against hypoxia+SU5416-induced pulmonary hypertension, lung vascular remodeling and right ventricular hypertrophy.

6. Summary

Pulmonary arterial hypertension (PAH) is characterized by vascular remodeling and right ventricular hypertrophy. Adenosine monophosphate kinase alpha 2 subunit (AMPKα2) protects against vascular remodeling and cardiac hypertrophy, yet the role of AMPKα2 in the development of PAH is unclear. Here we examined the role of AMPKα2 in Sugen/hypoxia-induced PAH in mice utilizing an AMPKα2 knockout (KO) mouse strain. Under normoxic conditions, AMPKα2 KO had no observable effect on pulmonary vascular remodeling, right ventricular pressure, or right ventricular hypertrophy in comparison to wild type mice. However, in response to hypoxia plus VEGF antagonist Sugen-5416, AMPKα2 KO mice exhibited increased vascular remodeling (i.e. muscularization of small pulmonary arteries), leucocyte infiltration, pulmonary fibrosis, and right ventricular pressure, leading to increased right ventricular hypertrophy. The impaired ability of AMPKα2 KO mice to adapt to hypoxic stress was associated with increased phosphorylation of mTORC1 targets p70S6 kinase^{Thr389} and S6 ribosomal protein^{Ser235}, as well as increased expression of Vascular Cell Adhesion Molecule-1 (VCAM-1). Surprisingly, disruption of AMPKα2 did not result in a significant loss in overall AMPK activity, which was partially compensated for by increased AMPKα1 expression. Our data indicate that AMPKα2 attenuates hypoxia-induced pulmonary hypertension, in part by reducing mTORC1 signaling and leukocyte recruitment. This protective role of AMPKα2 against PAH appears independent of the AMPK activity.

References

1. Archer SL, Weir EK, Wilkins MR. Basic science of pulmonary arterial hypertension for clinicians: new concepts and experimental therapies. Circulation. 2010;121(18):2045-2066.
2. Morrell NW, Adnot S, Archer SL, Dupuis J, Jones PL, MacLean MR, McMurtry IF, Stenmark KR, Thistlethwaite PA, Weissmann N, Yuan JX, Weir EK. Cellular and molecular basis of pulmonary arterial hypertension. J Am Coll Cardiol. 2009;54:S20-31.
3. Khoo JP, Zhao L, Alp NJ, Bendall JK, Nicoli T, Rockett K, Wilkins MR, Channon KM. Pivotal role for endothelial tetrahydrobiopterin in pulmonary hypertension. Circulation. 2005;111(16):2126-2133.
4. Stasch JP, Evgenov OV. Soluble quanylate cyclase stimulators in pulmonary hypertension. Handb Exp Pharmacol. 2013;218:279-313.
5. Preston IF, Suissa S, Humbert M. New perspectives in long-term outcomes in clinical trials of pulmonary arterial hypertension. Eur Respir Rev. 2013;22(130):495-502.
6. Hu X, Atzler D, Xu X, Zhang P, Guo H, Lu Z, Fassett J, Schwedhelm E, Boger RH, Bache RJ, Chen Y. Dimethhylarginine dimethylaminohydrolase-1 is the critical enzyme for degrading the cardiovascular risk factor asymmetrical dimethylarginine. Arterioscler Thromb Vasc Biol. 2011;31(7):1540-1546.
7. Millatt LJ, Whitley GS, Li D, Leiper JM, Siragy HM, Carey RM, Johns RA. Evidence for dysregulation of dimethylarginine dimethylaminohydrolase I in chronic hypoxia-induced pulmonary hypertension. Circulation. 2003;108:1493-1498.
8. Sasaki A, Doi S, Mizutani S, Azuma H. Roles of accumulated endogenous nitric oxide synthase inhibitors, enhanced arginase activity, and attenuated nitric oxide synthase

activity in endothelial cells for pulmonary hypertension in rats. Am J Physiol lung Cell Mol physiol. 2007;292:L1480-1487.

9. Kielstein JT, Bode-Boger SM, Hesse G, Martens-Lobenhoffer J, Takacs A, Fliser D, Hoeper MM. Asymmetrical dimethylarginine in idiopathic pulmonary arterial hypertension. Arterioscler Thromb Vasc Biol. 2005;25:1414-1418.
10. Boger RH. The emerging role of asymmetric dimethylarginine as a novel cardiovascular risk factor. Cardiovasc Res. 2003;59:824-833.
11. Ogawa T, Kimoto M, Sasaoka K. Occurrence of a new enzyme catalyzing the direct conversion of NG, NG-dimethyl-L-arginine to L-citrulline in rats. Biochem Biophys Res Commun. 1987;148:671-677.
12. Ding H, Wu B, Wang H, Lu Z, Yan J, Wang X, Shaffer JR, Hui R, Wang DW. A novel loss-of-function DDAH1 promoter polymorphism is associated with increased susceptibility to thrombosis stroke and coronary heart disease. Circ Res. 2010;106:1145-1152.
13. Valkonen V-P, Tuomainen T-P, Laaksonen R. DDAH gene and cardiovascular risk. Vasc Med. 2005;10:S45-S48.
14. Leiper JM, Santa Maria J, Chubb A, MacAllister RJ, Charles IG, Whitley GS, Vallance P. Identification of two human dimethylarginine dimethylaminohydrolases with distinct tissue distributions and homology with microbial arginine deiminases. Biochem J. 1999;343:209-214.
15. Hu X, Xu X, Zhu G, Atzler D, Kimoto M, Chen J, Schwedhelm E, Luneburg N, Boger RH, Zhang P, Chen Y. Vascular endothelial-specific dimethylarginine dimethylaminohydrolase-1-deficient mice reveal that vascular endothelium plays an important role in removing asymmetric dimethylarginine. Circulation. 2009;120:2222-2229.

16. Zhang P, Hu X, Xu X, Chen Y, Bache RJ. Dimethylarginine dimethylaminohydrolase 1 modulates endothelial cell growth through nitric oxide and Akt. Arterioscler Thromb Vasc Biol. 2011;31:890-897.

17. Arrigoni FI, Vallance P, Haworth SG, Leiper JM. Metabolism of asymmetric dimethylarginines is regulated in the lung developmentally and with pulmonary hypertension induced by hypobaric hypoxia. Circulation. 2003;107:1195-1201.

18. Gray GA, Patrizio M, Sherry L, Miller AA, Malaki M, Wallace AF, Leiper JM, Vallance P. Immunolocalisation and activity of DDAH I and II in the heart and modification post-myocardial infarction. Acta Histochem. 2010;112:413-423.

19. Hu T, Chouinard M, Cox AL, et al. Farnesoid X receptor agonist reduces serum asymmetric dimethylarginine levels through hepatic dimethylarginine dimethylaminohydrolase-1 gene regulation. J Biol Chem. 2006;281:39831-8.

20. Voelkel NF, Quaife RA, Leinwand LA, et al. Right ventricular function and failure: report of a National Heart, Lung, and Blood Institute working group on cellular and molecular mechanisms of right heart failure. Circulation. 2006;114:1883-91.

21. Rich S, Kaufmann E, Levy PS. The effect of high doses of calcium-channel blockers on survivial in primary pulmonary hypertension. N Engl J Med. 1992;327:76-81

22. Sitbon O, Humbert M, Jais X, et al. Long-term response to calcium channel blockers in idiopathic pulmonary arterial hypertension. Circulation. 2005;111:3105-11.

23. Archer S, Rich S. Primary pulmonary hypertension: a vascular biology and translational research “Work in progress.” Circulation. 2000;102:2781-91.

24. Chatterjee A, Black SM, Catravas JD. Endothelial nitric oxide (NO) and its pathophysiologic regulation. Vascul Pharmacol. 2008;49:134-140.

25. Mandegar M, Fung YC, Huang W, Remillard DV, Rubin LJ, Yuan JX. Cellular and molecular mechanisms of pulmonary vascular remodeling: role in the development of pulmonary hypertension. Microvasc. Res. 2004;68:75-103.

26. Furchgott RF. Studies on endothelium-dependent vasodilation and the endothelium-derived relaxing factor. Acta Physiol Scand 1990;139:257-70.

27. Furchgott RF, Zawadzki JV. The obligatory role of endothelial cells in the relaxation of arterial smooth muscle by acetylcholine. Nature 1980;288:373-6.

28. Palmer RMJ, Ashton DS, Moncada S. Vascular endothelial cells synthesize nitric oxide from L-arginine. Nature 1988:333:664-6.

29. Moncada S. The L-arginine: nitric oxide pathway. Acta Physiol Scand 1992;145:201-227.

30. Petros A, Bennett D, Vallance P. Effect of nitric oxide synthase inhibitors on hypotension patients with septic shock. Lancet 1991;338:1557-1558.

31. Vallance P, Moncada S. Role of endogenous nitric oxide in septic shock. New Horiz 1993;1:77-86.

32. Schulz R, Nava E, Moncada S. Induction and potential biological relevance of a Ca^{2+} independent nitric oxide synthase in the myocardium. Br J Pharmacol 1992;105:575-80.

33. Belder AJ, Radomski MW, Why HJF, et al. Nitric oxide synthase activities in human myocardium. Lancet 1993;341:84-5.

34. Wright CE, Rees DD, Moncada S. Protective and pathological roles of nitric oxide in endotoxin shock. Cardiovasc Res 1992;26:48-57.

35. Boerth NJ, Dey NB, Cornwell TL Lincoln TM. Cyclic GMP-dependent protein kinase regulates vascular smooth muscle cell phenotype. J Vasc Res 1997;34:245-259.

36. Cooke JP, Ghebremariam YT. Dietary nitrate, nitric oxide and restenosis. J Clin Invest. 2011;121(4):1258-1260.

37. Brown GC, Cooper CE. Nanomolar concentrations of nitric oxide reversibly inhibit synaptosomal respiration by competing with oxygen at cytochrome oxidase. FEBS Lett 1994;356:295-298.

38. Humbert M, Sitbon O, Chaouat A, et al. Pulmonary arterial hypertension in France: results from a national registry. Am J Respir Crit Care Med. 2006;173:1023-30.

39. Dayoub H, Achan V, Adimoolam S, et al. Dimethylarginine dimethylaminohydrolase regulates nitric oxide synthesis. Circulation 2003;108:3042-3047.

40. McBride AD, Sliver PA. State of the Arg: protein methylation at arginine comes of age. Cell 2001;106:1-10.

41. Boisvert FM, Cote J, Boulanger MC, Richard S. Aproteomic analysis of arginine-methylated protein complexes, Mol Cell Proteomics 2003;2:1319-1330.

42. Wada K, Inoue K, Hagiwara M. Identification of methylated proteins by protein arginine N-methyltransferase 1, PRMT1, with a new expression cloning strategy. Biochim Biophys Acta 2002;1591:1-10.

43. Onozato ML, Tojo A, Leiper J, Fujita T, Palm F, Wilcox CS. Expression of DDAH and PRMT isoforms in the diabetic rat kidney; effects of angiotensin II receptor blocker. Diabetes. 2007;57:172-180.

44. Achan V, Broadhead M. Malaki M, et al. Asymmetric dimethylarginine causes hypertension and cardiac dysfunction in humans and is actively metabolized by dimethylarginine dimethylaminohydrolase. Arterioscler Thromb Vasc Biol 2003;23:1455-1459.

45. Vallance P, Leone A, Calver A, et al. Accumulation of an endogenous inhibitor of nitric oxide synthesis in chronic renal failure. Lancet 1992;339:572-575.

46. Murray-Rust J, Leiper JM, McAlister M, et al. Structural insights into the hydrolysis of cellular nitric oxide synthase inhibitors by dimethylarginine dimethylaminohydrolase. Nat Struct Biol 2001;8:679-683.

47. Leiper JM, Santa Maria J, Chubb A, et al. Identification of two human dimethylarginine dimethylaminohydrolases with distinct tissue distributions and homology with microbial arginine deiminases. Biochem J 1999;343:209-214.

48. Ito A, Tsao PS, Adimoolam S, et al. Novel mechanism for endothelial dysfunction: dysregulation of dimethylarginine dimethylaminohydrolase. Circulation 1999;99:3092-3095.

49. Leiper J, Vallance P. Biological significance of endogenous methylarginines that inhibit nitric oxide synthases. Cardiovasc Res. 1999;43(3):542-548.

50. Lee Y, Stallcup M. Minireview: protein arginine methylation of nonhistone proteins in transcriptional regulation. Mol Endocrinol 2009;23:425-433.

51. Bedford MT, Richard S. Arginine methylartion an emerging regulator of protein function. Mol Cell 2005;18:263-272.

52. Boulanger MC, Liang C, Russell RS, Lin R, Bedford MT, Wainberg MA, Richard S. Methylation of Tat by PRMT6 regulates human immunodeficiency virus type 1 gene expression. J Virol 2005;79:124-131.

53. Najbauer J, Johnson BA, Young AL, Aswad DW. Peptides with sequences similar to glycine, arginine-rich motifs in proteins interacting with RNA are efficiently recognized by methyltransferase(s) modifying arginine in numerous proteins. J Biol Chem 1993;268:10501-10509.

54. Cheng D, Cote J, Shaaban S, Bedford MT. The arginine methyltransferase CARM1 regulates the coupling of transcription and mRNA processing. Mol Cell 2007;25:71-83.

55. Chang B, Chen Y, Zhao Y, Bruick RK. JMJD6 is a histone arginine demethylase. Science 2007;318:444-447.

56. Wang Y, Wysocka J, Sayegh J, Lee YH, Perlin JR, Leonelli L, Sonbuchner LS, McDonald CH, Cook RG, Bou Y, Roeder RG, Clarke S, Stallcup MR, Allis CD, Coonrod SA. Human PAD4 regulates histone arginine methylation levels via demethylimination. Science 2004'306:279-283.

57. Shi Y, Lan C, Matson C, Mulligan P, Wheststine JR, Cole PA, Casero RA, Shi Y Histone demethylation mediated by the nuclear amine oxidase homolog LSD1. Cell 2004;119:941-953.

58. Scorilas A, Black MH, Talieri M, Diamandis EP. Genomic organization, physical mapping, and expression analysis of the human protein arginine methyltransferase 1 gene. Biochem Biophys Res Commun 2000;278:349-359.

59. Pawlak MR, Scherer CA, Chen J, Roshon MJ, Ruley HE. Arginine N-methyltransferase 1 is required for early postimplantation mouse development, but cells deficient in the enzyme are viable. Mol Cell Biol 2000;20:4859-4869.

60. Yadav N, Lee J, Kim J, Chen J, Hu MC, Aldaz CM, Bedford MT. Specific protein methylation defets and gene expression perturbations in coactivator associated arginine methyltransferase 1 deficient mice. Proc Natl Acad Sci 2003;100:6464-6468.

61. Lin WJ, Gary JD, Yang MC, Clarke S, Herschman HR. The mammalian immediate-early TIS21 protein and the leukemia associated BTG1 protein interact with a protein arginine N-methyltransferase. J Biol Chem 1996;271:15034-15044.

62. Singh V, Miranda TB, Jiang W, Frankel A, Roemer ME, Robb VA, Gutmann DH, Herschman HR, Clarke S, Newsham IF. DAL-1/4.1B tumor suppressor interacts with protein arginine N-methyltransferase 3 (PRMT3) and inhibits its ability to methylate substrates in vitro and in vivo. Oncogene 2004;23:7761-7771.

63. Zhang X, Cheng X. Structure of the predominant protein arginine methyltransferase PRMT-1 and analysis of its binding to substrate peptides. Structure 2003;11:509-520.

64. Chen Y, Xu X, Sheng M, Zhang X, Gu Q, Zheng Z. PRMT-1 and DDAHs-induced ADMA upregulation in involved in ROS and RAS mediated diabetic retinopathy. Exp Eye Res 2009;89:1028-1034.

65. Osanai T, Saitoh M, Sasaki S, Tomita H, Matsunaga T, Okumura K. Effect of shear stress on asymmetric dimethylarginine release from vascular endothelial cells. Hypertension 2003;42:985-990.

66. Ogawa T, Kimoto M, Sasaoka K. Purification and properties of a new enzyme, N^G,N^G-dimethylarginine dimethylaminohydrolase, from rat kidney. J Biol Chem 1989;264:10205-9.

67. MacAllister RJ, Parry H, Kimoto M, et al. Regulation of nitric oxide synthesis by dimethylarginine dimethylaminohydrolase. Br J Pharmacol 1996;119:1533-1540.

68. Stuhlinger MC, Tsao PS, Her JH, et al. Homocysteine impairs the nitric oxide synthase pathway: role of asymmetric dimethylarginine. Circulation 2001;104:2569-2575.

69. Leiper JM, Murray-Rust J, McDonald N, et al. S-Nitrosylation of dimethylarginine dimethylaminohydrolase regulates enzyme activity: further interactions between nitric oxide synthase and dimethylarginine dimethylaminohydrolase. Proc Natl Acad Sci U S A 2002;99:13527-32.

70. Jang J, Ho H-K, Kwan HH, et al. Angiogenesis is impaired by hypercholesterolemia: role of asymmetric dimethylarginine. Circulation 2000;102:1414-19.

71. Kostourou V, Robinson SP, Cartwright JE, et al. Dimethylarginine dimethylaminohydrolase I promotes tumour growth and angiogenesis. Br J Cancer 2002;87:673-80.

72. Achan V, Tran CT, Arrigoni F, et al. All-trans-retinoic acid increases nitric oxide synthesis by endothelial cells: a role for the induction of dimethylarginine dimethylaminohydrolase. Cir Res 2002;90:764-9.

73. Mehta S, Stewart DJ, Langleben D, et al. Short-term pulmonary vasodilation with L-arginine in pulmonary hypertension. Circulation 1995;92:1539-45.

74. Tuder RM, Flook BE, Voelkel NF. Increased gene expression for VEGF receptor KDR/Flk and Flt in lungs exposed to acute or to chronic hypoxia: modulation of gene expression by nitric oxide. J Clin Invest 1995;95:1798-1807.

75. Fong TAT, Shawver LK, Sun L, Tang C, App H, Powell TJ, Kim YH, Schreck R, Wang X, Risau W, Ullrich A, Hirth P, McMahon G. SU5416 is a potent and selective inhibitor of the vascular endothelial growth factor receptor (Flk-1/KDR) that inhibits tyrosine kinase catalysis, tumor vascularization, and growth of multiple tumor types. Cancer Res 1999;59:99-106.

76. Mendel DB, Laird AD, Smolich BD, Blake RA, Liang C, Hannah AL, Shaheen RM, Ellis LM, Weitman S, Shawver LK, Cherrington JM. Development of SU5416, a selective small molecule inhibitor of VEGF receptor tyrosinekinase activity, as an anti-antigen-esis agent. Anticancer Drug Design 2000;15:29-41.

77. Rosen L, Mulay M, Mayers A, Kabbinavar F, Rosen P, Cropp G, Hannah A. Pahse I dose escalating trial of SU5416, a novel angiogenesis inhibitor in patients with advanced malignancies. Proc Am Soc Clin Oncol 1999;18:618.

78. Stopeck A, Sheldon M, Vahedian M, Cropp G, Gosalia R, Hannah A. Results of a phase I does –escalating study of the antiangiogenic agent, SU5416, in patients with advanced malignancies. Clin Cancer Res 2002;8:2798-2805.

79. Kasahara Y, Tuder RM, Taraseviciene-Stewart L, Ke Cras TD, Abman SH, Hirth P, Waltenberger J, Voelkel NF. Inhibition of vascular endothelial growth factor receptors causes lung cell apoptosis and emphysema. J Clin Invest 2000;106:1311-1319.

80. Taraseviciene-Stewart L, Scerbavicius R, Choe KH, Moore M, Sullivan A, Nicolls MR, Fontenot AP, Tuder RM, Voelkel NF. An animal model of autoimmune emphysema. Am J Respir Crit Care Med 2005;171:734-742.

81. Kang K, Wagner PD, Breen EC. Lung-specific inactivation of VEGF in adult mice leads to emphysema like changes. Am J Respir Crit Care Med 2002;165:B54.

82. Tuder RM, Zhen L, Cho CY, Taraseviciene-Stewart L, Kasahara Y, Salvemini D, Voelkel NF, Flores SC. Oxidative stress and apoptosis interact and cause emphysema due to vascular endothelial growth factor receptor blockade. Am J Respir Cell Mol Biol 2003;29:88-97.

83. Taraseviciene-Stewart L, Kasahara Y, Alger L, Hirth P, Mc Mahon G, Waltenberger J, Voelkel NF, Tuder RM. Inhibition of the VEGF receptor 2 combined with chronic hypoxia causes cell death dependent pulmonary EC proliferation and severe pulmonary hypertension. FASEB J 2001;15:427-438.

84. Abe K, Toba M, Alzoubi A, Ito M, Fagan KA, Cool CD, Voelkel NF, McMurtry IF, Oka M. Formation of plexiform lesions in experimental severe pulmonary arterial hypertension. Circulation 2010;121:2747-2754.

85. Kwapiszewska G, Wygrecka M, Marsh LM, Schmitt S, Tosser R, Wilhelm J, Helmus K, Eul B, Zakrzewicz A, Ghofrani HA, Schermuly RT, Bohle RM, Grimminger F, Seeger W, Eickelberg O, Fink L, Weissmann N. Fhl-1, a new key protein in pulmonary hypertension. Circulation 2008;118:1183-1194.

86. Moreno-Vinasco L, Gomberg-Maitland M, Maitland ML, Desai AA, Singleton PA, Sammani S, Sam L, Liu Y, Husain AN, Lang RM, Ratain MJ, Lussier YA, Garcia JG.

Genomic assessment of a multikinase inhibitor, sorafenib, in a rodent model of pulmonary hypertension. Physiol Genomics 2008;33:278-291.

87. Taraseviciene-Stewart L, Nicolls MR, Kraskauskas D, Scerbavicius R, Burns N, Cool C, Wood K, Parr JE, Boackle SA, Voelkel NF. Absence of T cells confers increased pulmonary arterial hypertension and vascular remodeling. Am J Respir Crit Care Med 2007;175:1280-1289.
88. Oka M, Homma N, Taraseviciene-Stewart L, Morris KG, Kraskauskas D, Burns N, Voelkel NF, McMurtry IF. Rho kinase-mediated vasoconstriction is important in severe occlusive pulmonary arterial hypertension in rats. Circ Res 2007;100:923-929.
89. Taraseviciene-Stewart L, Gera L, Hirth P, Voelkel NF, Tuder RM, Stewart JM. A brady-kinin antagonist and a caspase inhibitor prevent severe pulmonary hypertension in a rat model. Can J Physiol Pharmacol 2002;80:269-274.
90. Tuder RM, Chacon M, Alger L, Wang J, Taraseviciene-Stewart L, Kasahara Y, Cool CD, Bishop AE, Geraci M, Semenza GL, Yacoub M, Polak JM, Voelkel NF. Expression of angiogenesis-related molecules in plexiform lesions in severe pulmonary hypertension: evidence for a process of disordered angiogenesis. J Pathol 2001;195:367-374.
91. Lee SD, Shroyer KR, Markham NE, Cool CD, Voelkel NF, Tuder RM. Monoclonal endothelial cell proliferation is present in primary but not secondary pulmonary hypertension. J Clin Invest 1998;101:927-934.
92. Yeager ME, Voelkel NF, Tuder RM. Mutational analysis of endothelial cell TGF-b receptor type II in plexiform lesions of patients with primary pulmonary hypertension. Circulation 1999;100:I-587.
93. Meyrick B, Reid L. Hypoxia-induced structural changes in the media and adventitia of the rat hilar pulmonary artery and their regression. Am J Pathol 1980;100:151-178.

94. Jones PL, Cowan KN, Rabinovitch M. Tenascin-C, proliferation and subendothelial fibronectin in progressive pulmonary vascular disease. Am J Pathol 1997;150:1349-1360.

95. Jeffery TK, Wanstall JC. Pulmonary vascular remodeling: a target for therapeutic intervention in pulmonary hypertension. Pharmacol Ther 2001;92:1-20.

96. Kakusaka I, Kabeko N, Kiyatake K, Fujita A, Suzuki A, Nakano K, Okada O, Sugita T, Watanabe S, Kuriyama T. Effects of various doses of monocrotaline administration on the development of pulmonary hypertension and its regression in rats. Nihon Hyobu Shikkan Gakkai Zasshi 1989;27:51-56.

97. Sakao S, Tatsumi K, Voelkel NF. Reversible or irreversible remodeling in pulmonary arterial hypertension. Am J Respir Cell Mol Biol 2010;43:629-634.

98. Nagasaka H, Okano Y, Aizawa M, et al. Altered metabolisms of mediators controlling vascular function and enhanced oxidative stress in asymptomatic children with congenital portosystemic venous shunt. Metabolism. 2010;59:107-13.

99. Lu Z, Xu X, Hu X, et al. Oxidative stress regulates left ventricular PDE5 expression in the failing heart. Circulation. 2010;121:1474-83.

100. Lu Z, Fassett J, Xu X, et al. Adenosine A3 receptor deficiency exerts unanticipated cardiac protective effects on the pressure overloaded induced ventricle hypertrophy. Circulation. 2008;118:1713-21.

101. Xu X, Fassett J, Hu X, et al. Ecto-5'-nucleotidase deficiency exacerbates pressure-overload-induced left ventricular hypertrophy and dysfunction. Hypertension. 2008;51:1557-64.

102. Xu D, Guo H, Xu X, et al. Exacerbated pulmonary arterial hypertension and right ventricular hypertrophy in animals with loss of function of extracellular superoxide dismutase. Hypertension. 2011;58:303-9.

103. Handoko ML, de Man FS, Happe CM, et al. Opposite effects of training in rats with stable and progressive pulmonary hypertension. Circulation. 2009;120:42-49.

104. Urboniene D, Haber I, Fang YH, Thenappan T, Archer DL. Validation of high-resolution echocardiography and magnetic resonance imaging versus high-fidelity catheterization in experimental pulmonary hypertension. Am J Physiol Lung Cell Mol Physiol. 2010;299:410-12.

105. Mass R, Tan-Andreesen J, Schwedhelm E, Schulze F, Boger RH. A stable-isotope based technique for the determination of dimethylarginine dimethylaminohydrolase (DDAH) activity in mouse tissue. J Chromatogr B Analyt Technol Biomed Life Sci. 2007;851:220-8.

106. Lu Z, Xu X, Hu X, et al. PGC-1 alpha regulates expression of myocardial mitochondrial antioxidants and myocardial oxidative stress after chronic systolic overload. Antioxid Redox Signal. 2010;13:1011-22.

107. Weis M, Kledal TN, Lin KY, et al. Cytomegalovirus infection impairs the nitric oxide synthase pathway: role of asymmetric dimethylarginine in transplant arteriosclerosis. Circulation. 2004;109:500-5.

108. Zhang P, Xu X, Hu X, Vandeel ED, Zhu G, Chen Y. Inducible nitric oxide synthase deficiency protects the heart from systolic overload-induced ventricular hypertrophy and congestive heart failure. Circ Res. 2007;100:1089-98.

109. Machado RF, Londhe Nerkar MV, Dweik RA, Hammel J, Janocha A, Pyle J, Laskowski D, Jennings C, Arroliga AC, Erzurum SC. Nitric oxide and pulmonary arterial pressures in pulmonary hypertension. *Free Radic Biol Med*. 2004;37:1010-1017.

110. Klinger JR, Abman SH, Gladwin MT. Nitric oxide deficiency and endothelial dysfunction in pulmonary arterial hypertension. *Am J Respir Crit Care Med*.188:639-646.

111. Fagan KA, Fouty BW, Tyler RC, Morris KG, Jr., Hepler LK, Sato K, LeCras TD, Abman SH, Weinberger HD, Huang PL, McMurtry IF, Rodman DM. The pulmonary circulation of homozygous or heterozygous enos-null mice is hyperresponsive to mild hypoxia. *J Clin Invest*. 1999;103:291-299.

112. Cooper CJ, Landzberg MJ, Anderson TJ, Charbonneau F, Creager MA, Ganz P, Selwyn AP. Role of nitric oxide in the local regulation of pulmonary vascular resistance in humans. *Circulation*. 1996;93:266-271.

113. Radomski MW, Palmer RM, Moncada S. Characterization of the l-arginine:Nitric oxide pathway in human platelets. *Br J Pharmacol*. 1990;101:325-328.

114. Kubes P, Suzuki M, Granger DN. Nitric oxide: An endogenous modulator of leukocyte adhesion. *Proc Natl Acad Sci U S A*. 1991;88:4651-4655.

115. Niu XF, Ibbotson G, Kubes P. A balance between nitric oxide and oxidants regulates mast cell-dependent neutrophil-endothelial cell interactions. *Circ Res*. 1996;79:992-999.

116. Humbert M, Morrell NW, Archer SL, Stenmark KR, MacLean MR, Lang IM, Christman BW, Weir EK, Eickelberg O, Voelkel NF, Rabinovitch M. Cellular and molecular pathobiology of pulmonary arterial hypertension. *J Am Coll Cardiol*. 2004;43:13S-24S.

117. Michelakis ED. The role of the no axis and its therapeutic implications in pulmonary arterial hypertension. *Heart Fail Rev*. 2003;8:5-21.

118. Crosswhite P, Sun Z. Nitric oxide, oxidative stress and inflammation in pulmonary arterial hypertension. *J Hypertens*.28:201-212.

119. Hassoun PM, Mouthon L, Barbera JA, Eddahibi S, Flores SC, Grimminger F, Jones PL, Maitland ML, Michelakis ED, Morrell NW, Newman JH, Rabinovitch M, Schermuly R, Stenmark KR, Voelkel NF, Yuan JX, Humbert M. Inflammation, growth factors, and pulmonary vascular remodeling. *J Am Coll Cardiol*. 2009;54:S10-19.

120. Zuckerbraun BS, Shiva S, Ifedigbo E, Mathier MA, Mollen KP, Rao J, Bauer PM, Choi JJ, Curtis E, Choi AM, Gladwin MT. Nitrite potently inhibits hypoxic and inflammatory pulmonary arterial hypertension and smooth muscle proliferation via xanthine oxidoreductase-dependent nitric oxide generation. *Circulation*. 2010;121:98-109.

121. Maruhashi T, Noma K, Iwamoto Y, Iwamoto A, Oda N, Kajikawa M, Matsumoto T, Hidaka T, Kihara Y, Chayama K, Nakashima A, Goto C, Liao JK, Higashi Y. Critical role of exogenous nitric oxide in rock activity in vascular smooth muscle cells. *PLoS One*.9:e109017.

122. Kolpakov V, Gordon D, Kulik TJ. Nitric oxide-generating compounds inhibit total protein and collagen synthesis in cultured vascular smooth muscle cells. *Circ Res*. 1995;76:305-309.

123. Wells SM, Holian A. Asymmetric dimethylarginine induces oxidative and nitrosative stress in murine lung epithelial cells. *Am J Respir Cell Mol Biol*. 2007;36:520-528.

124. Druhan LJ, Forbes SP, Pope AJ, Chen CA, Zweier JL, Cardounel AJ. Regulation of enos-derived superoxide by endogenous methylarginines. *Biochemistry*. 2008;47:7256-7263.

125. Li XH, Peng J, Tan N, Wu WH, Li TT, Shi RZ, Li YJ. Involvement of asymmetric dimethylarginine and rho kinase in the vascular remodeling in monocrotaline-induced pulmonary hypertension. *Vascul Pharmacol*. 2010;53:223-229.

126. Wells SM, Buford MC, Migliaccio CT, Holian A. Elevated asymmetric dimethylarginine alters lung function and induces collagen deposition in mice. *Am J Respir Cell Mol Biol*. 2009;40:179-188.

127. Kielstein JT, Bode-Boger SM, Hesse G, Martens-Lobenhoffer J, Takacs A, Fliser D, Hoeper MM. Asymmetrical dimethylarginine in idiopathic pulmonary arterial hypertension. *Arterioscler Thromb Vasc Biol*. 2005;25:1414-1418.

128. Dimitroulas T, Giannakoulas G, Sfetsios T, Karvounis H, Dimitroula H, Koliakos G, Settas L. Asymmetrical dimethylarginine in systemic sclerosis-related pulmonary arterial hypertension. *Rheumatology (Oxford)*. 2008;47:1682-1685.

129. Shao Z, Wang Z, Shrestha K, Thakur A, Borowski AG, Sweet W, Thomas JD, Moravec CS, Hazen SL, Tang WH. Pulmonary hypertension associated with advanced systolic heart failure: Dysregulated arginine metabolism and importance of compensatory dimethylarginine dimethylaminohydrolase-1. *J Am Coll Cardiol*. 2012;59:1150-1158.

130. Gorenflo M, Zheng C, Werle E, Fiehn W, Ulmer HE. Plasma levels of asymmetrical dimethyl-l-arginine in patients with congenital heart disease and pulmonary hypertension. *J Cardiovasc Pharmacol*. 2001;37:489-492.

131. Michell BJ, Griffiths JE, Mitchelhill KI, Rodriguez-Crespo I, Tiganis T, Bozinovski S, de Montellano PR, Kemp BE, Pearson RB. The akt kinase signals directly to endothelial nitric oxide synthase. *Curr Biol*. 1999;9:845-848.

132. Masri FA, Xu W, Comhair SA, Asosingh K, Koo M, Vasanji A, Drazba J, Anand-Apte B, Erzurum SC. Hyperproliferative apoptosis-resistant endothelial cells in idiopathic pulmonary arterial hypertension. *Am J Physiol Lung Cell Mol Physiol*. 2007;293:L548-554.

133. Tang H, Chen J, Fraidenburg DR, Song S, Sysol JR, Drennan AR, Offermanns S, Ye RD, Bonini MG, Minshall RD, Garcia JG, Machado RF, Makino A, Yuan JX. Deficiency of akt1, but not akt2, attenuates the development of pulmonary hypertension. *Am J Physiol Lung Cell Mol Physiol*. 2015;308:L208-220.

134. Iannone L, Zhao L, Dubois O, Duluc L, Rhodes CJ, Wharton J, Wilkins MR, Leiper J, Wojciak-Stothard B. Mir-21/ddah1 pathway regulates pulmonary vascular responses to hypoxia. *Biochem J*. 2014;462:103-112.

135. Bakr A, Pak O, Taye A, Hamada F, Hemeida R, Janssen W, Gierhardt M, Ghofrani HA, Seeger W, Grimminger F, Schermuly RT, Witzenrath M, Brandes RP, Huang N, Cooke JP, Weissmann N, Sommer N. Effects of dimethylarginine dimethylaminohydrolase-1 overexpression on the response of the pulmonary vasculature to hypoxia. *Am J Respir Cell Mol Biol*.49:491-500.

136. Takimoto E, Champion HC, Li M, Belardi D, Ren S, Rodriguez ER, Bedja D, Gabrielson KL, Wang Y, Kass DA. Chronic inhibition of cyclic gmp phosphodiesterase 5a prevents and reverses cardiac hypertrophy. *Nat Med*. 2005;11:214-222.

137. Moens AL, Takimoto E, Tocchetti CG, Chakir K, Bedja D, Cormaci G, Ketner EA, Majmudar M, Gabrielson K, Halushka MK, Mitchell JB, Biswal S, Channon KM, Wolin MS, Alp NJ, Paolocci N, Champion HC, Kass DA. Reversal of cardiac hypertrophy and fibrosis from pressure overload by tetrahydrobiopterin: Efficacy of recoupling nitric oxide synthase as a therapeutic strategy. *Circulation*. 2008;117:2626-2636.

138. Bogaard HJ, Abe K, Vonk Noordegraaf A, Voelkel NF. The right ventricle under pressure: Cellular and molecular mechanisms of right-heart failure in pulmonary hypertension. *Chest*. 2009;135:794-804.

139. Carling D, Thornton C, Woods A, Sanders MJ. Amp-activated protein kinase: New regulation, new roles? *Biochem J*. 2012;445:11-27.

140. Hardie DG, Ross FA, Hawley SA. Ampk: A nutrient and energy sensor that maintains energy homeostasis. *Nat Rev Mol Cell Biol*. 2012;13:251-262.

141. Igata M, Motoshima H, Tsuruzoe K, Kojima K, Matsumura T, Kondo T, Taguchi T, Nakamaru K, Yano M, Kukidome D, Matsumoto K, Toyonaga T, Asano T, Nishikawa T, Araki E. Adenosine monophosphate-activated protein kinase suppresses vascular smooth muscle cell proliferation through the inhibition of cell cycle progression. *Circ Res*. 2005;97:837-844.

142. Nagata D, Takeda R, Sata M, Satonaka H, Suzuki E, Nagano T, Hirata Y. Amp-activated protein kinase inhibits angiotensin ii-stimulated vascular smooth muscle cell proliferation. *Circulation*. 2004;110:444-451.

143. Zhang M, Dong Y, Xu J, Xie Z, Wu Y, Song P, Guzman M, Wu J, Zou MH. Thromboxane receptor activates the amp-activated protein kinase in vascular smooth muscle cells via hydrogen peroxide. *Circ Res*. 2008;102:328-337.

144. Goncharov DA, Kudryashova TV, Ziai H, Ihida-Stansbury K, DeLisser H, Krymskaya VP, Tuder RM, Kawut SM, Goncharova EA. Mammalian target of rapamycin complex 2 (mtorc2) coordinates pulmonary artery smooth muscle cell metabolism, proliferation, and survival in pulmonary arterial hypertension. *Circulation*. 2014;129:864-874.

145. Song P, Zhou Y, Coughlan KA, Dai X, Xu H, Viollet B, Zou MH. Adenosine monophosphate-activated protein kinase-alpha2 deficiency promotes vascular smooth muscle cell migration via s-phase kinase-associated protein 2 upregulation and e-cadherin downregulation. *Arterioscler Thromb Vasc Biol*. 2013;33:2800-2809.

146. Song P, Wang S, He C, Wang S, Liang B, Viollet B, Zou MH. Ampkalpha2 deletion exacerbates neointima formation by upregulating skp2 in vascular smooth muscle cells. *Circ Res*. 2011;109:1230-1239.

147. Zhang P, Hu X, Xu X, Fassett J, Zhu G, Viollet B, Xu W, Wiczer B, Bernlohr DA, Bache RJ, Chen Y. Amp activated protein kinase-alpha2 deficiency exacerbates pressure-overload-induced left ventricular hypertrophy and dysfunction in mice. *Hypertension*. 2008;52:918-924.

148. Sasaki H, Asanuma H, Fujita M, Takahama H, Wakeno M, Ito S, Ogai A, Asakura M, Kim J, Minamino T, Takashima S, Sanada S, Sugimachi M, Komamura K, Mochizuki N, Kitakaze M. Metformin prevents progression of heart failure in dogs: Role of amp-activated protein kinase. *Circulation*. 2009;119:2568-2577.

149. Gundewar S, Calvert JW, Jha S, Toedt-Pingel I, Ji SY, Nunez D, Ramachandran A, Anaya-Cisneros M, Tian R, Lefer DJ. Activation of amp-activated protein kinase by metformin improves left ventricular function and survival in heart failure. *Circ Res*. 2009;104:403-411.

150. Xu X, Lu Z, Fassett J, Zhang P, Hu X, Liu X, Kwak D, Li J, Zhu G, Tao Y, Hou M, Wang H, Guo H, Viollet B, McFalls EO, Bache RJ, Chen Y. Metformin protects against systolic overload-induced heart failure independent of amp-activated protein kinase alpha2. *Hypertension*. 2014;63:723-728.

151. Hu X, Xu X, Lu Z, Zhang P, Fassett J, Zhang Y, Xin Y, Hall JL, Viollet B, Bache RJ, Huang Y, Chen Y. Amp activated protein kinase-alpha2 regulates expression of estrogen-related receptor-alpha, a metabolic transcription factor related to heart failure development. *Hypertension*. 2012;58:696-703.

152. Fassett JT, Hu X, Xu X, Lu Z, Zhang P, Chen Y, Bache RJ. Ampk attenuates microtubule proliferation in cardiac hypertrophy. *Am J Physiol Heart Circ Physiol*. 2013;304:H749-758.

153. Viollet B, Andreelli F, Jorgensen SB, Perrin C, Geloen A, Flamez D, Mu J, Lenzner C, Baud O, Bennoun M, Gomas E, Nicolas G, Wojtaszewski JF, Kahn A, Carling D, Schuit FC, Birnbaum MJ, Richter EA, Burcelin R, Vaulont S. The amp-activated protein kinase alpha2 catalytic subunit controls whole-body insulin sensitivity. *J Clin Invest*. 2003;111:91-98.

154. Chen Y, Guo H, Xu D, Xu X, Wang H, Hu X, Lu Z, Kwak D, Xu Y, Gunther R, Huo Y, Weir EK. Left ventricular failure produces profound lung remodeling and pulmonary hypertension in mice: Heart failure causes severe lung disease. *Hypertension*. 2012;59:1170-1178.

155. Ciuclan L, Bonneau O, Hussey M, Duggan N, Holmes AM, Good R, Stringer R, Jones P, Morrell NW, Jarai G, Walker C, Westwick J, Thomas M. A novel murine model of severe pulmonary arterial hypertension. Am J Respir Crit Care Med. 2011;184:1171-82.

156. Lu Z, Xu X, Fassett J, Kwak D, Liu X, Hu X, Wang H, Guo H, Xu D, Yan S, McFalls EO, Lu F, Bache RJ, Chen Y. Loss of the eukaryotic initiation factor 2alpha kinase general control nonderepressible 2 protects mice from pressure overload-induced congestive heart failure without affecting ventricular hypertrophy. *Hypertension*. 2014;63:128-135.

157. Xu D, Guo H, Xu X, Lu Z, Fassett J, Hu X, Xu Y, Tang Q, Hu D, Somani A, Geurts AM, Ostertag E, Bache RJ, Weir EK, Chen Y. Exacerbated pulmonary arterial hypertension and right ventricular hypertrophy in animals with loss of function of extracellular superoxide dismutase. Hypertension. 2011;58:303-309.

158. Houssaini A, Abid S, Mouraret N, Wan F, Rideau D, Saker M, Marcos E, Tissot CM, Dubois-Rande JL, Amsellem V, Adnot S. Rapamycin reverses pulmonary artery smooth muscle cell proliferation in pulmonary hypertension. *Am J Respir Cell Mol Biol*. 2013;48:568-577.

159. Burke DL, Frid MG, Kunrath CL, Karoor V, Anwar A, Wagner BD, Strassheim D, Stenmark KR. Sustained hypoxia promotes the development of a pulmonary artery-specific chronic inflammatory microenvironment. *Am J Physiol Lung Cell Mol Physiol*. 2009;297:L238-250.

160. Isoda K, Young JL, Zirlik A, MacFarlane LA, Tsuboi N, Gerdes N, Schonbeck U, Libby P. Metformin inhibits proinflammatory responses and nuclear factor-kappab in human vascular wall cells. *Arterioscler Thromb Vasc Biol*. 2006;26:611-617.

161. Hattori Y, Suzuki K, Hattori S, Kasai K. Metformin inhibits cytokine-induced nuclear factor kappab activation via amp-activated protein kinase activation in vascular endothelial cells. *Hypertension*. 2006;47:1183-1188.

162. Frid MG, Brunetti JA, Burke DL, Carpenter TC, Davie NJ, Reeves JT, Roedersheimer MT, van Rooijen N, Stenmark KR. Hypoxia-induced pulmonary vascular remodeling requires recruitment of circulating mesenchymal precursors of a monocyte/macrophage lineage. *Am J Pathol*. 2006;168:659-669.

163. Frid MG, Brunetti JA, Burke DL, Carpenter TC, Davie NJ, Stenmark KR. Circulating mononuclear cells with a dual, macrophage-fibroblast phenotype contribute robustly to hypoxia-induced pulmonary adventitial remodeling. *Chest*. 2005;128:583S-584S.

164. Bai J, Zhang N, Hua Y, Wang B, Ling L, Ferro A, Xu B. Metformin inhibits angiotensin ii-induced differentiation of cardiac fibroblasts into myofibroblasts. *PLoS One*. 2013;8:e72120.

165. Xiao H, Ma X, Feng W, Fu Y, Lu Z, Xu M, Shen Q, Zhu Y, Zhang Y. Metformin attenuates cardiac fibrosis by inhibiting the tgfbeta1-smad3 signalling pathway. *Cardiovasc Res*. 2010;87:504-513.

166. Huang X, Fan R, Lu Y, Yu C, Xu X, Zhang X, Liu P, Yan S, Chen C, Wang L. Regulatory effect of amp-activated protein kinase on pulmonary hypertension induced by chronic hypoxia in rats: In vivo and in vitro studies. *Mol Biol Rep*. 2014;41:4031-4041.

167. Agard C, Rolli-Derkinderen M, Dumas-de-La-Roque E, Rio M, Sagan C, Savineau JP, Loirand G, Pacaud P. Protective role of the antidiabetic drug metformin against chronic experimental pulmonary hypertension. *Br J Pharmacol*. 2009;158:1285-1294.

168. Fu X, Zhao JX, Zhu MJ, Foretz M, Viollet B, Dodson MV, Du M. Amp-activated protein kinase alpha1 but not alpha2 catalytic subunit potentiates myogenin expression and myogenesis. *Mol Cell Biol*. 2013;33:4517-4525.

169. Crawford RM, Treharne KJ, Best OG, Riemen CE, Muimo R, Gruenert DC, Arnaud-Dabernat S, Daniel JY, Mehta A. Ndpk-a (but not ndpk-b) and ampk alpha1 (but not ampk alpha2) bind the cystic fibrosis transmembrane conductance regulator in epithelial cell membranes. *Cell Signal*. 2006;18:1595-1603.

170. Gusarova GA, Dada LA, Kelly AM, Brodie C, Witters LA, Chandel NS, Sznajder JI. Alpha1-amp-activated protein kinase regulates hypoxia-induced na,k-atpase endocytosis via direct phosphorylation of protein kinase c zeta. *Mol Cell Biol*. 2009;29:3455-3464.